

Early-type stars observed in the ESO UVES Paranal Observatory Project: I – Interstellar Na I UV, Ti II and Ca II K observations.

I. Hunter^{1,2*}, J. V. Smoker^{1,2}, F. P. Keenan¹, C. Ledoux², E. Jehin²,
R. Cabanac³, C. Melo², S. Bagnulo².

¹*Astrophysics and Planetary Science Research Division, Department of Physics and Astronomy, The Queen's University of Belfast, University Road, Belfast, BT7 1NN, U.K.*

²*European Southern Observatory, Alonso de Cordova 3107, Casilla 19001, Vitacura, Santiago 19, Chile*

³*Canada-France-Hawaii Telescope Corporation, 65-1238 Mamalahoa Hwy. Kamuela, Hawaii 96743, USA*

Accepted Received in original form

ABSTRACT

We present an analysis of interstellar Na I ($\lambda_{\text{air}}=3302.37\text{\AA}$, 3302.98\AA), Ti II ($\lambda_{\text{air}}=3383.76\text{\AA}$) and Ca II K ($\lambda_{\text{air}}=3933.66\text{\AA}$) absorption features for 74 sightlines towards O- and B-type stars in the Galactic disc. The data were obtained from the UVES Paranal Observatory Project, at a spectral resolution of 3.75 km s^{-1} and with mean signal to noise ratios per pixel of 260, 300 and 430 for the Na I, Ti II and Ca II observations, respectively. Interstellar features were detected in all but one of the Ti II sightlines and all of the Ca II sightlines. The dependence of the column density of these three species with distance, height relative to the Galactic plane, H I column density, reddening and depletion relative to the solar abundance has been investigated. We also examine the accuracy of using the Na I column density as an indicator of that for H I. In general we find similar strong correlations for both Ti and Ca, and weaker correlations for Na. Our results confirm the general belief that Ti and Ca occur in the same regions of the interstellar medium and also that the Ti II/Ca II ratio is constant over all parameters. We hence conclude that the absorption properties of Ti and Ca are essentially constant under the general interstellar medium conditions of the Galactic disc.

Key words: ISM: general – ISM: clouds – ISM: abundances – ISM: structure – stars: early-type

1 INTRODUCTION

The study of the interstellar medium in our Galaxy has a long history, dating back a century when interstellar Ca II absorption was first detected (Hartmann 1904). Historically, ground-based work has concentrated on the Ca II K and Na I D lines at around 3933 \AA and 5980 \AA . Studies such as Albert et al. (1993), Sembach, Danks & Savage (1993), Welty, Hobbs & Kulkarni (1994), Welty, Morton & Hobbs (1996) and Smoker et al. (2003) have observed the Ca II K and

Na I D lines in an attempt to provide information on the structure and physical characteristics of interstellar clouds, in particular their spatial distribution (e.g. Lallement et al. 2003), kinematics (e.g. Sembach & Danks 1994) and depletion patterns of these elements (e.g. Crinklaw, Federman & Joseph 1994; Wakker & Mathis 2000). The general situation can be summarised as follows; Ca II, with its ionisation potential of $\sim 11.9\text{ eV}$, is typically a trace ionisation stage in diffuse, neutral clouds, plus a more extended intercloud medium. However Na I is found to trace the neutral clouds only. Ca II is thought to be heavily depleted onto dust in denser clouds, with Na I a little-depleted element (Welty et al. 1996).

Other interstellar lines which have been studied much less frequently are the UV Na I doublet at $\lambda_{\text{air}}=3302.37\text{\AA}$,

* email: i.hunter@qub.ac.uk.

Based on observations taken at UT2, Kueyen, Cerro Paranal, Chile, ESO DDT programme 2665.D-5655, UVES Paranal Observatory Project.

Table 1. Main transitions studied.

Transition	λ_{air} (Å)	f -value
Na I	3302.368	0.00921
Na I	3302.978	0.00460
Ti I	3383.759	0.358
Ca II	3933.661	0.627

3302.98 Å, and Ti II at $\lambda_{\text{air}}=3383.76\text{Å}$. The relative paucity of observations is for two main reasons. First, the oscillator strengths of $f=0.0092$, 0.0046 and 0.358 for the Na I doublet and Ti II, respectively, are somewhat smaller than for the Ca II K ($f=0.627$) and Na I D lines ($f=0.318$, 0.631). Second, both the Na I UV doublet and Ti II lines lie toward the blue end of the optical range, where detectors are less efficient. Although the weakness of the lines clearly makes them more difficult to observe, it has the advantage that (especially in the case of Na I UV doublet) saturation effects are much less of an issue. Hence these transitions can be used to probe quite dense regions of the ISM, without having to apply large corrections for the effects of line saturation. In the case of Ti II, the ionisation potential of 13.57 eV is nearly the same as that of H I, so that this species is the dominant ionisation stage in H I regions and no ionisation corrections are necessary to obtain the total abundance of Ti in these regions. This is in contrast to Ca II K in warm neutral or weakly ionized gas, where the species is not the dominant ionisation stage (e.g. Sembach et al. 2000).

Previous observations of the Na I UV lines have been published by only a handful of authors including Hobbs (1978), Vallerga et al. (1993) and Welsh et al. (1997); corresponding results for Ti II appear in Stokes (1978), Hobbs (1984) and Welsh et al. (1997). In total approximately 110 Ti II sightlines have been studied to date, although many of these were non-detections.

The results for the Na I UV lines are complementary to previous studies of Na I D. Data for Ti II thus far indicate that this element appears to be associated with a smoothly distributed neutral medium. Although, unlike Ca II, Ti II is the dominant ionisation stage in neutral gas, the Ti II abundance shows a similar amount of scatter when plotted against N_{HI} (Wakker & Mathis 2000), with the Ti II/Ca II abundance ratio being constant over a range of interstellar density conditions (Welsh et al. 1997).

The current paper concerns observations of the Na I UV doublet, Ti II and Ca II K towards a sample of 74 early-type stars in the Southern Hemisphere. The wavelengths and transition strengths for the studied lines are shown in Table 1.

In contrast to previous surveys which generally have signal-to-noise (S/N) ratios in the Na I UV lines and Ti II of around 40, the current paper utilises data that typically have S/N ratios exceeding 250. This enables features with equivalent widths of $< 1\text{ mÅ}$ to be detected. This contrasts with the only previously existing Southern Hemisphere survey of Ti II by Welsh et al. (1997; hereafter W97) in which, with a S/N of 40, 18 out of 42 of the observed sightlines in Ti II were non-detections.

In Sect. 2 we describe the sample of stars observed,

while Sect. 3 discusses the data analysis and methods used to obtain equivalent widths, b -values, velocities of components and column densities, including an estimate of the errors in the derived parameters and comparison with previous work. Sect. 4 presents correlations between the derived column densities and parameters such as reddening and height above the Galactic disc (z). Finally, in Sect. 5 we list the main conclusions. A future paper will deal in more detail with the search for intermediate and high velocity gas along the current sightlines.

2 THE SAMPLE

We have extracted spectra for three interstellar species, namely the Na I UV doublet, Ti II and Ca II K along the sightlines to 74 O- and B-type field stars from *An Atlas of High-Resolution Spectra of Stars across the Hertzsprung-Russell Diagram*, available from the UVES Paranal Observatory Project (POP; Bagnulo et al. 2003). Although Ca H is also present in the spectra, it is on the wing of an H I line, so was not used in the bulk of the analysis.

High resolution spectra of the stars in the POP survey were obtained using the Ultraviolet and Visual Echelle Spectrograph (UVES) mounted on the 8.2-m UT2 (Kueyen) telescope at the European Southern Observatory (ESO), Paranal, Chile. The observations were taken between February 2001 and February 2003, with the field stars generally being observed during twilight. Further details of the observations and data reduction methods are available at <http://www.sc.eso.org/santiago/uvespop/>. The combination of bright stars, an efficient detector and an 8.2-m telescope results in very high S/N ratios for the merged spectra, the average per pixel being 260, 300 and 430 in the regions of the Na I UV, Ti II and Ca II K lines, respectively. There are 2 pixels per resolution element. For all the spectra, the velocity resolution is 3.75 km s^{-1} .

Spectra were selected on the criteria that the continuum in the region of interest was relatively unaffected by stellar features. As the stars of our sample are O- and B-type, in most cases the stellar lines were sufficiently broad that they could easily be classified as stellar and not interstellar lines. In Table 2 we list the field stars in our sample, and also their spectral types, peculiarities and visual magnitudes as listed by UVES POP. Spectral types range from O4 V to B9.5 V, and all objects are brighter than $m_v = 8.0$. Note that the peculiarities are taken from UVES POP and hence are not listed in the standard international nomenclature; <http://sc.eso.org/santiago/uvespop/> should be consulted for full details.

In Table 2 we also include the reddening, $E(B - V)$, along the line-of-sight and the spectroscopic distance estimate to each star. The spectra obtained from UVES POP had already been shifted to the helio-centric frame of rest. Each spectrum was furthermore shifted to the kinematic Local Standard of Rest using the corrections generated by the program RV (Wallace & Clayton 1996). In the majority of cases the LSR velocity of the stars were calculated from the positions of strong stellar lines such as Si II 3852 Å or Si III 4552 Å and these are given in Fig. 3.

Distance estimates have been calculated using the spec-

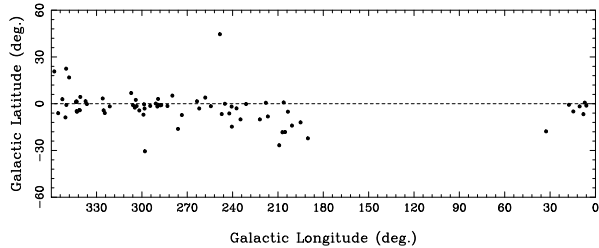


Figure 1. Galactic location of the stellar sample in latitude and longitude.

troscopic parallax equations given in DiPas & Savage (1994). Absolute magnitudes have been estimated from the spectral type and these estimates are based on data from Schmidt-Kaler (1982) and have random errors of some 25 per cent. Reddenings have been estimated using the observed $(B - V)$ colour in combination with the colours and spectral types from stars taken from Wegner (1994). We note that especially for mid O-type stars, the absolute magnitudes from Schmidt-Kaler (1982) are systematically fainter than in, for example, Wegner (2000), although show better agreement with the estimates from Vacca, Garmany & Shull (1996). The Schmidt-Kaler (1982) magnitudes are chosen as these cover all of our spectral types with the exception of WR stars, whose distances we have obtained from the literature. We find that agreement between the Hipparcos stellar parallax distance (obtained from the SIMBAD database, operated at CDS, Strasbourg, France) and our spectroscopic distances are better than 20 per cent for luminosity class V objects. For luminosity class III objects the stellar and spectroscopic distance estimates can differ by as much as a factor of two. There are no luminosity class I or II objects in our sample within 300 pc and so this relationship cannot be tested for the highest luminosity class objects. We have decided to adopt the spectroscopic distance estimates for all the stars to maintain consistency.

In Table 2 we also list the height, z , of the star relative to the plane of the Galaxy ($z = d_{\text{spec}} \times \sin(b)$). In Figs. 1 and 2 we present a plot of the Galactic location of the field stars. The majority of the stars lie close to the Galactic plane and have Galactic longitudes in the range $l = 270 - 360^\circ$.

3 DATA ANALYSIS

The spectra presented in this paper are the merged versions of the POP survey available on-line at <http://www.eso.org/uvespop>. No further data processing was undertaken. The following sections detail the methods used to analyse the reduced data.

3.1 The spectra

Spectra for the three species were normalised in the region of the interstellar lines by fitting a low order polynomial to the continuum using the spectrum analysis program DIPSO (Howarth et al. 2003). It should be noted that both the Na I UV doublet and the Ti II line lie well within the Free Spectral Range of the CCD and so problems with order-merging will not affect the spectra. The Ca II K line lies closer to the

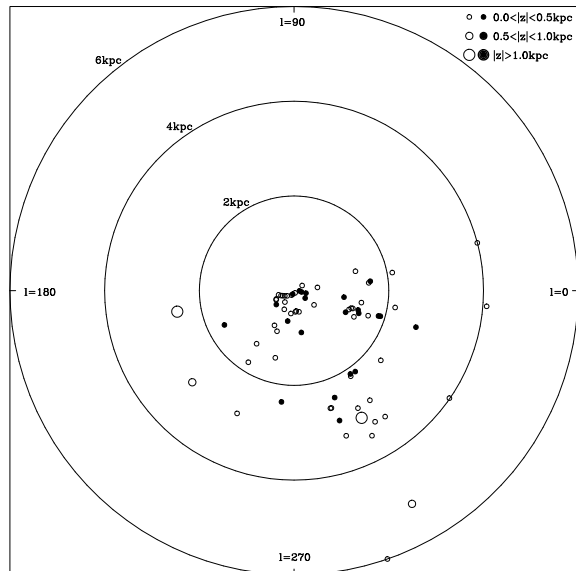


Figure 2. Heliocentric Galactic location of the stellar sample projected onto the Galactic plane. Filled circles are stars above the plane of the Galaxy and open circles are stars below the plane of the Galaxy.

edge of an echelle order, although no obvious problems were visible in the spectra due to order-merging. The online table of wavelength ranges effected by flattening artefacts has also been checked, and none of the species studied fall in effected regions.

In Fig. 3 we present the spectra for Na I UV, Ti II and Ca II K for each line-of-sight. Note that we have plotted the two lines of the Na I UV doublet on the same figure, to allow for an easy comparison, and hence only the feature at 3302.37 \AA is in the LSR. Therefore one must add -55.3 km s^{-1} to the velocity of the line at 3302.97 \AA in order to correct it to the kinematical LSR rest frame. We also plot the extent of the full width half maximum (FWHM) of the stellar line, centred on the LSR velocity of the star. The LSR velocity and FWHM of the stellar lines were estimated by Gaussian fitting using the Emission Line Fitting suite (ELF) within DIPSO. We generally fitted the stellar lines of the Si II doublet at 3853 \AA or the Si III triplet at 4552 \AA to determine these values. In some cases we were unable to estimate the FWHM due to the stellar lines being merged into the continuum. We therefore approximated the FWHM of the stellar line as the $v \sin i$ value for the star, taken from the literature for the following stars; HD 148184 (Krelowski, Schmidt & Snow, 1997), HD 52918 (Goraya & Tur, 1988), HD 58978 (Mennickent et al., 1994), HD 67536 (Grady, Bjorkman & Snow, 1987), HD 88661 (Ballereau, Chauville & Zorec, 1995), HD 45725 (Slettebak, 1982), HD 143275 (Hurwitz & Bowyer, 1996), HD 148937 and HD 164794 (Penny, 1996). For the Wolf-Rayet stars we have generally been unable to detect stellar lines with certainty and have not found $v \sin i$ values from the literature. Hence we have not plotted the extent of the stellar line. We have estimated the LSR velocity of these stars from the hydrogen emission lines and this is listed with the plot for these stars in Fig. 3.

It can be seen that in almost all cases the stellar contam-

Table 2. The stellar sample and basic parameters. Distances for the majority of the stars were calculated spectroscopically and errors are of the order of 25 per cent, excluding systematic errors (see Sect. 2). For some objects the distance was taken from the literature, references to which are given at the bottom of the table.

Star	l (deg.)	b (deg.)	Sp. type	m_v (mag.)	$(B - V)$ (mag.)	$E(B - V)$ (mag.)	d (pc)	z (pc)
HD 164794	6.01	-1.21	O4V f,el	5.93	0.00	0.00	1585 ¹	-33
HD 163800	7.05	0.69	O7III f	7.01	0.31	0.60	1621	19
HD 170235	7.95	-6.73	B2V n,el	6.59	0.07	0.28	501	-58
HD 167264	10.46	-1.74	B0.5Ia/Iab	5.35	0.00	0.20	2109	-64
HD 171432	14.62	-4.98	B1/B2Iab	7.11	0.15	0.32	4014	-348
HD 169454	17.54	-0.67	B1Ia el	6.65	0.74	0.93	1359	-15
HD 188294	32.65	-17.77	B8V d	6.44	-0.02	0.09	212	-64
HD 30677	190.18	-22.22	B1II/III n	6.84	-0.02	0.17	2707	-1023
HD 36861	195.05	-11.99	O8III f el	3.30	0.18	0.45	347	-72
HD 37490	200.73	-14.03	B3III el	4.57	-0.11	0.05	304	-73
HD 43285	203.42	-5.13	B6V el	6.05	-0.11	0.03	265	-23
HD 36646	205.31	-18.17	B4V n	6.63	-0.12	0.04	437	-136
HD 48099	206.21	0.80	O7V f,el	6.37	-0.08	0.21	1640	22
HD 37055	207.04	-18.34	B3IV v	6.41	-0.12	0.04	449	-141
HD 33328	209.14	-26.69	B2IV n,el,BCep	4.25	-0.18	0.01	251	-112
HD 45725	216.66	-8.21	B3V el	4.60	-0.10	0.08	184	-26
HD 52918	218.01	0.61	B1V bCep	4.99	-0.20	0.03	477	5
HD 46185	221.97	-10.08	B2/B3II?	6.79	-0.16	-0.02	2937	-514
HD 58343	231.09	-0.21	B2V n,el	5.20	-0.04	0.17	309	-1
HD 50896	234.76	-10.08	WN5 wr	6.74	-0.06	0.17	1393 ²	-243
HD 58978	237.41	-3.00	B1II el	5.61	-0.13	0.06	1796	-93
HD 49131	240.50	-14.73	B2III	5.80	-0.19	0.00	870	-221
HD 61429	240.65	-1.84	B8IV v	4.70	-0.11	-0.01	108	-3
HD 58377	242.20	-6.26	B5IV	6.81	-0.17	-0.02	448	-48
HD 64972	245.09	-0.02	B8 p (B6 II)	7.18	-0.11	-0.05	2858	0
HD 60498	247.20	-6.64	B4III	7.35	-0.12	0.03	936	-108
HD 90882	248.41	44.59	B9.5V	5.18	-0.04	0.01	112	78
HD 68761	254.37	-1.62	B0.5III	6.53	-0.09	0.13	1473	-41
HD 74966	258.08	3.93	B4IV	7.43	-0.14	0.01	658	45
HD 72067	262.08	-3.08	B2V n,el	5.83	-0.16	0.05	488	-26
HD 76341	263.54	1.52	O9Ib el	7.17	0.22	0.49	2365	62
HD 76131	273.58	-7.27	B6III	6.69	-0.05	0.08	453	-57
HD 67536	276.11	-16.14	B2.5V n	6.24	-0.09	0.12	450	-125
HD 89587	279.83	5.19	B3III	6.87	-0.13	0.03	900	81
HD 88661	283.08	-1.48	B2IV el	5.76	-0.12	0.08	458	-11
HD 92740	287.17	-0.85	WN7A wr	6.42	0.08	0.08	2600 ¹	-38
HD 93131	287.67	-1.08	WN6A wr	6.48	-0.03	0.08	2600 ¹	-49
HD 94910	289.18	-0.69	B2 pe wr	7.09	0.49	0.08	6000 ³	-72
HD 96917	289.28	3.06	O8.5Ib v	7.11	0.05	0.32	2910	155
HD 94963	289.76	-1.81	O6.5III f,el	7.14	-0.10	0.19	3257	-102
HD 97253	290.79	0.09	O5.5III f,cl,el	7.11	0.15	0.45	2415	3
HD 100841	294.47	-1.40	B9III d	3.12	-0.04	0.03	52	-1
HD 29138	297.99	-30.54	B1Iab	7.19	-0.09	0.10	3530	-1793
HD 105071	298.24	-3.09	B6Ia/Ib	6.31	0.13	0.19	3482	-187
HD 106068	298.51	-0.41	B8Ia/Ib	5.95	0.23	0.26	2824	-20
HD 105056	298.94	-7.05	ON9.7Ia pv,el	7.42	0.09	0.26	5184 ¹	-636
HD 109867	301.71	-4.35	B1Ia v	6.26	0.00	0.19	3264	-247
HD 112272	303.49	-1.50	B0.5Ia v	7.39	0.64	0.84	2168	-56
HD 112842	304.06	2.48	B4IV	7.08	0.15	0.25	2126	91
HD 113904	304.68	-2.49	WC5/B0Ia wr	5.69	-0.11	0.11	2817	-122
HD 115363	305.88	-0.97	B1Ia	7.82	0.50	0.69	3282	-55
HD 115842	307.08	6.83	B0.5Ia el	6.04	0.21	0.41	2157	256
HD 136239	321.23	-1.75	B1.5Ia v	7.87	0.77	0.94	2350	-71
HD 143448	324.55	-5.97	B3IV el	7.10	0.00	0.16	520	-54
HD 142758	325.31	-4.28	B1.5Ia v	7.08	0.14	0.31	4000	-298
HD 137753	325.93	3.34	B7IV	6.70	-0.03	0.09	282	16
HD 148937	336.37	-0.22	O6.5 pn,el	6.77	0.24	0.09	1380 ¹	-5
HD 148379	337.25	1.58	B1.5Ia el	5.36	0.44	0.61	1180	32
HD 148688	340.72	4.35	B1Ia el	5.33	0.27	0.46	1452	110
HD 154811	341.06	-4.22	OC9.7Ib	6.93	0.40	0.46	1230 ⁴	-90

Table 2. *ctd.*

Star	l (deg.)	b (deg.)	Sp. type	m_v (mag.)	$(B - V)$ (mag.)	$E(B - V)$ (mag.)	d (pc)	z (pc)
HD 154873	341.35	-4.11	B1Ib d	6.70	0.28	0.47	1654	-118
HD 156575	342.94	-5.16	B1.5III	7.35	0.15	0.35	1267	-113
HD 156385	343.16	-4.76	WC7 wr	6.92	0.05	0.35	1300 ⁵	-107
HD 151932	343.22	1.43	WN7A wr	6.49	0.23	0.35	1413 ¹	35
HD 152235	343.31	1.10	B1Ia el	6.34	0.42	0.61	1861	35
HD 152003	343.33	1.41	O9.7Iab v	6.99	0.29	0.53	2687	66
HD 152270	343.49	1.16	WC7 wr	6.60	0.23	0.53	1900 ⁶	38
HD 145482	348.12	16.84	B2V	4.57	-0.15	0.06	268	77
HD 157038	349.95	-0.79	B1/B2Ia d	6.41	0.64	0.81	1444	-19
HD 143275	350.10	22.49	B0.2IV	2.29	-0.09	0.14	173	66
HD 163745	350.56	-8.79	B5II	6.50	-0.09	-0.01	2189	-334
HD 155806	352.59	2.87	O7.5V el	5.61	-0.06	0.23	1064	53
HD 163758	355.36	-6.10	O6.5Ia f	7.32	0.02	0.34	4103	-436
HD 148184	357.93	20.68	B2V n,el	4.28	0.31	0.52	122	43

Reference codes: (1) Diplas & Savage (1994), (2) Fruscione et al. (1994), (3) Hoekzema, Lamers & van Genderen (1993), (4) Winkler (1997), (5) Conti & Vacca (1990), (6) Conti et al. (1983).

ination of the interstellar line is minimal, since the stellar feature is sufficiently broad to merge into the continuum or has been easily removed through the normalisation process. In cases where some stellar contribution is evident, this was fitted using ELF and the column density was calculated in the IS fitting process within DIPSO. Hence when we fit the interstellar components the stellar contribution was removed. It should be noted that stellar contamination is usually only seen in the Ca II K line. In cases where it was not possible to easily fit the stellar line, i.e. when it is of a similar width to the interstellar profile and hence causes significant contamination, we have not calculated column densities for the components, but we have listed the velocities of each component in Table 3.

The high S/N of our data means that we detect interstellar Ca II in every one of our spectra and Ti II in all but one. Even in this case, the Ti II spectrum towards HD 90882 does indeed show some evidence for absorption, although we have chosen not to fit this as it is close to the noise level. The S/N ratio of this Ti spectrum (190) is somewhat lower than the mean for Ti (300), and the star is also one of the closest in our sample at $d=112$ pc, with an upper limit to the column density of $\sim 1.2 \times 10^{11} \text{ cm}^{-2}$ (Sect.3.2 and Sect.3.3). We have fewer detections in the Na I UV lines, with 15 sightlines showing no interstellar Na I absorption and upper limits to the column density have been calculated along these sightlines.

3.2 Equivalent Width Measurements and upper limits

The equivalent width (EW), FWHM and the central velocity (v) of each component of each interstellar line were measured by fitting Gaussian profiles to the normalised spectra using the line fitting suite of programs ELF. The equivalent widths and the velocities for each interstellar component are listed in Table 3 along with their errors. The errors in equivalent width are based on the 3σ errors in column density as described in Sect.3.5. Errors in the velocities were taken from ELF. In order to check their reliability, test data at S/N ra-

tios of 200 and 400 were created with different b -values and the estimated errors compared with the known values for the centres of the lines. Agreement was found to be excellent between the calculated error and known position of the lines.

The determination of upper limits in the case of non-detections is non-trivial. Non-detections were estimated using a velocity width and a 3σ cutoff derived from the S/N ratio. Clearly, the non-detections have an unknown velocity width, and often lie in between other detected components. Hence the following scheme was adopted. If the undetected component c_{undet}^2 lies in the middle of three detected components in another species c_{detet}^1 , c_{detet}^2 , c_{detet}^3 of velocities v_{detet}^1 , v_{detet}^2 , v_{detet}^3 , the lower-velocity limit was set at $v_{\text{detet}}^2 - ((v_{\text{detet}}^2 - v_{\text{detet}}^1)/2.0)$ and the upper velocity limit at $v_{\text{detet}}^2 + ((v_{\text{detet}}^3 - v_{\text{detet}}^2)/2.0)$. In the cases where there were more than one species detected in for example component 3, the average of these velocities was taken for v_{detet}^3 . We stress that due to the unknown b -value of the undetected components, the upper limits may not be reliable.

3.3 Column Density Measurements - Component fitting

The Gaussian velocity dispersion parameter, b , and the column density, N , were initially estimated based on the FWHM and the EW of each of the individual components as measured using ELF. Values of b were determined to be $0.6006 \times \text{FWHM}$ of the profile, corrected for instrumental broadening. The column density was initially derived from the equation:

$$N(\text{cm}^{-2}) = 1.13 \times 10^{17} \times \frac{EW(\text{m}\text{\AA})}{f \times \lambda^2(\text{\AA})}, \quad (1)$$

where λ is the rest wavelength of the line and f is the oscillator strength (e.g. Vergely et al. 2000). Oscillator strengths and rest wavelengths were taken from Morton (2003, 2004).

Eq. 1 assumes that the medium is optically thin, which, while a reasonable approximation for the Na I UV interstellar line doublet at 3302 Å, and to a lesser extent for Ti II

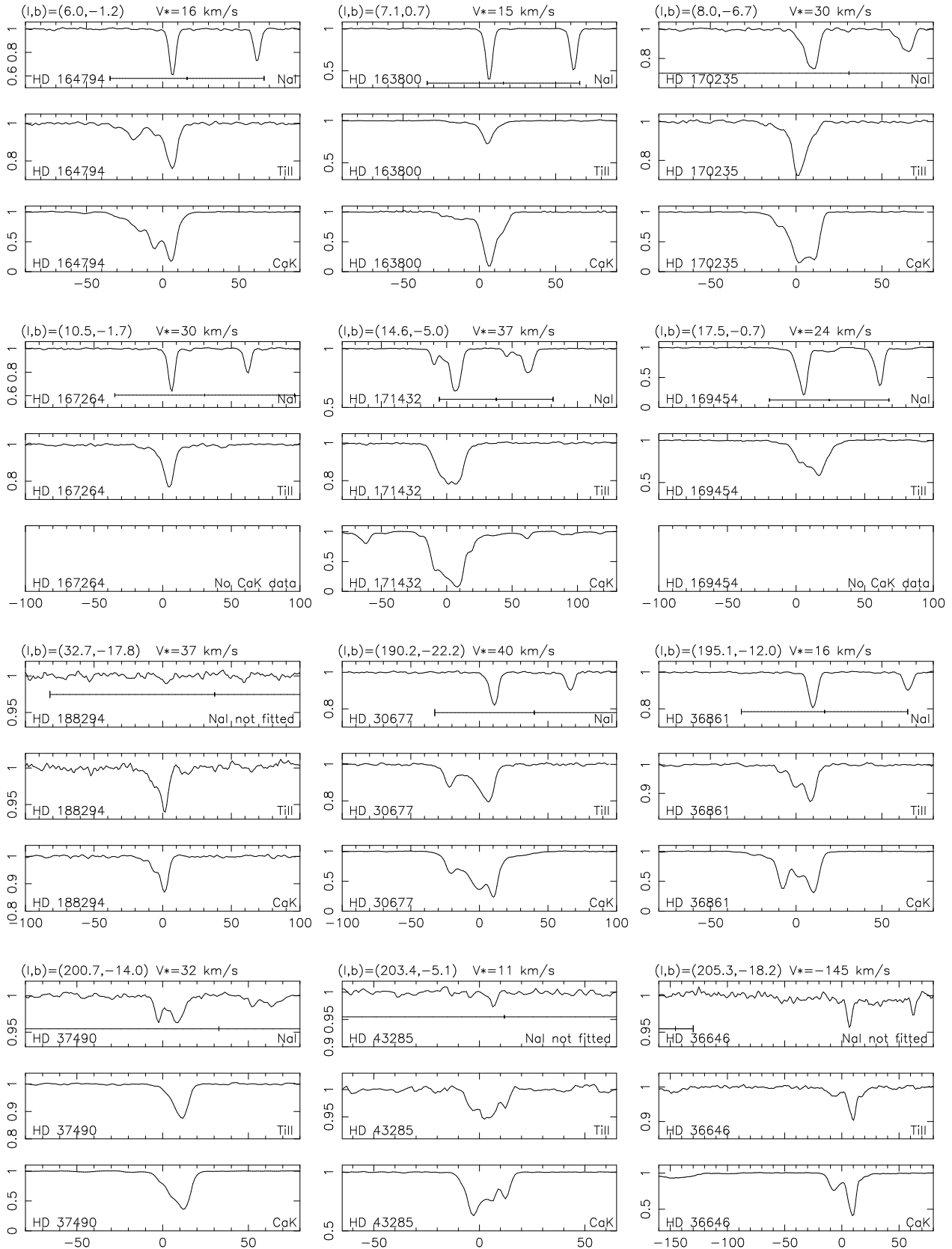


Figure 3. The interstellar Na I UV (3302.37Å), Ti II (3383.76Å) and Ca II K (3933.66Å) absorption profiles along each line-of-sight. The abscissa is the kinematic LSR velocity in km s^{-1} and the ordinate is the normalised flux. Note that the two lines of Na I UV have been plotted on the same figure, and a correction of -55.3 km s^{-1} should be added to the weaker line at 3302.98Å to move it to a LSR velocity. The horizontal bars indicate the extent of the FWHM of a stellar line and the stellar velocity is marked in the centre of each line. V_* is the stellar velocity in the LSR.

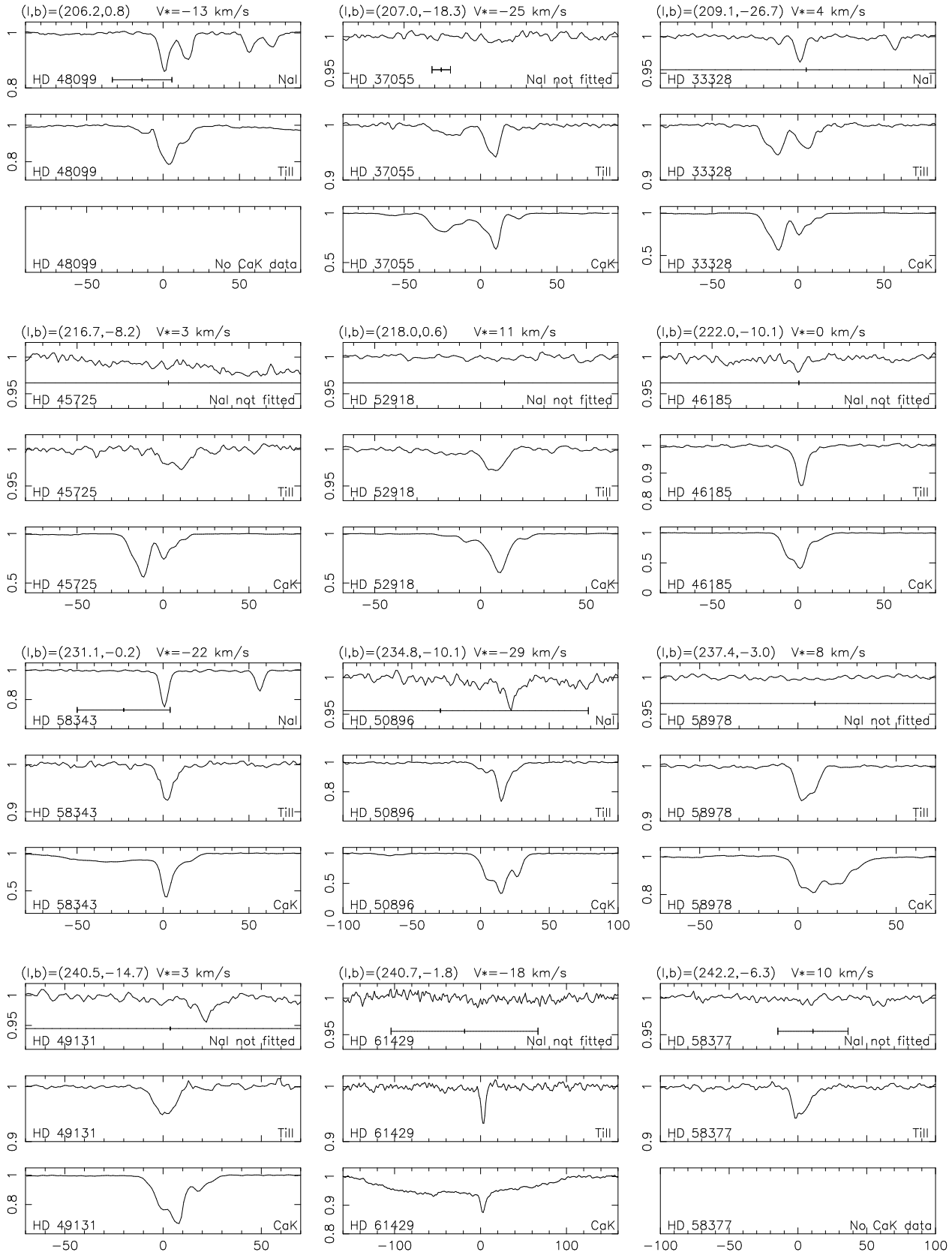


Figure 3. *ctd.*

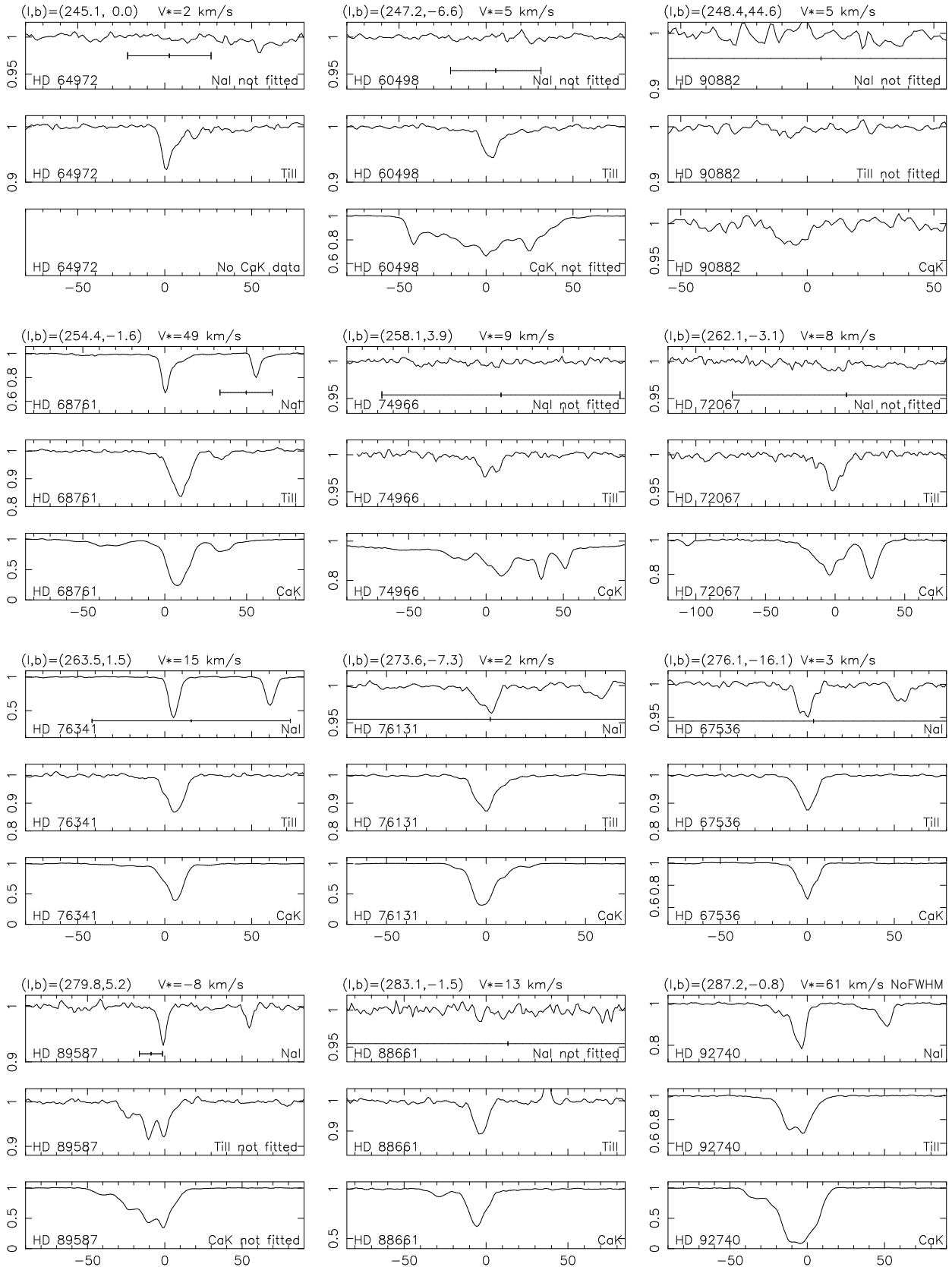


Figure 3. *ctd.*

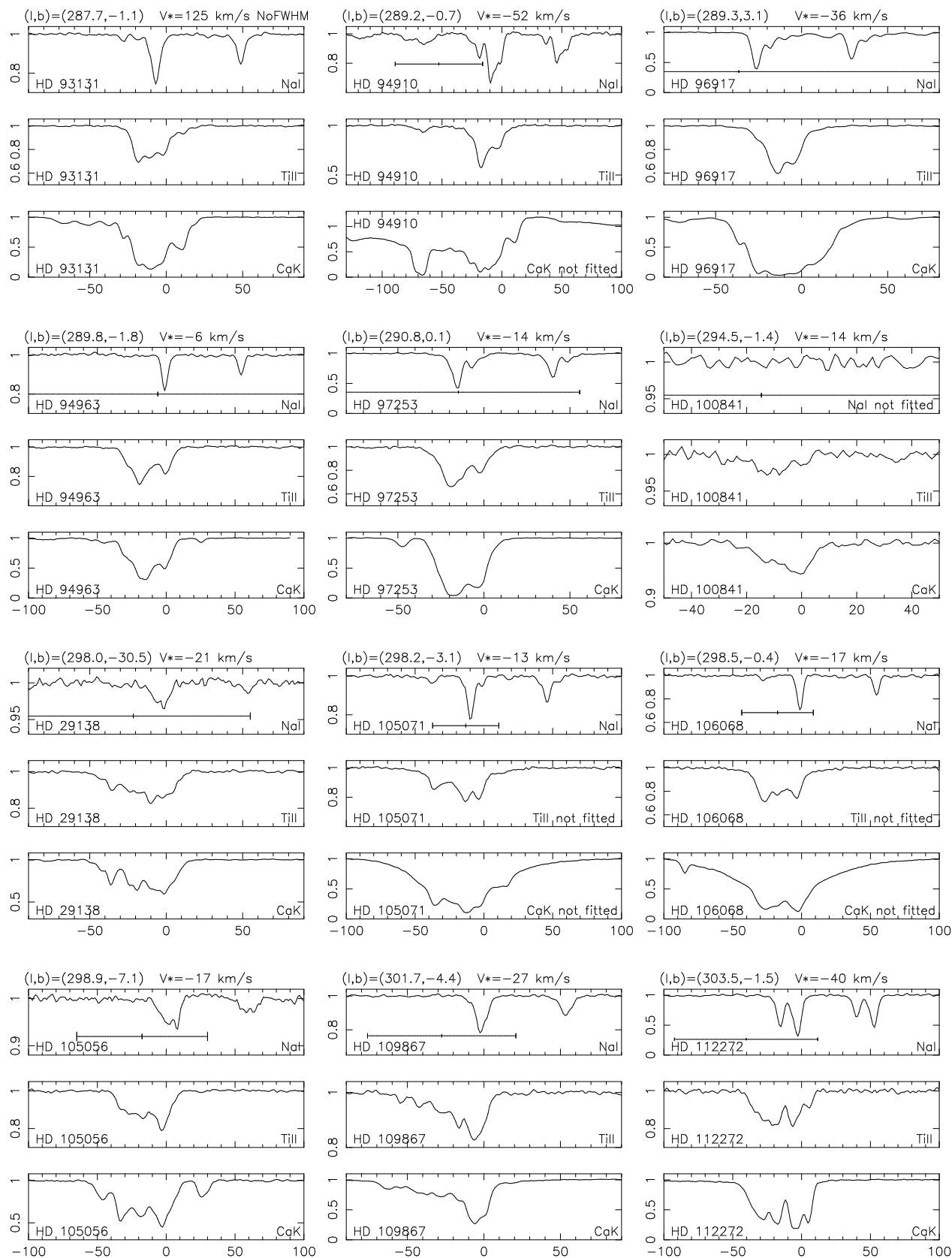


Figure 3. *ctd.*

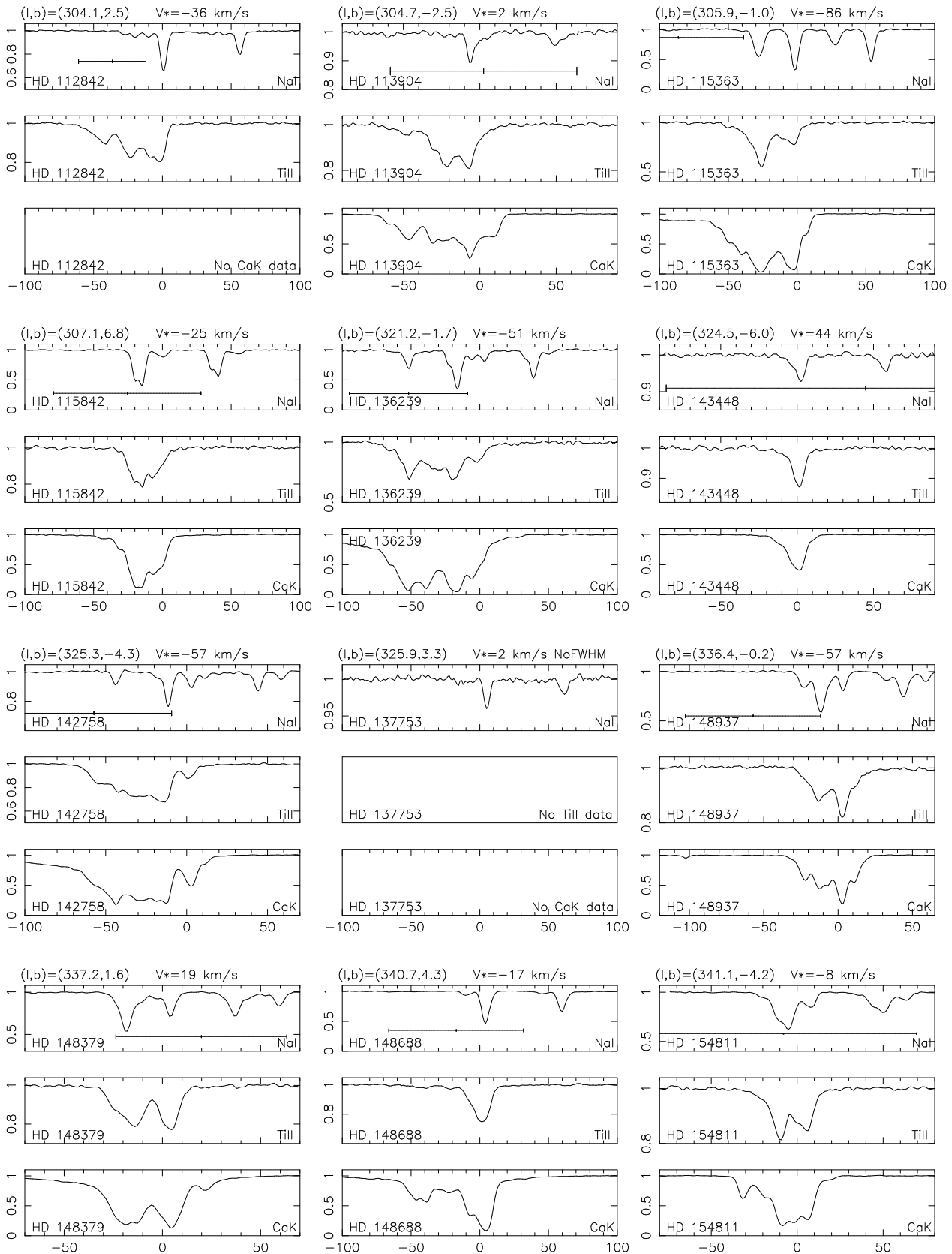


Figure 3. *ctd.*

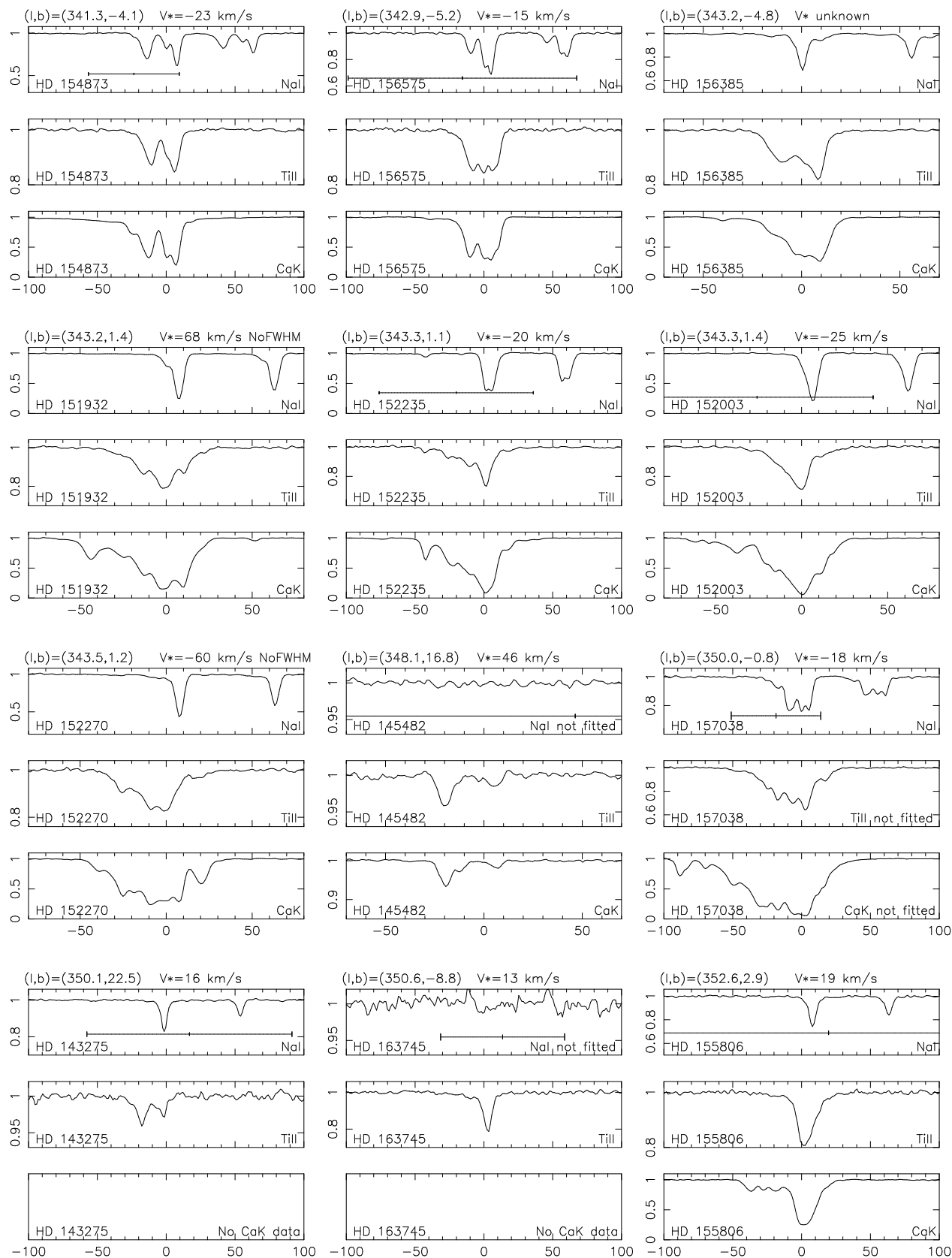
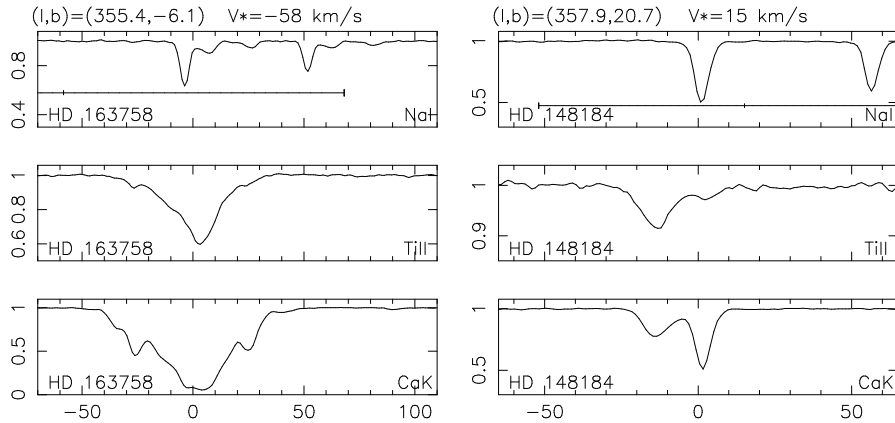


Figure 3. *ctd.*

Figure 3. *ctd.*

3383 Å is a poor assumption for Ca II 3933 Å. Nevertheless, this method was useful in gaining initial estimates of the column density for each component. The IS suite of programs within DIPSO was then used to refine the column density, and in some cases the b -values of the individual components. In every case the theoretical interstellar spectrum generated by the IS program was in excellent agreement with the observed one.

The upper limits to the column density for each component was estimated using the upper limits to the EW (see Sect. 3.2) and Eq. 1 and are given in Table 3.

3.4 Column Density Measurements - Apparent optical depth method

We have also calculated the total column density by the apparent optical depth (AOD) method. In this, the observed interstellar line profiles are converted first to AOD and then to apparent column density by integrating across the line profile. The method and its accuracy are described in detail in Savage & Sembach (1991). In Table 4 we present the total column density, derived by both component fitting and by the AOD method for each interstellar line observed along each line-of-sight. Where a stellar line was fitted, as discussed in Section 3.1, the column density of this line was subtracted from the total derived by the AOD method. In Fig. 4 we present plots comparing the column density derived by profile fitting and the AOD method. It can be seen that the scatter in the plots is minimal especially in the case of Ti and Ca. We also see that at higher column densities, the profile fitting and AOD methods are in better agreement for Ti and Ca. It should be noted that in the profile fitting and the AOD methods we have used the same baseline fit. We note that each of the lines in the Na I doublet were measured independently.

3.5 Uncertainty in individual cloud column densities

From the instrumental FWHM resolution, $\Delta\lambda_{\text{inst}}$, and the S/N ratio of the spectra, we can calculate the smallest equivalent width, EW_{lim} , of an unresolved feature that we would expect to see at the 3σ level by the relationship:

$$EW_{\text{lim}} = 3 \times \Delta\lambda_{\text{inst}} (S/N)^{-1}.$$

Using this, we find that EW_{lim} for Na I UV, Ti II and Ca II are 0.45 mÅ, 0.39 mÅ and 0.33 mÅ, respectively and this is in reasonable agreement with the smallest interstellar features we have actually measured, see Table 3. Converting the calculated EW_{lim} to a column density using Eq. 1, we find that we should be able to observe changes of 0.10 dex, 0.10 dex and 0.05 dex in the column density of an individual component for Na, Ti and Ca respectively, where these values have been calculated for a component with an EW of the mode of the EW's given in Table 3. This agrees with the observations and errors estimates for the column densities of individual components given in Table 3. The error estimates in the b -values and column densities for each component were derived as follows. For each detected component of each species, the column density was increased, in steps of one per cent between 1 and 15 per cent and in steps of five between 15 and 100 per cent, leaving the other components in the best-fit model constant, until the peak residual (in the data–model fit) exceeded 3σ . The difference between the column density of the fit at the 3σ level for this component and the best-fit column density, was taken to be the uncertainty. An identical procedure was performed to estimate the b -value errors. Where no 3σ limit was found, the error was set to be 95 per cent of the observed profile. This occurs in the case of weak features where we may be fitting noise. Finally, errors in the equivalent widths were derived from the errors in the column density measurements using Eq. 1.

3.6 Uncertainty in total column densities

In this section we estimate the uncertainties in the column densities, by comparing the total value derived from the stronger and weaker lines in the Na and Ca doublets. In the case of Ca this allows us to take into account all sources of error, for example in the continuum fit. For the Na lines the baseline fit is not independent. In Fig. 5 we plot the total column density derived from each line of the Na I UV doublet and, in general, there is excellent agreement between the total column density of each line, from which we can deduce the accuracy of our base-line fitting and column density measurements. The few discrepant cases can normally be accounted for by noise features affecting weak detections, saturation affecting strong detections, and in one

Table 3. Component table. Velocities are in the LSR. ‘Vel. Range’ is the velocity range over which upper limits were estimated.

Star name	Cmp. Num	v	Na I (3302.37)			log(N)	v	Na I (3302.98)			log(N)	v	Ti II (3383.76)			log(N)	v	Ca II (3393.66)			Vel. Range
			b	EW				b	EW				b	EW				b	EW		
HD 164794	1	-	-	<2.3	<12.41	-	-	<2.3	<12.71	-	-	<2.0	<10.74	-51.0±0.6	3.4±2.9	2.7±1.1	10.60±0.15	-57.7 -41.1			
HD 164794	2	-	-	<2.4	<12.42	-	-	<2.4	<12.73	-31.2±0.6	3.2±3.1	1.7±1.2	10.69±0.22	-	-	<1.9	<10.35	-41.1 -24.0			
HD 164794	3	-	-	<1.8	<12.31	-	-	<1.8	<12.61	-18.7±0.2	5.6±1.3	10.2±2.2	11.47±0.08	-14.7±0.4	2.3±0.5	6.0±1.1	11.04±0.05	-24.0 -10.9			
HD 164794	4	-	-	<1.4	<12.18	-	-	<1.4	<12.48	-4.6±0.7	3.9±1.6	5.4±1.5	11.21±0.10	-5.7±0.5	3.2±0.2	21.3±2.6	11.80±0.02	-10.9 -1.1			
HD 164794	5	-	-	<0.8	<11.94	-	-	<0.8	<12.25	-	-	<0.7	<10.27	2.9±1.5	8.5±0.5	76.3±5.6	11.96±0.03	-1.1 4.6			
HD 164794	6	6.5±0.4	1.9±0.4	22.8±2.2	13.54±0.03	6.7±0.3	1.8±0.4	15.6±1.4	13.63±0.03	5.9±0.8	4.5±0.4	24.2±1.8	11.85±0.03	5.7±0.5	2.7±0.3	37.7±5.6	12.14±0.02	4.6 11.7			
HD 163800	1	-	-	<0.6	<11.84	-	-	<0.6	<12.14	-	-	<0.5	<10.15	-23.8±0.1	0.4±0.4	3.3±0.4	10.61±0.05	-24.6 -18.6			
HD 163800	2	-	-	<1.3	<12.15	-	-	<1.3	<12.46	-14.8±0.9	5.5±4.4	2.9±1.2	10.90±0.15	-12.3±1.4	8.4±0.3	26.1±1.3	11.52±0.02	-18.6 -6.4			
HD 163800	3	1.2±0.3	1.8±1.7	1.5±0.8	12.24±0.18	0.1±0.2	1.3±1.7	0.6±0.6	12.15±0.29	-	-	<0.9	<10.37	0.6±0.4	5.0±0.1	6.7±1.4	11.55±0.02	-6.4 3.4			
HD 163800	4	6.4±0.3	1.8±0.7	35.5±2.8	13.83±0.02	6.8±0.3	1.7±0.5	28.5±2.0	13.97±0.02	5.3±0.5	2.8±0.3	11.4±1.1	11.61±0.03	6.3±0.5	2.8±0.5	113.2±11.1	12.44±0.02	3.4 6.0			
HD 163800	5	-	-	<0.4	<11.67	-	-	<0.4	<11.97	5.9±0.1	9.6±1.2	22.6±2.7	11.79±0.05	-	-	<0.8	<0.97	6.0 10.0			
HD 163800	6	-	-	<1.3	<12.16	-	-	<1.3	<12.46	-	-	<1.1	<10.47	14.2±0.5	4.1±0.1	29.0±1.1	11.75±0.01	10.0 22.4			
HD 170235	1	-	-	<1.0	<12.07	-	-	<1.0	<12.37	-17.8±0.2	1.0±1.0	0.5±0.4	10.10±0.29	-18.5±0.5	3.0±2.1	2.6±1.0	10.52±0.13	-22.1 -14.2			
HD 170235	2	-	-	<0.9	<12.01	-	-	<0.9	<12.32	-	-	<0.9	<10.99	-10.3±0.2	3.6±0.2	15.9±1.8	11.46±0.03	-14.2 -7.2			
HD 170235	3	-	-	<0.8	<11.95	-	-	<0.8	<12.25	-4.2±4.2	9.6±4.3	9.6±3.5	11.44±0.13	-	-	<0.9	<10.04	-7.2 -1.2			
HD 170235	4	-	-	<0.7	<11.90	-	-	<0.7	<12.20	1.0±0.3	3.0±0.4	14.9±1.7	11.69±0.04	2.4±0.9	5.5±0.2	158.4±12.5	12.49±0.02	-1.2 4.1			
HD 170235	5	8.0±0.1	5.0±0.5	25.0±2.5	13.46±0.04	5.3±0.3	4.5±2.5	5.0±1.8	13.07±0.13	6.4±1.1	5.6±1.1	12.6±2.0	11.58±0.06	-	-	<0.7	<0.92	4.1 8.8			
HD 170235	6	11.3±0.2	0.8±0.8	4.8±1.4	12.89±0.08	10.6±0.6	3.3±0.6	10.8±1.4	13.42±0.05	-	-	<1.5	<10.63	11.0±0.4	2.4±0.3	41.7±5.1	12.10±0.02	8.8 20.7			
HD 170235	7	30.5±0.2	1.0±1.0	0.7±0.4	11.92±0.20	-	-	<1.5	<12.54	-	-	<1.5	<10.62	-	-	<1.8	<10.33	20.7 32.5			
HD 167264	1	-	-	<1.7	<12.29	-	-	<1.7	<12.59	-13.8±0.8	4.8±4.6	2.1±1.1	10.76±0.19	-	-	-	-	-23.5 -5.6			
HD 167264	2	2.7±1.8	3.9±3.7	2.5±1.1	12.45±0.16	-	-	<1.0	<12.34	2.7±0.3	7.8±1.1	16.6±2.2	11.69±0.05	-	-	-	-	-5.6 4.4			
HD 167264	3	6.0±0.3	1.7±0.3	21.1±1.2	13.47±0.02	6.7±0.4	2.1±0.4	12.5±1.0	13.51±0.03	5.1±0.1	3.2±0.4	11.1±1.2	11.55±0.04	-	-	-	-	4.4 12.5			
HD 167264	4	19.1±0.4	1.5±1.5	1.0±0.7	12.06±0.22	18.3±0.3	1.5±1.5	0.6±0.6	12.14±0.29	19.0±0.5	2.9±2.7	0.9±0.8	10.41±0.27	-	-	-	-	12.5 31.2			
HD 167264	5	-	-	<1.8	<12.31	-	-	<1.8	<12.61	43.7±0.3	3.1±2.9	1.4±0.9	10.58±0.22	-	-	-	-	31.2 49.9			
HD 171432	1	-	-	<1.6	<12.27	-	-	<1.6	<12.57	-	-	<2.0	<10.74	-65.2±1.0	12.2±1.6	14.3±1.8	11.24±0.05	-89.7 -63.8			
HD 171432	2	-	-	<0.6	<11.81	-	-	<0.6	<12.11	-	-	<0.7	<10.28	-62.5±0.6	3.6±0.2	14.4±0.8	11.28±0.02	-63.8 -54.8			
HD 171432	3	-	-	<1.7	<12.28	-	-	<1.7	<12.58	-	-	<2.0	<10.75	-47.2±0.6	3.5±1.4	2.5±0.5	10.47±0.08	-54.8 -28.2			
HD 171432	4	-9.9±0.1	1.3±0.4	6.0±0.5	12.86±0.03	-9.6±0.2	0.4±1.3	2.4±0.5	12.75±0.08	-	-	<1.7	<10.68	-8.0±0.3	6.0±0.1	93.1±3.4	12.23±0.01	-28.2 -5.3			
HD 171432	5	0.5±1.6	8.4±0.9	15.4±1.5	13.25±0.04	-1.8±1.4	8.3±2.0	6.4±1.4	13.18±0.08	-3.7±1.2	7.3±0.4	26.3±2.1	11.90±0.03	-	-	<0.4	<0.69	-5.3 -0.2			
HD 171432	6	-	-	<0.3	<11.46	-	-	<0.3	<11.76	1.4±0.3	1.9±0.6	5.0±0.7	11.20±0.05	0.9±0.2	4.5±0.1	76.3±3.2	12.21±0.01	-0.2 3.9			
HD 171432	7	7.4±0.1	4.0±0.1	30.3±1.7	13.61±0.02	7.4±0.1	4.2±0.2	18.6±1.0	13.66±0.02	5.4±0.1	1.3±1.0	2.9±0.6	10.94±0.08	6.3±0.1	2.5±0.2	42.3±5.6	12.14±0.02	3.9 8.3			
HD 171432	8	-	-	<0.4	<11.61	-	-	<0.4	<11.91	9.4±0.3	4.6±0.3	19.4±1.6	11.78±0.03	10.5±0.4	2.1±0.6	55.5±7.7	12.28±0.02	8.3 14.0			
HD 171432	9	-	-	<0.8	<11.96	-	-	<0.8	<12.27	18.6±2.2	6.1±5.8	2.0±1.1	10.74±0.19	17.5±0.2	5.3±0.1	41.6±1.3	11.81±0.01	14.0 26.9			
HD 171432	10	-	-	<1.4	<12.18	-	-	<1.4	<12.49	-	-	<1.6	<10.65	35.8±2.5	14.9±1.3	21.3±2.2	11.42±0.04	26.9 48.4			
HD 171432	11	-	-	<1.8	<12.31	-	-	<1.8	<12.61	-	-	<2.2	<10.78	61.0±0.6	3.2±0.2	9.8±0.8	11.10±0.03	48.4 76.8			
HD 171432	12	-	-	<1.8	<12.30	-	-	<1.8	<12.60	-	-	<2.2	<10.77	92.6±0.5	7.0±0.8	8.9±1.1	11.04±0.05	76.8 105.0			
HD 171432	13	-	-	<1.1	<12.09	-	-	<1.1	<12.39	-	-	<1.3	<10.56	117.4±0.4	2.5±0.9	2.7±0.4	10.63±0.06	105.0 122.3			
HD 169454 ¹	1	-	-	<5.4	<12.79	-	-	<5.4	<13.09	-40.2±3.6	15.4±14.7	1.6±1.5	10.64±0.29	-	-	-	-	-71.1 -23.7			
HD 169454 ¹	2	-3.7±1.9	10.0±4.0	10.1±2.8	13.08±0.10	-7.3±0.5	2.8±9.5	1.2±1.0	12.43±0.26	-10.4±1.1	6.6±2.6	5.1±1.4	11.16±0.10	-	-	-	-	-23.7 -3.4			
HD 169454 ¹	3	0.8±0.4	2.2±0.3	14.8±1.4	13.34±0.03	0.0±0.4	2.6±0.5	8.7±1.2	13.36±0.05	-	-	<0.5	<10.14	-	-	-	-	-3.4 2.6			
HD 169454 ¹	4	5.8±0.4	2.3±0.7	53.5±8.0	14.10±0.03	5.9±0.4	2.2±0.4	43.7±3.3	14.20±0.02	2.9±0.3	5.2±0.2	31.6±1.6	11.97±0.02	-	-	-	-	2.6 7.1			
HD 169454 ¹	5	-	-	<0.6	<11.86	-	-	<0.6	<12.16	9.2±0.2	2.5±0.3	12.0±1.1	11.62±0.03	-	-	-	-	7.1 12.6			
HD 169454 ¹	6	16.2±0.6	3.1±1.7	3.7±1.2	12.64±0.12	16.3±0.6	3.7±2.9	1.4±1.2	12.51±0.26	15.7±0.3	4.0±0.2	31.5±2.0	12.06±0.02	-	-	-	-	12.6 20.0			
HD 169454 ¹	7	24.6±0.2	4.9±1.5	7.7±1.6	12.96±0.08	25.4±0.9	5.2±4.7	3.0±1.6	12.85±0.18	21.8±0.7	5.7±0.3	22.9±1.9	11.86±0.03	-	-	-	-	20.0 28.1			
HD 169454 ¹	8	-	-	<1.0	<12.07	-	-	<1.0	<12.37	32.3±0.4	2.5±2.1	1.9±0.7	10.72±0.13	-	-	-	-	28.1 37.3			
HD 188294	1	-	-	<1.0	<12.05	-	-	<1.0	<12.35	-	-	<0.9	<10.37	-13.0±0.5	3.0±2.8	1.3±0.7	10.19±0.18	-18.9 -8.8			
HD 188294	2	-	-	<0.8	<11.93	-	-	<0.8	<12.23	-4.0±1.0	6.8±2.7	3.7±1.2	11.02±0.12	-5.1±0.2	3.0±0.9	4.8±0.7	10.75±0.06	-8.8 -1.2			
HD 188294	3	-	-	<1.1	<12.09	-	-	<1.1	<12.39	2.6±0.2	2.3±0.8	3.2±0.5	10.96±0.06	1.8±0.1	3.0±0.3	11.3±0.9	11.15±0.03	-1.2 10.0			
HD 188294	4	-	-	<1.5	<12.22	-	-	<1.5	<12.52	17.8±0.7	3.5±3.4	0.8±0.6	10.35±0.25	-	-	<1.4	<10.22	10.0 24.9			
HD 30677	1	-	-	<0.6	<11.82	-	-	<0.6	<12.12	-22.0±0.3	3.1±0.6	6.4±1.0	11.27±0.06	-21.0±0.5	3.0±0.2	15.9±1.3	11.33±0.03	-27.6 -21.1			
HD 30677	2	-	-	<0.8	<11.95	-	-	<0.8	<12.26	-20.6±13.8	10.7±7.5	5.7±2.4	11.20±0.15	-	-	<0.8	<0.98	-21.1 -12.2			
HD 30677	3	-	-	<0.3	<11.53	-	-	<0.3	<11.83	-3.8±7.3	15.8±3.8	18.9±4.0	11.74±0.08	-	-	<0.3	<0.55	-12.2 -8.9			
HD 30677	4	-	-	<0.3	<11.47	-	-	<0.3	<11.77	-	-	<0.3	<0.93	-14.0±1.1	12.6±0.4	76.6±4.4	12.04±0.02	-8.9 -6.0			
HD 30677	5	3.5±0.4	2.0±1.9	1.1±0.6	12.12±0.18	-	-	<1.0	<12.37	2.0±1.1	5.2±1.0	10.3±1.3	11.48±0.05	0.6±0.2	7.8±0.1	106.5±3.9	12.29±0.01	-6.0 5.5			
HD 30677	6	-	-	<0.4	<11.67	-	-	<0.4	<11.97	8.0±0.4	3.6±0.4	11.5±1.3	11.56±0.04	9.9±0.3	2.0±0.4	19.7±2.8	11.84±0.02	5.5 10.0			
HD 30677	7	10.8±0.6	3.2±0.3	14.2±1.1	13.24±0.03	10.8±0.1	3.2±0.6	7.5±0.8	13.26±0.04	-	-	<0.6	<10.22	11.8±0.7	4.0±0.3	34.1±2.0	11.70±0.02	10.0 15.7			
HD 30677	8	-	-	<3.7	<12.62	-	-	<3.7	<12.92	-	-	<4.4	<11.08	20.3±1.2	18.4±1.3	42.3±4.4	11.73±0.04	15.7 57.0			

Table 3. *ctd.*

Star name	Cmp. Num	Na I (3302.37)				Na I (3302.98)				Ti II (3383.76)				Ca II (3393.66)				Vel. Range
		<i>v</i>	<i>b</i>	EW	log(<i>N</i>)	<i>v</i>	<i>b</i>	EW	log(<i>N</i>)	<i>v</i>	<i>b</i>	EW	log(<i>N</i>)	<i>v</i>	<i>b</i>	EW	log(<i>N</i>)	
HD 36861 ²	1	-	-	<0.9	<11.98	-	-	<0.9	<12.28	-	-	<0.9	<10.37	-25.2±0.2	1.0±1.0	1.9±0.6	10.36±0.12	-27.2 -16.9
HD 36861 ²	2	-	-	<0.7	<11.92	-	-	<0.7	<12.22	-9.2±0.2	1.7±1.6	1.6±0.5	10.63±0.13	-7.9±0.4	2.5±0.2	37.6±3.1	11.89±0.02	-16.9 -7.9
HD 36861 ²	3	-	-	<0.4	<11.63	-	-	<0.4	<11.93	-	-	<0.4	<10.02	-7.3±1.1	14.2±1.6	50.1±4.9	11.77±0.04	-7.9 -3.3
HD 36861 ²	4	-	-	<0.7	<11.89	-	-	<0.7	<12.19	-0.4±0.1	3.4±0.6	6.5±0.8	11.27±0.05	1.8±0.2	4.0±0.2	34.2±2.3	11.75±0.02	-3.3 5.1
HD 36861 ²	5	9.8±0.5	2.5±0.3	12.9±1.1	13.22±0.03	9.9±0.1	2.4±0.4	6.4±0.8	13.18±0.05	8.5±0.1	3.4±0.4	10.7±1.1	11.50±0.04	10.1±0.6	3.6±0.1	64.6±4.9	12.08±0.02	5.1 12.3
HD 36861 ²	6	-	-	<0.9	<12.00	-	-	<0.9	<12.30	15.0±0.7	4.0±3.8	0.2±0.2	9.70±0.29	-	-	<1.1	<10.10	12.3 23.0
HD 37490	1	-	-	<1.4	<12.21	-	-	<1.4	<12.51	-	-	<1.4	<10.58	-45.7±0.6	5.3±2.4	2.1±0.7	10.40±0.12	-56.2 -31.5
HD 37490	2	-	-	<1.2	<12.15	-	-	<1.2	<12.45	-	-	<1.2	<10.52	-17.3±0.5	5.3±1.9	2.7±0.7	10.51±0.10	-31.5 -19.0
HD 37490	3	-2.5±0.1	1.6±1.0	1.9±0.4	12.36±0.08	-2.8±0.3	2.3±1.5	0.9±0.4	12.32±0.16	-	-	<0.6	<10.20	-	-	<0.6	<9.84	-10.0 0.2
HD 37490	4	2.7±0.2	1.0±0.9	0.5±0.3	11.71±0.23	-	-	<0.3	<11.88	1.3±4.5	6.4±6.1	1.6±0.9	10.66±0.18	4.9±0.2	6.8±0.1	11.9±1.8	11.95±0.01	0.2 5.9
HD 37490	5	8.7±0.2	4.5±1.3	3.6±0.7	12.62±0.08	8.0±0.5	4.7±4.3	1.4±0.7	12.51±0.18	7.8±1.1	4.9±0.7	6.6±0.8	11.28±0.05	10.8±0.6	3.0±0.1	84.5±1.1	11.75±0.01	5.9 11.2
HD 37490	6	-	-	<0.4	<11.67	14.6±0.9	0.6±0.0	0.2±0.0	11.59±0.00	12.4±0.3	3.5±0.4	7.5±0.8	11.34±0.04	13.8±0.1	3.0±0.1	26.5±1.0	11.70±0.01	11.2 18.4
HD 43285	1	-	-	<1.5	<12.21	-	-	<1.5	<12.52	-	-	<1.2	<10.51	-6.3±0.9	5.2±1.6	6.0±1.3	10.86±0.08	-16.8 -4.9
HD 43285	2	-	-	<0.7	<11.88	-	-	<0.7	<12.18	-3.9±0.3	2.1±2.0	1.9±0.8	10.72±0.15	-2.8±0.1	3.3±0.1	32.9±1.9	11.67±0.02	-4.9 0.6
HD 43285	3	-	-	<1.0	<12.04	-	-	<1.0	<12.34	3.9±0.3	4.8±1.7	5.9±1.5	11.21±0.10	5.4±0.2	3.5±0.2	22.9±1.3	11.51±0.02	0.6 8.5
HD 43285	4	-	-	<0.7	<11.92	-	-	<0.7	<12.22	12.4±0.2	0.8±0.8	1.5±0.6	10.60±0.15	12.5±0.1	1.3±0.3	13.3±0.7	11.26±0.02	8.5 14.5
HD 36646 ¹	1	-	-	<0.9	<12.01	-	-	<0.9	<12.31	-6.7±1.2	7.0±3.5	3.6±1.3	11.00±0.13	-7.7±0.3	4.4±0.3	20.5±1.1	11.44±0.02	-18.6 -3.6
HD 36646 ¹	2	-	-	<0.4	<11.63	-	-	<0.4	<11.93	-	-	<0.5	<10.14	0.0±6.5	9.0±0.5	24.5±1.9	11.49±0.03	-3.6 2.7
HD 36646 ¹	3	-	-	<0.3	<11.51	-	-	<0.3	<11.81	5.3±0.6	1.3±1.2	1.5±0.5	10.61±0.12	<9.85	-	<0.6	<9.85	2.7 7.4
HD 36646 ¹	4	-	-	<0.3	<11.88	-	-	<0.3	<11.85	9.9±0.6	3.6±0.5	6.3±0.7	11.27±0.04	8.9±0.1	3.2±0.1	50.8±1.8	11.95±0.01	7.4 13.0
HD 36646 ¹	5	-	-	<0.2	<11.45	-	-	<0.2	<11.75	17.0±1.6	9.2±8.8	0.3±0.0	9.85±0.29	16.0±1.8	10.4±1.2	13.8±1.7	11.22±0.05	13.0 17.1
HD 36646 ¹	6	-	-	<0.3	<11.54	-	-	<0.3	<11.85	17.7±0.3	2.3±1.8	1.6±0.6	10.65±0.13	-	-	<0.7	<9.89	17.1 22.3
HD 48099	1	-	-	<1.5	<12.23	-	-	<1.5	<12.53	-12.4±0.2	6.1±1.5	5.8±1.2	11.21±0.08	-	-	-	-	-24.6 -6.3
HD 48099	2	0.7±0.1	3.1±0.4	9.9±1.1	13.09±0.04	0.7±0.1	2.7±0.8	4.4±0.7	13.01±0.06	-1.9±0.2	2.1±0.5	5.4±0.5	11.19±0.04	-	-	-	-	-6.3 2.6
HD 48099	3	6.0±0.7	3.7±2.6	2.4±0.9	12.44±0.13	6.1±0.6	3.6±3.5	1.6±0.8	12.55±0.18	4.2±0.2	4.8±0.3	22.4±1.2	11.84±0.02	-	-	-	-	2.6 10.3
HD 48099	4	15.6±0.1	3.8±0.5	8.8±1.1	13.01±0.05	15.7±0.2	3.6±1.3	4.2±0.8	12.97±0.08	14.4±0.3	4.9±0.5	9.7±1.0	11.45±0.04	-	-	-	-	10.3 23.5
HD 37055 ²	1	-	-	<1.5	<12.23	-	-	<1.5	<12.53	-13.4±0.5	1.0±1.0	0.2±0.2	9.83±0.29	-12.5±0.6	6.5±0.5	15.6±1.3	11.21±0.04	-20.5 -3.8
HD 37055 ²	2	-	-	<1.1	<12.08	-	-	<1.1	<12.38	5.8±0.7	4.0±1.2	4.0±0.8	11.06±0.08	4.7±0.2	6.9±0.2	30.6±1.7	11.62±0.02	-3.8 7.9
HD 37055 ²	3	-	-	<0.9	<11.99	-	-	<0.9	<12.30	10.6±0.3	2.0±1.1	2.4±0.5	10.83±0.08	10.4±0.4	2.2±0.2	20.6±1.2	11.47±0.02	7.9 17.6
HD 37055 ²	4	-	-	<1.3	<12.17	-	-	<1.3	<12.47	-	-	<1.0	<10.45	24.7±0.2	3.7±0.7	5.7±0.7	10.84±0.05	17.6 32.1
HD 33328	1	-	-	<0.5	<11.77	-16.2±0.6	7.2±0.0	0.8±0.8	12.30±0.29	-17.4±0.7	3.9±1.4	3.0±0.6	10.93±0.08	-18.9±0.1	2.2±0.2	8.9±0.5	11.11±0.02	-26.4 -14.4
HD 33328	2	-11.2±0.2	1.0±1.0	0.4±0.3	11.71±0.22	-	-	<0.4	<11.97	-11.0±0.6	3.4±0.8	3.9±0.6	11.05±0.06	-11.8±0.7	4.0±0.1	51.1±1.4	11.86±0.01	-14.4 -5.1
HD 33328	3	1.1±0.1	2.3±0.8	2.2±0.5	12.41±0.08	1.0±0.1	2.2±1.5	1.2±0.4	12.47±0.12	2.4±1.3	4.8±1.4	3.6±0.8	11.01±0.08	0.0±0.4	2.2±0.1	17.1±0.5	11.38±0.01	-5.1 3.7
HD 33328	4	-	-	<0.2	<11.43	-	-	<0.2	<11.73	7.2±0.3	2.0±1.5	1.5±0.5	10.62±0.12	5.4±0.6	3.6±0.2	12.3±0.6	11.20±0.02	3.7 9.1
HD 33328	5	10.6±0.3	1.0±1.0	0.3±0.2	11.48±0.20	-	-	<0.3	<11.79	13.2±0.3	0.8±0.8	0.5±0.3	10.13±0.22	12.2±0.6	3.3±0.6	4.3±0.5	10.71±0.05	9.1 15.4
HD 45725	1	-	-	<0.9	<12.03	-	-	<0.9	<12.33	-	-	<0.8	<10.35	-3.2±0.4	3.0±0.7	4.3±0.7	10.71±0.06	-9.2 -0.4
HD 45725	2	-	-	<0.7	<11.92	-	-	<0.7	<12.22	1.7±0.8	4.5±4.3	2.0±1.0	10.75±0.18	3.1±0.2	2.8±0.2	11.4±0.6	11.15±0.02	-0.4 6.5
HD 45725	3	-	-	<0.8	<11.95	-	-	<0.8	<12.25	11.0±0.6	3.8±3.0	2.4±1.0	10.82±0.15	10.9±0.2	2.8±0.2	9.3±0.7	11.06±0.03	6.5 13.8
HD 45725	4	-	-	<0.8	<11.94	-	-	<0.8	<12.24	18.1±0.1	0.8±0.8	0.4±0.4	10.03±0.29	16.0±0.7	3.1±0.8	4.6±0.6	10.75±0.05	13.8 21.0
HD 52918	1	-	-	<1.4	<12.20	-	-	<1.4	<12.51	-14.1±1.0	9.8±9.3	1.4±1.4	10.60±0.29	-16.0±0.9	5.1±2.0	3.1±0.8	10.57±0.10	-29.9 -10.8
HD 52918	2	-	-	<0.8	<11.97	-	-	<0.8	<12.27	-	-	<0.7	<10.28	-6.5±0.4	2.3±0.5	5.6±0.6	10.85±0.04	-10.8 0.3
HD 52918	3	-	-	<1.0	<12.07	-	-	<1.0	<12.37	6.5±0.2	5.8±2.1	3.8±1.0	11.01±0.10	7.7±0.1	7.3±0.2	40.2±2.1	11.71±0.02	0.3 14.2
HD 52918	4	-	-	<0.8	<11.95	-	-	<0.8	<12.25	-	-	<0.7	<10.26	21.3±0.3	1.7±0.8	2.7±0.4	10.62±0.06	14.2 24.8
HD 46185	1	-	-	<1.1	<12.08	-	-	<1.1	<12.38	-1.6±2.6	5.6±3.1	3.4±1.2	10.98±0.13	-5.3±0.7	4.0±0.1	41.1±1.2	11.79±0.01	-13.1 -0.8
HD 46185	2	-	-	<0.6	<11.80	-	-	<0.6	<12.10	2.1±0.2	2.4±0.5	8.2±0.9	11.39±0.04	1.5±0.5	3.2±0.1	51.4±1.8	11.95±0.01	-0.8 5.6
HD 46185	3	-	-	<1.4	<12.18	-	-	<1.4	<12.48	8.2±4.1	5.4±5.1	2.3±1.2	10.80±0.18	10.7±1.1	6.3±0.4	20.7±1.0	11.39±0.02	5.6 21.1
HD 58343 ³	1	0.8±0.4	2.0±0.2	15.2±1.2	13.29±0.03	0.8±0.3	2.1±0.5	8.2±0.9	13.31±0.04	1.9±0.3	3.2±1.3	3.5±1.0	11.02±0.10	1.6±0.4	2.5±0.2	35.0±2.8	11.84±0.02	-3.6 3.2
HD 58343 ³	2	-	-	<2.2	<12.39	-	-	<2.2	<12.70	3.3±0.7	7.3±3.6	4.9±1.7	11.13±0.13	7.0±0.2	10.8±0.7	39.0±2.9	11.68±0.03	3.2 23.2
HD 50896	1	-	-	<5.7	<12.80	-	-	<5.7	<13.10	-	-	<5.5	<11.18	-65.0±0.6	9.6±4.8	7.5±2.6	10.94±0.13	-84.2 -32.9
HD 50896	2	-	-	<3.9	<12.64	-	-	<3.9	<12.94	-0.8±0.7	4.3±2.6	3.6±1.3	11.00±0.13	-	-	<3.8	<10.64	-32.9 2.3
HD 50896	3	-	-	<0.9	<11.99	-	-	<0.9	<12.29	5.0±0.5	3.0±1.3	4.0±1.1	11.05±0.10	5.7±0.2	5.4±0.2	58.3±3.7	11.96±0.02	2.3 10.1
HD 50896	4	-	-	<0.6	<11.81	-	-	<0.6	<12.11	14.8±0.2	0.8±0.8	3.7±1.0	11.29±0.06	-	-	<0.6	<9.81	10.1 15.2
HD 50896	5	-	-	<0.4	<11.63	-	-	<0.4	<11.93	16.1±0.6	5.1±0.6	21.2±2.0	11.76±0.04	15.2±0.1	4.2±0.2	78.6±5.5	12.13±0.02	15.2 18.7
HD 50896	6	22.0±0.3	2.7±1.9	2.6±1.0	12.50±0.13	21.5±0.5	2.7±2.6	1.0±0.9	12.38±0.26	-	-	<0.6	<10.19	-	-	<0.6	<9.82	18.7 23.9
HD 50896	7	-	-	<1.2	<12.14	-	-	<1.2	<12.44	25.7±1.4	5.0±2.2	5.0±1.6	11.14±0.12	26.5±0.1	4.0±0.2	41.5±2.5	11.79±0.02	23.9 35.0

Table 3. ctd.

Star name	Cmp. Num	v	Na I (3302.37)			v	Na I (3302.98)			v	Ti II (3383.76)			v	Ca II (3393.66)			Vel. Range
			b	EW	log(N)		b	EW	log(N)		b	EW	log(N)		b	EW	log(N)	
HD 58978	1	-	-	<0.5	<11.76	-	-	<0.5	<12.06	1.7±0.3	2.8±0.5	4.2±0.5	11.08±0.05	1.8±0.2	3.3±0.2	12.2±0.6	11.19±0.02	-4.4 4.8
HD 58978	2	-	-	<0.5	<11.72	-	-	<0.5	<12.02	7.8±0.3	3.3±0.8	3.7±0.6	11.02±0.06	8.1±0.2	2.9±0.2	10.1±0.5	11.13±0.02	4.8 13.3
HD 58978	3	-	-	<0.2	<11.42	-	-	<0.2	<11.72	-	-	<0.2	<9.80	18.7±0.8	14.3±0.9	35.6±2.6	11.63±0.03	13.3 17.6
HD 58978	4	-	-	<0.1	<11.04	-	-	<0.1	<11.34	-	-	<0.1	<9.42	16.5±0.5	2.9±0.7	3.5±0.6	10.64±0.06	17.6 19.4
HD 58978	5	-	-	<0.5	<11.72	-	-	<0.5	<12.02	-	-	<0.4	<10.10	22.2±0.5	2.8±0.8	3.1±0.5	10.59±0.06	10.4 27.8
HD 49131	1	-	-	<1.3	<12.17	-	-	<1.3	<12.47	0.9±0.2	6.8±0.7	7.6±0.9	11.31±0.05	0.9±0.2	6.5±0.1	37.3±1.0	11.70±0.01	-12.4 4.4
HD 49131	2	-	-	<0.6	<12.15	-	-	<0.6	<12.15	-	-	<0.4	<10.00	7.9±0.1	2.6±0.1	20.8±0.6	11.45±0.01	4.4 12.5
HD 49131	3	-	-	<0.6	<11.81	-	-	<0.6	<12.11	-	-	<0.3	<9.96	17.0±0.8	3.3±0.2	8.4±0.4	11.02±0.02	12.5 19.9
HD 49131	4	-	-	<0.9	<12.03	-	-	<0.9	<12.33	-	-	<0.6	<10.18	22.7±2.7	4.7±0.6	5.3±0.5	10.80±0.04	19.9 32.1
HD 61429 ³	1	-	-	<0.8	<11.94	-	-	<0.8	<12.25	3.1±0.1	2.5±1.0	4.5±0.9	11.11±0.08	2.6±0.2	2.5±0.5	5.1±0.5	10.81±0.04	-2.1 5.4
HD 61429 ³	2	-	-	<0.8	<11.97	-	-	<0.8	<12.27	-	-	<0.8	<10.36	8.0±1.2	2.7±2.6	1.1±0.5	10.09±0.18	5.4 13.4
HD 58377	1	-	-	<0.2	<11.33	-	-	<0.2	<11.63	-2.1±0.1	0.4±0.4	1.0±0.5	10.50±0.15	-	-	-	-	-2.9 0.1
HD 58377	2	-	-	<0.5	<11.73	-	-	<0.5	<12.03	2.3±1.1	6.7±1.6	6.6±1.4	11.27±0.08	-	-	-	-	0.1 7.6
HD 58377	3	-	-	<1.3	<12.16	-	-	<1.3	<12.46	12.9±1.2	7.4±7.0	1.0±1.0	10.46±0.29	-	-	-	-	7.6 27.7
HD 64972	1	-	-	<0.7	<11.88	-	-	<0.7	<12.18	0.6±0.3	2.4±0.7	4.8±0.8	11.16±0.06	-	-	-	-	-4.2 3.8
HD 64972	2	-	-	<0.7	<11.90	-	-	<0.7	<12.20	7.0±0.7	3.6±2.2	2.6±0.9	10.87±0.13	-	-	-	-	3.8 12.1
HD 64972	3	-	-	<0.8	<11.94	-	-	<0.8	<12.24	17.3±0.3	2.0±1.8	1.3±0.6	10.56±0.16	-	-	-	-	12.1 21.2
HD 60498 ⁴	1	-	-	<0.8	<11.94	-	-	<0.8	<12.24	-	-	<0.6	<10.22	-41.2	-	-	-	-45.9 -36.2
HD 60498 ⁴	2	-	-	<0.5	<11.77	-	-	<0.5	<12.07	-	-	<0.4	<10.05	-31.2	-	-	-	-36.2 -29.6
HD 60498 ⁴	3	-	-	<0.8	<11.95	-	-	<0.8	<12.25	-	-	<0.6	<10.23	-28.1	-	-	-	-29.6 -19.8
HD 60498 ⁴	4	-	-	<1.0	<12.05	-	-	<1.0	<12.35	-	-	<0.8	<10.33	-11.4	-	-	-	-19.8 -7.3
HD 60498 ⁴	5	-	-	<0.6	<11.83	-	-	<0.6	<12.13	-	-	<0.5	<10.11	-3.3	-	-	-	-7.3 0.1
HD 60498 ⁴	6	-	-	<0.4	<11.69	-	-	<0.4	<12.00	2.4±0.2	4.6±1.1	4.9±1.0	11.13±0.08	4.6	-	-	-	0.1 5.6
HD 60498 ⁴	7	-	-	<0.3	<11.49	-	-	<0.3	<11.80	7.7±1.3	31.9±30.3	5.9±4.8	11.21±0.26	-	-	-	-	5.6 9.1
HD 60498 ⁴	8	-	-	<0.3	<11.53	-	-	<0.3	<11.83	10.5±0.8	4.8±4.6	0.6±0.6	10.22±0.29	-	-	-	-	9.1 12.9
HD 60498 ⁴	9	-	-	<0.6	<11.80	-	-	<0.6	<12.10	-	-	<0.4	<10.08	15.3	-	-	-	12.9 19.9
HD 60498 ⁴	10	-	-	<0.8	<11.95	-	-	<0.8	<12.25	-	-	<0.6	<10.23	24.5	-	-	-	19.9 29.9
HD 60498 ⁴	11	-	-	<1.1	<12.11	-	-	<1.1	<12.41	-	-	<0.9	<10.39	35.3	-	-	-	29.9 44.3
HD 60498 ⁴	12	-	-	<1.1	<12.09	-	-	<1.1	<12.39	-	-	<0.9	<10.37	53.4	-	-	-	44.3 58.1
HD 90882	1	-	-	<4.1	<12.66	-	-	<4.1	<12.97	-	-	<4.4	<11.08	-6.0±0.5	7.2±6.8	5.1±2.9	10.79±0.19	-10.2 8.4
HD 68761 ^{5,6}	1	-	-	<2.0	<12.35	-	-	<2.0	<12.65	-	-	<2.0	<10.75	-55.3±1.0	6.0±2.1	5.1±1.4	10.79±0.10	-67.3 -47.2
HD 68761 ^{5,6}	2	-	-	<1.3	<12.16	-	-	<1.3	<12.47	-	-	<1.3	<10.56	-39.2±1.0	6.0±0.5	15.7±1.6	11.28±0.04	-47.2 -34.0
HD 68761 ^{5,6}	3	-	-	<1.5	<12.24	-	-	<1.5	<12.54	-	-	<1.6	<10.64	-28.9±1.0	5.8±0.5	13.5±1.5	11.25±0.04	-34.0 -18.4
HD 68761 ^{5,6}	4	-	-	<1.4	<12.21	-	-	<1.4	<12.51	-8.0±2.4	6.4±6.1	1.3±1.2	10.54±0.29	-	-	<1.7	<10.29	-18.4 -3.9
HD 68761 ^{5,6}	5	0.2±0.3	1.6±0.3	14.4±1.4	13.33±0.03	0.3±0.3	1.5±0.4	10.2±0.9	13.43±0.03	-	-	<0.6	<10.21	-	-	<0.7	<9.89	-3.9 2.0
HD 68761 ^{5,6}	6	-	-	<0.3	<11.57	-	-	<0.3	<11.87	-	-	<0.3	<9.97	3.7±3.0	17.5±5.2	24.3±6.7	11.48±0.10	2.0 5.3
HD 68761 ^{5,6}	7	5.3±0.3	8.5±1.6	14.8±2.2	13.23±0.06	6.2±0.5	5.4±3.3	3.6±1.3	12.92±0.13	8.2±0.7	6.6±0.6	18.4±1.9	11.73±0.04	8.0±0.1	6.8±0.1	142.3±5.1	12.41±0.01	5.3 9.4
HD 68761 ^{5,6}	8	-	-	<1.4	<12.18	-	-	<1.4	<12.49	12.0±1.9	5.9±2.3	5.8±1.5	11.20±0.10	-	<1.6	<10.27	9.4 23.3	
HD 68761 ^{5,6}	9	-	-	<1.9	<12.33	-	-	<1.9	<12.63	34.0±0.3	4.6±2.8	3.1±1.1	10.94±0.13	35.1±0.2	6.8±0.3	33.2±1.8	11.64±0.02	23.3 42.7
HD 68761 ^{5,6}	10	-	-	<2.7	<12.49	-	-	<2.7	<12.79	-	-	<2.8	<10.89	50.8±1.7	9.8±3.4	7.2±1.9	10.93±0.10	42.7 70.4
HD 74966 ³	1	-	-	<0.8	<11.96	-	-	<0.8	<12.26	-	-	<1.1	<10.47	-19.7±0.9	5.0±1.5	3.9±0.8	10.67±0.08	-29.7 -16.3
HD 74966 ³	2	-	-	<0.4	<11.68	-	-	<0.4	<11.98	-	-	<0.6	<10.18	-12.8±0.4	2.3±0.9	2.5±0.5	10.49±0.08	-16.3 -9.3
HD 74966 ³	3	-	-	<0.4	<11.63	-	-	<0.4	<11.93	-5.8±0.5	3.0±2.8	0.6±0.6	10.23±0.29	-	<0.5	<9.78	-9.3 -3.0	
HD 74966 ³	4	-	-	<0.4	<11.68	-	-	<0.4	<11.98	-0.3±0.3	2.6±1.8	2.0±0.7	10.75±0.13	-	<0.6	<9.83	-3.0 4.0	
HD 74966 ³	5	-	-	<0.8	<11.97	-	-	<0.8	<12.27	7.2±0.3	2.5±2.4	1.6±0.7	10.65±0.15	9.3±0.1	9.3±0.6	25.6±1.4	11.55±0.02	4.0 17.7
HD 74966 ³	6	-	-	<0.8	<11.97	-	-	<0.8	<12.27	-	-	<1.1	<10.48	27.2±0.6	3.5±0.8	4.2±0.6	10.70±0.06	17.7 31.5
HD 74966 ³	7	-	-	<0.7	<11.90	-	-	<0.7	<12.20	-	-	<0.9	<10.41	35.7±0.1	2.7±0.2	11.9±0.7	11.21±0.02	31.5 43.1
HD 74966 ³	8	-	-	<0.9	<12.01	-	-	<0.9	<12.31	-	-	<1.2	<10.52	50.5±0.1	3.8±0.3	9.6±0.8	11.09±0.03	43.1 58.0
HD 72067 ⁷	1	-	-	<4.8	<12.74	-	-	<4.8	<13.04	-	-	<3.2	<10.95	-105.8±0.2	2.8±1.1	2.8±0.6	10.54±0.08	-111.3 -59.5
HD 72067 ⁷	2	-	-	<4.6	<12.72	-	-	<4.6	<13.02	-13.1±0.3	1.9±1.8	0.9±0.4	10.44±0.16	-	<5.0	<10.76	-59.5 -10.1	
HD 72067 ⁷	3	-	-	<0.4	<11.69	-	-	<0.4	<11.99	-	-	<0.3	<9.90	-6.9±0.5	12.7±0.8	37.1±2.9	11.68±0.03	-10.1 -5.4
HD 72067 ⁷	4	-	-	<0.2	<11.39	-	-	<0.2	<11.69	-4.2±4.5	4.2±3.1	1.9±0.8	10.72±0.15	-3.5±2.7	32.2±27.4	13.2±6.1	11.20±0.16	-5.4 -3.0
HD 72067 ⁷	5	-	-	<0.4	<11.70	-	-	<0.4	<12.00	-1.1±2.7	3.5±1.4	2.8±0.8	10.91±0.10	-3.4±0.2	2.7±0.6	5.9±0.8	10.89±0.05	-3.0 1.7
HD 72067 ⁷	6	-	-	<1.3	<12.17	-	-	<1.3	<12.48	5.5±1.5	3.8±2.3	2.0±0.7	10.75±0.13	5.8±0.2	3.1±0.9	4.2±0.9	10.70±0.08	1.7 15.9
HD 72067 ⁷	7	-	-	<1.9	<12.34	-	-	<1.9	<12.64	-	-	<1.3	<10.55	26.2±0.9	5.2±0.2	30.1±1.5	11.58±0.02	15.9 36.6

Table 3. ctd.

Star name	Cmp. Num	Na I (3302.37)				Na I (3302.98)				Ti II (3383.76)				Ca II (3393.66)				Vel. Range
		v	b	EW	log(N)	v	b	EW	log(N)	v	b	EW	log(N)	v	b	EW	log(N)	
HD 76341	1	-	-	<3.7	<12.62	-	-	<3.7	<12.92	-13.0±0.8	4.8±4.5	1.2±1.2	10.54±0.29	-14.0±3.3	19.6±5.9	20.3±5.2	11.37±0.10	-37.9 -7.9
HD 76341	2	-	-	<0.9	<12.03	-	-	<0.9	<12.33	-	-	<1.0	<10.43	-2.3±0.1	2.3±0.3	9.1±0.9	11.18±0.03	-7.9 -0.2
HD 76341	3	-	-	<0.5	<11.77	-	-	<0.5	<12.07	1.9±0.7	4.9±2.0	6.8±1.8	11.28±0.10	-	-	<0.4	<9.68	-0.2 4.0
HD 76341	4	5.2±0.6	3.2±0.2	45.4±5.2	13.88±0.02	5.3±0.5	2.9±0.2	30.7±1.9	13.96±0.02	7.9±0.5	4.9±0.9	11.7±1.9	11.55±0.06	6.3±0.8	4.8±0.1	83.2±5.3	12.12±0.02	4.0 15.2
HD 76341	5	-	-	<2.3	<12.42	-	-	<2.3	<12.72	-	-	<2.4	<10.82	24.3±0.9	5.1±3.0	3.7±1.3	10.64±0.13	15.2 34.5
HD 76131	1	-	-	<0.5	<11.79	-	-	<0.5	<12.09	-13.6±0.2	1.4±1.4	0.5±0.4	10.11±0.26	-14.1±0.4	2.6±0.6	4.3±0.6	10.73±0.05	-17.9 -8.5
HD 76131	2	-2.8±0.8	3.5±2.3	1.7±0.7	12.33±0.13	-4.2±0.6	3.4±3.3	1.1±0.6	12.42±0.18	-3.5±1.9	4.4±0.5	8.8±0.9	11.41±0.04	-2.0±0.1	5.7±0.0	110.2±4.0	12.30±0.01	-8.5 -0.3
HD 76131	3	3.1±0.5	2.2±1.4	1.8±0.5	12.33±0.10	2.7±0.4	2.9±2.3	1.5±0.6	12.54±0.15	1.5±0.9	3.0±0.4	6.6±0.7	11.29±0.04	-	-	<0.6	<9.85	-0.3 5.7
HD 76131	4	-	-	<0.6	<11.80	-	-	<0.6	<12.10	9.2±0.8	4.5±1.6	3.2±0.9	10.98±0.10	-	-	-	-	5.7 15.4
HD 76131	5	-	-	<0.8	<11.94	-	-	<0.8	<12.25	-	-	<0.9	<10.42	21.7±0.6	3.6±0.7	5.5±0.7	10.83±0.05	15.4 28.9
HD 67536	1	-	-	<0.9	<12.01	-	-	<0.9	<12.31	-	-	<0.9	<10.40	-14.3±0.5	2.9±2.7	1.2±0.5	10.17±0.15	-20.1 -8.9
HD 67536	2	-4.7±0.6	1.3±1.3	1.9±0.5	12.33±0.10	-4.0±0.5	2.3±1.3	1.6±0.7	12.55±0.15	-0.9±0.4	7.6±1.8	9.0±2.0	11.44±0.08	-4.0±0.5	3.6±0.2	16.2±0.9	11.34±0.02	-8.9 -0.5
HD 67536	3	-	-	<0.2	<11.28	-	-	<0.2	<11.58	-	-	<0.2	<9.67	-	-	<0.2	<9.30	-0.5 1.6
HD 67536	4	0.4±0.5	2.4±1.1	3.1±0.7	12.56±0.08	1.2±0.4	1.1±2.3	1.2±0.5	12.42±0.15	0.9±0.3	4.6±1.1	7.0±1.1	11.30±0.06	0.4±0.1	1.6±0.2	16.9±1.0	11.38±0.02	1.6 3.5
HD 67536	5	6.6±0.4	0.8±0.8	0.4±0.4	11.76±0.27	7.1±0.7	0.4±0.8	0.3±0.3	11.86±0.29	-	-	<0.4	<10.66	5.3±0.2	2.2±0.2	10.8±0.6	11.17±0.02	3.5 8.6
HD 89587 ^{4,6}	1	-	-	<0.9	<12.02	-	-	<0.9	<12.32	-	-	-	-	-	-	-	-	-44.8 -31.7
HD 89587 ^{4,6}	2	-	-	<0.8	<11.94	-	-	<0.8	<12.24	-24.8	-	-	-	-	-	-	-	-31.7 -21.0
HD 89587 ^{4,6}	3	-	-	<0.5	<11.72	-	-	<0.5	<12.02	-18.7	-	-	-	-	-	-	-	-21.0 -14.5
HD 89587 ^{4,6}	4	-	-	<0.6	<11.86	-	-	<0.6	<12.16	-10.2	-	-	-	-	-	-	-	-14.5 -5.5
HD 89587 ^{4,6}	5	-1.0±0.1	2.1±0.8	4.2±0.9	12.71±0.08	-0.8±0.2	1.7±1.5	2.0±0.7	12.70±0.12	-0.5	-	-	-	-	-	-	-	-5.5 3.2
HD 89587 ^{4,6}	6	-	-	<0.4	<11.63	-	-	<0.4	<11.94	7.0	-	-	-	-	-	-	-	3.2 8.5
HD 89587 ^{4,6}	7	-	-	<0.4	<11.70	-	-	<0.4	<12.00	-	-	-	-	-	-	-	-	8.5 14.7
HD 88661	1	-	-	<2.3	<12.42	-	-	<2.3	<12.72	-	-	<2.4	<10.82	-28.8±0.2	5.2±1.2	9.0±1.9	11.05±0.08	-39.2 -22.2
HD 88661	2	-	-	<1.6	<12.25	-	-	<1.6	<12.55	-15.6±0.4	1.1±1.0	0.9±0.8	10.41±0.27	-	-	<1.5	<10.24	-22.2 -10.7
HD 88661	3	-	-	<0.8	<11.97	-	-	<0.8	<12.27	-	-	<0.9	<10.37	-5.7±0.9	5.5±0.2	51.5±2.9	11.85±0.02	-11.7 -4.7
HD 88661	4	-	-	<0.6	<11.80	-	-	<0.6	<12.10	-3.3±0.1	5.2±1.2	12.3±2.6	11.55±0.08	-3.9±1.2	22.0±16.5	16.6±7.6	11.30±0.16	-4.7 -0.6
HD 88661	5	-	-	<0.7	<11.89	-	-	<0.7	<12.19	-	-	<0.7	<10.29	2.3±0.2	1.0±1.0	3.0±0.8	10.58±0.10	-0.6 4.3
HD 92740 ⁷	1	-	-	<1.6	<12.26	-	-	<1.6	<12.56	-	-	<1.9	<10.71	-33.9±1.0	6.2±0.4	26.9±1.3	11.55±0.02	-46.2 -27.7
HD 92740 ⁷	2	-20.7±0.4	2.0±1.3	2.5±0.6	12.45±0.10	-	-	<0.9	<12.29	-21.4±0.9	11.5±4.6	7.1±2.3	11.29±0.12	-22.2±0.9	5.1±0.2	30.4±1.8	11.66±0.02	-27.7 -17.7
HD 92740 ⁷	3	-15.2±0.2	1.2±1.0	2.9±0.6	12.54±0.08	-16.8±1.1	6.7±4.4	3.6±1.5	12.91±0.15	-11.8±0.9	5.2±0.2	29.1±1.6	11.97±0.02	-12.2±0.2	4.5±0.1	95.4±3.9	12.36±0.02	-17.7 -11.2
HD 92740 ⁷	4	-8.0±0.6	3.0±0.4	10.0±1.0	13.08±0.04	-8.8±0.3	2.1±1.2	2.7±0.7	12.80±0.10	-	-	<0.5	<10.17	-	-	<0.6	<9.83	-11.2 -5.8
HD 92740 ⁷	5	-3.0±0.4	2.3±0.3	11.7±1.0	13.18±0.03	-3.4±0.5	2.8±0.5	7.7±0.8	13.27±0.04	-2.4±0.8	4.6±0.2	30.6±1.7	11.99±0.02	-4.2±0.9	5.5±0.2	113.1±14.0	12.54±0.02	-5.8 1.1
HD 92740 ⁷	6	4.9±0.3	1.4±1.4	0.9±0.6	12.01±0.21	5.7±0.2	1.0±1.4	0.3±0.3	11.86±0.29	6.0±0.8	4.9±0.7	8.2±1.1	11.38±0.05	5.1±0.4	5.8±0.1	84.2±2.5	12.10±0.01	1.1 11.9
HD 93131 ⁷	1	-	-	<2.1	<12.38	-	-	<2.1	<12.68	-	-	<2.1	<10.77	-67.4±0.2	6.2±0.5	15.9±1.1	11.27±0.03	-79.7 -59.4
HD 93131 ⁷	2	-	-	<1.6	<12.25	-	-	<1.6	<12.55	-	-	<1.6	<10.64	-51.4±1.4	7.9±0.5	25.1±1.9	11.48±0.03	-59.4 -44.3
HD 93131 ⁷	3	-	-	<1.2	<12.13	-	-	<1.2	<12.44	-	-	<1.2	<10.53	-37.3±0.7	4.2±0.3	15.1±1.1	11.25±0.03	-44.3 -32.7
HD 93131 ⁷	4	-28.2±0.2	1.1±1.1	1.8±0.6	12.32±0.13	-27.8±0.4	1.4±1.1	0.9±0.6	12.32±0.22	-27.9±0.6	2.9±2.6	1.7±0.7	10.66±0.15	-28.2±0.3	1.9±0.1	20.2±1.3	11.49±0.02	-32.7 -23.2
HD 93131 ⁷	5	-18.5±0.3	3.7±3.4	2.2±0.9	12.41±0.15	-18.2±0.3	2.0±3.5	0.7±0.6	12.22±0.27	-18.7±0.3	3.7±0.2	27.0±1.5	11.93±0.02	-18.4±0.8	4.6±0.1	104.2±4.1	12.31±0.01	-23.2 -14.8
HD 93131 ⁷	6	-11.5±0.2	1.0±0.9	2.3±0.6	12.41±0.10	-12.4±0.2	1.0±0.9	0.9±0.6	12.32±0.21	-10.6±0.3	4.1±0.2	23.0±1.3	11.88±0.02	-10.4±0.7	4.2±0.1	67.1±9.1	12.33±0.02	-14.8 -9.0
HD 93131 ⁷	7	-6.8±0.4	2.3±0.3	16.0±1.4	13.33±0.03	-6.6±0.4	2.3±0.4	9.8±1.0	13.38±0.04	-	-	<0.5	<10.15	-	-	<0.6	<9.84	-9.0 -4.1
HD 93131 ⁷	8	-1.5±0.2	1.0±0.9	1.8±0.6	12.31±0.13	0.4±0.2	1.0±0.9	0.7±0.6	12.22±0.25	-2.1±0.3	4.5±0.3	24.8±1.3	11.88±0.02	-2.9±0.7	4.1±0.1	106.2±3.6	12.25±0.01	-4.1 2.2
HD 93131 ⁷	9	-	-	<0.6	<11.84	-	-	<0.6	<12.14	5.8±0.3	1.4±1.0	2.6±0.5	10.85±0.08	-	-	<0.7	<9.93	2.2 8.0
HD 93131 ⁷	10	-	-	<0.7	<11.89	-	-	<0.7	<12.19	11.3±0.2	2.4±0.7	4.5±0.7	11.09±0.06	9.1±1.7	5.4±0.1	71.9±2.5	12.10±0.01	8.0 14.6
HD 93131 ⁷	11	-	-	<0.7	<11.88	-	-	<0.7	<12.18	18.6±0.3	1.0±0.9	0.9±0.5	10.40±0.18	19.4±0.2	1.1±0.7	3.3±0.5	10.64±0.05	14.6 21.1
HD 94910 ⁴	1	-117.3±0.7	8.6±8.2	5.5±3.6	12.81±0.21	-	-	<5.7	<13.11	-	-	<5.5	<11.18	-	-	-	-	-134.6 -98.3
HD 94910 ⁴	2	-79.4±0.5	4.7±4.5	4.2±1.9	12.69±0.16	-	-	<4.1	<12.96	-	-	<4.0	<11.04	-	-	-	-	-98.3 -72.4
HD 94910 ⁴	3	-64.5±0.4	8.4±3.4	11.7±3.9	13.14±0.12	-	-	<4.2	<12.98	-66.2±0.3	7.0±3.5	8.4±3.0	11.38±0.13	-	-	-	-	-72.4 -45.7
HD 94910 ⁴	4	-25.1±0.6	3.3±2.1	4.7±1.7	12.74±0.13	-	-	<3.7	<12.92	-27.0±1.5	8.6±3.4	11.0±3.8	11.52±0.12	-	-	-	-	-45.7 -22.0
HD 94910 ⁴	5	-18.6±0.1	1.9±0.7	9.5±1.3	13.09±0.05	-18.5±0.2	1.6±1.5	3.9±1.3	12.96±0.12	-17.1±0.1	4.7±0.3	43.0±3.8	12.17±0.03	-	-	-	-	-22.0 -13.8
HD 94910 ⁴	6	-9.4±0.1	2.7±0.3	22.5±1.9	13.48±0.03	-9.8±0.3	1.8±0.7	9.2±1.6	13.38±0.06	-	-	<1.1	<10.49	-	-	-	-	-13.8 -6.6
HD 94910 ⁴	7	-2.4±0.4	3.5±0.7	17.0±2.3	13.32±0.05	-3.4±0.7	4.6±1.1	13.7±2.7	13.48±0.08	-4.7±0.2	7.6±0.7	37.2±4.0	12.06±0.04	-	-	-	-	-6.6 6.9
HD 96917	1	-	-	<4.1	<12.67	-	-	<4.1	<12.97	-	-	<3.5	<10.98	-70.8±0.3	9.8±1.2	17.8±2.3	11.34±0.05	-90.3 -54.3
HD 96917	2	-	-	<2.0	<12.35	-	-	<2.0	<12.65	-	-	<1.7	<10.66	-37.7±0.3	5.3±0.3	34.3±1.8	11.65±0.02	-54.3 -36.8
HD 96917	3	-	-	<0.7	<11.90	-	-	<0.7	<12.20	-	-	<0.6	<10.21	-35.9±0.2	1.4±0.4	9.0±1.6	11.42±0.03	-36.8 -30.6
HD 96917	4	-26.2±0.4	2.4±0.2	42.9±3.2	13.88±0.02	-26.3±0.4	2.5±0.2	28.8±1.8	13.94±0.02	-22.4±1.1	8.0±1.0	20.3±2.5	11.76±0.05	-26.6±0.1	4.0±0.3	97.5±11.1	12.44±0.02	-30.6 -21.0
HD 96917	5	-18.3±0.5	2.5±0.3	16.9±1.4	13.35±0.03	-18.3±0.1	3.0±0.6	10.8±1.1	13.41±0.04	-14.2±0.2	5.0±0.2	38.8±2.4	12.15±0.02	-15.9±1.2	7.0±0.5	158.7±40.6	12.82±0.03	-21.0 -13.3
HD 96917	6	-10.3±0.2	2.6±0.6	7.6±1.1	12.94±0.06	-9.7±0.2	2.3±1.3	3.9±1.0	12.94±0.10	-	-	<0.6	<10.24	-	-	<0.6	<9.81	-13.3 -6.7
HD 96917	7	-2.3±0.4	4.7±1.9	5.9±1.5	12.82±0.10	-2.2±0.5	3.5±3.3	2.5±1.1	12.75±0.16	-4.3±0.1	5.2±0.3	32.2±1.9	12.04±0.02	-4.9±0.1	6.0±0.4	140.8±17.3	12.63±0.02	-6.7 1.4
HD 96917	8	-	-	<1.0	<12.07	-	-	<1.0	<12.37	5.3±2.3	10.4±4.7	8.0±2.8	11.34±0.13	7.2±1.2	7.0±0.1	131.8±11.1	12.44±0.02	1.4 10.6
HD 96917	9	14.6±0.2	5.8±1.4															

Table 3. ctd.

Star name	Cmp. Num	NaI (3302.37)				NaI (3302.98)				TiII (3383.76)				CaII (3393.66)				Vel. Range
		ν	b	EW	log(N)	ν	b	EW	log(N)	ν	b	EW	log(N)	ν	b	EW	log(N)	
HD 94963	1	-	-	<4.2	<12.68	-	-	<4.2	<12.98	-	-	<2.7	<10.87	-89.0±1.8	10.4±4.2	6.9±2.2	10.90±0.12	-109.9 -71.5
HD 94963	2	-	-	<2.4	<12.44	-	-	<2.4	<12.74	-	-	<1.6	<10.63	-54.0±0.3	1.9±1.2	2.3±0.6	10.43±0.10	-71.5 -49.4
HD 94963	3	-	-	<1.5	<12.21	-	-	<1.5	<12.51	-	-	<1.0	<10.41	-44.8±0.9	5.6±0.6	11.6±1.1	11.14±0.04	-49.4 -36.2
HD 94963	4	-	-	<1.4	<12.20	-	-	<1.4	<12.50	-25.7±0.6	6.4±0.6	18.4±1.9	11.73±0.04	-29.6±0.2	4.6±0.2	32.0±1.8	11.64±0.02	-36.2 -23.5
HD 94963	5	-	-	<0.8	<11.97	-	-	<0.8	<12.27	-18.9±0.3	3.6±0.3	13.8±1.2	11.66±0.03	-19.9±0.9	5.5±0.2	65.9±0.0	12.09±0.02	-23.5 -15.9
HD 94963	6	-	-	<1.0	<12.06	-	-	<1.0	<12.36	-11.5±0.5	6.4±0.6	18.6±1.9	11.74±0.04	-13.4±0.2	5.7±0.1	82.5±2.8	12.14±0.01	-15.9 -6.6
HD 94963	7	-0.9±0.1	1.9±0.5	10.2±1.1	13.12±0.04	-0.8±0.1	1.6±0.7	5.5±0.9	13.12±0.06	-0.2±0.3	4.3±0.3	16.5±1.3	11.70±0.03	-1.3±0.9	5.3±0.1	70.5±2.2	12.04±0.01	-6.6 2.6
HD 94963	8	-	-	<1.4	<12.21	-	-	<1.4	<12.51	5.9±0.8	4.1±3.9	2.0±1.0	10.74±0.18	-	-	-	<10.19	2.6 15.7
HD 94963	9	-	-	<1.6	<12.24	-	-	<1.6	<12.54	-	-	<1.0	<10.44	25.4±0.2	2.2±0.5	5.3±0.6	10.79±0.05	15.7 29.8
HD 97253	1	-	-	<2.8	<12.50	-	-	<2.8	<12.80	-	-	<3.0	<10.91	-47.4±0.1	3.6±0.4	14.3±1.4	11.23±0.04	-54.6 -35.6
HD 97253	2	-28.7±0.6	3.1±2.9	2.3±1.3	12.44±0.19	-26.8±0.6	3.4±2.9	2.6±1.4	12.76±0.19	-20.1±0.7	4.3±0.6	17.9±3.1	11.85±0.05	-19.7±0.3	7.5±0.5	70.9±26.0	12.61±0.03	-35.6 -21.3
HD 97253	3	-19.6±0.4	2.3±0.7	10.5±1.6	13.09±0.06	-17.1±0.3	3.2±0.6	14.4±1.9	13.54±0.05	-19.5±1.6	12.2±2.9	33.6±6.8	11.97±0.08	-	-	<0.6	<0.81	-21.3 -16.6
HD 97253	4	-15.1±0.4	2.0±0.5	33.4±3.8	13.78±0.03	-14.6±0.1	1.2±0.8	13.4±2.0	13.67±0.04	-12.2±1.2	4.5±0.8	15.9±2.6	11.69±0.06	-15.9±0.2	4.5±1.1	185.4±26.3	12.40±0.05	-16.6 -10.7
HD 97253	5	-6.9±0.1	2.3±0.4	15.4±1.7	13.30±0.04	-7.1±0.1	1.5±0.8	7.1±1.1	13.24±0.06	-	-	<1.0	<10.42	-	-	<0.7	<0.92	-10.7 -4.6
HD 97253	6	-0.6±0.5	2.3±1.7	4.2±1.4	12.68±0.12	-2.3±0.5	3.1±2.6	3.6±1.5	12.90±0.15	-1.8±0.2	3.9±0.5	17.5±2.0	11.75±0.04	-3.9±0.2	5.8±0.2	98.3±11.9	12.47±0.02	-4.6 2.3
HD 97253	7	-	-	<1.6	<12.24	-	-	<1.6	<12.55	5.1±0.6	2.8±2.6	3.4±1.4	10.97±0.15	8.4±0.3	3.3±1.2	6.4±1.3	10.88±0.08	2.3 12.8
HD 100841	1	-	-	<0.7	<11.88	-	-	<0.7	<12.18	-27.9±0.1	0.8±0.8	0.6±0.6	10.23±0.29	-	-	<0.5	<0.77	-29.5 -25.4
HD 100841	2	-	-	<1.3	<12.17	-	-	<1.3	<12.47	-	-	<0.9	<10.41	-22.9±0.1	0.4±0.4	0.4±0.4	9.70±0.29	-25.4 -17.3
HD 100841	3	-	-	<1.9	<12.32	-	-	<1.9	<12.62	-11.0±0.5	7.5±6.4	4.4±2.0	11.10±0.16	-12.3±0.8	5.7±3.4	4.6±1.7	10.76±0.13	-17.3 -5.9
HD 100841	4	-	-	<2.0	<12.36	-	-	<2.0	<12.66	1.0±0.5	1.0±1.0	0.6±0.5	10.20±0.29	-1.1±0.5	5.8±2.0	8.0±2.2	10.99±0.10	-5.9 6.7
HD 29138 ⁸	1	-	-	<2.0	<12.35	-	-	<2.0	<12.65	-	-	<2.4	<10.82	-77.6±0.5	3.7±2.6	2.0±0.7	10.38±0.13	-85.0 -62.3
HD 29138 ⁸	2	-	-	<1.5	<12.24	-	-	<1.5	<12.54	-	-	<1.9	<10.71	-47.1±0.7	3.3±0.8	4.2±0.7	10.73±0.06	-62.3 -44.8
HD 29138 ⁸	3	-	-	<0.5	<11.76	-	-	<0.5	<12.06	-42.3±1.1	6.3±2.8	4.9±1.6	11.14±0.12	-42.6±0.2	1.0±0.6	4.8±0.6	10.88±0.04	-44.8 -39.0
HD 29138 ⁸	4	-	-	<0.5	<11.76	-	-	<0.5	<12.07	-34.8±0.5	3.2±0.8	6.5±1.0	11.28±0.06	-36.0±0.1	3.2±0.1	28.0±1.5	11.57±0.02	-39.0 -33.1
HD 29138 ⁸	5	-30.7±1.6	6.3±6.0	0.8±0.5	11.94±0.20	-	-	<0.5	<12.06	-	-	<0.6	<10.24	-	-	<0.6	<0.82	-33.1 -27.2
HD 29138 ⁸	6	-	-	<0.6	<11.79	-	-	<0.6	<12.09	-23.7±1.1	6.5±0.8	14.9±1.9	11.64±0.05	-23.7±0.2	4.5±0.1	33.4±1.9	11.68±0.02	-27.2 -20.9
HD 29138 ⁸	7	-	-	<0.6	<11.82	-	-	<0.6	<12.12	-17.6±0.4	2.1±1.1	3.3±0.7	11.00±0.08	-18.6±0.1	1.1±0.5	10.4±1.0	11.19±0.03	-20.9 -14.2
HD 29138 ⁸	8	-	-	<0.5	<11.76	-10.4±0.3	1.5±1.4	0.3±0.2	11.77±0.20	-10.9±2.7	3.3±0.5	9.5±1.0	11.46±0.04	-9.5±1.2	7.0±0.1	60.4±3.5	11.94±0.02	-14.2 -8.3
HD 29138 ⁸	9	-6.3±1.3	7.0±6.7	2.9±1.9	12.50±0.22	-	-	<0.4	<11.93	-	-	<0.5	<10.10	-	-	<0.4	<0.69	-8.3 -4.0
HD 29138 ⁸	10	-0.9±0.6	3.5±3.3	1.8±1.0	12.33±0.19	-1.7±0.5	2.8±3.3	1.0±0.9	12.37±0.26	-2.7±12.1	0.4±0.4	0.4±0.4	10.04±0.29	-1.6±0.2	3.4±0.2	18.0±1.1	11.45±0.02	-4.0 -1.5
HD 29138 ⁸	11	-	-	<0.3	<11.50	-	-	<0.3	<11.81	-1.3±16.6	8.5±0.8	25.6±2.5	11.86±0.04	-	-	<0.3	<0.57	-1.5 1.7
HD 29138 ⁸	12	-	-	<0.9	<11.99	-	-	<0.9	<12.29	5.2±3.5	0.8±0.8	0.7±0.6	10.27±0.26	4.4±0.2	6.1±0.2	34.3±1.8	11.65±0.02	1.7 11.7
HD 105071 ^{4,6}	1	-37.7±0.2	3.2±2.4	2.8±1.0	12.51±0.13	-36.9±0.4	1.0±3.0	1.0±0.7	12.36±0.22	-36.3	-	-	-	-35.8	-	-	-	-41.1 -33.0
HD 105071 ^{4,6}	2	-	-	<0.7	<11.88	-	-	<0.7	<12.19	-29.7	-	-	-	-28.8	-	-	-	-33.0 -27.0
HD 105071 ^{4,6}	3	-	-	<0.6	<11.82	-	-	<0.6	<12.12	-	-	-	-	-24.8	-	-	-	-27.0 -22.0
HD 105071 ^{4,6}	4	-	-	<0.6	<11.79	-	-	<0.6	<12.09	-19.1	-	-	-	-	-	-	-	-22.0 -17.2
HD 105071 ^{4,6}	5	-15.3±0.2	1.0±1.0	1.1±0.7	12.14±0.19	-15.2±0.2	1.0±1.0	1.4±0.7	12.51±0.18	-	-	-	-	-	-	-	-	-17.2 -13.1
HD 105071 ^{4,6}	6	-9.6±0.4	2.2±0.4	14.4±1.1	13.25±0.03	-9.4±0.1	2.4±0.6	8.7±1.1	13.32±0.05	-13.1	-	-	-	-11.8	-	-	-	-13.1 -6.6
HD 105071 ^{4,6}	7	-1.6±0.2	1.4±1.4	2.8±0.7	12.51±0.10	-1.4±0.3	2.5±1.4	2.1±0.9	12.69±0.15	-3.8	-	-	-	-2.0	-	-	-	-6.6 -1.4
HD 105071 ^{4,6}	8	-	-	<0.4	<11.67	-	-	<0.4	<11.97	-	-	-	-	-0.5	-	-	-	-1.4 2.2
HD 105071 ^{4,6}	9	-	-	<0.8	<11.92	-	-	<0.8	<12.23	5.0	-	-	-	-	-	-	-	2.2 8.7
HD 105071 ^{4,6}	10	-	-	<1.2	<12.13	-	-	<1.2	<12.43	-	-	-	-	12.5	-	-	-	8.7 19.2
HD 105071 ^{4,6}	11	-	-	<1.3	<12.17	-	-	<1.3	<12.47	-	-	-	-	26.0	-	-	-	19.2 30.6
HD 106068 ^{4,6}	1	-	-	<2.2	<12.38	-	-	<2.2	<12.69	-	-	-	-	-85.0	-	-	-	-89.7 -80.3
HD 106068 ^{4,6}	2	-	-	<6.6	<12.87	-	-	<6.6	<13.17	-	-	-	-	-75.6	-	-	-	-80.3 -51.5
HD 106068 ^{4,6}	3	-27.4±0.4	2.5±2.4	2.7±1.9	12.50±0.22	-26.1±0.6	2.9±2.4	1.5±1.5	12.54±0.29	-27.6	-	-	-	-28.2	-	-	-	-51.5 -24.1
HD 106068 ^{4,6}	4	-	-	<1.1	<12.11	-	-	<1.1	<12.41	-21.5	-	-	-	-20.5	-	-	-	-24.1 -19.2
HD 106068 ^{4,6}	5	-	-	<2.1	<12.38	-	-	<2.1	<12.68	-16.4	-	-	-	-18.4	-	-	-	-19.2 -9.9
HD 106068 ^{4,6}	6	-1.3±0.3	1.8±0.6	16.6±2.5	13.36±0.05	-1.0±0.1	1.7±0.9	9.2±2.1	13.36±0.08	-4.0	-	-	-	-3.2	-	-	-	-9.9 0.0
HD 106068 ^{4,6}	7	-	-	<1.2	<12.13	-	-	<1.2	<12.43	2.4	-	-	-	-	-	-	-	0.0 5.2
HD 106068 ^{4,6}	8	-	-	<1.7	<12.29	-	-	<1.7	<12.59	-	-	-	-	8.0	-	-	-	5.2 12.7
HD 105056	1	-	-	<1.9	<12.32	-	-	<1.9	<12.62	-	-	<2.3	<10.80	-46.0±1.0	6.1±0.4	33.2±2.7	11.64±0.03	-58.1 -39.8
HD 105056	2	-	-	<1.0	<12.04	-	-	<1.0	<12.35	-33.5±0.1	3.5±1.1	6.5±1.4	11.27±0.08	-33.8±0.5	23.1±2.4	11.60±0.03	-39.8 -30.2	
HD 105056	3	-	-	<0.8	<11.98	-	-	<0.8	<12.28	-26.0±0.8	4.8±0.9	12.2±1.9	11.55±0.06	-27.4±0.3	8.0±0.3	64.9±3.6	11.95±0.02	-30.2 -22.0
HD 105056	4	-	-	<0.9	<12.01	-	-	<0.9	<12.31	-16.6±0.2	5.0±0.6	15.4±2.1	11.67±0.05	-17.8±0.7	4.1±0.2	32.4±3.4	11.74±0.03	-22.0 -13.1
HD 105056	5	-	-	<0.7	<11.91	-7.5±1.2	4.2±3.0	0.8±0.4	12.33±0.20	-10.4±0.3	1.0±1.0	1.5±0.8	10.65±0.18	-	-	<1.4	<10.22	-13.1 -5.9
HD 105056	6	-4.3±2.7	4.1±3.5	2.8±1.2	12.50±0.15	-1.0±0.4	1.0±0.9	1.0±0.6	12.37±0.21	-3.0±0.3	5.8±0.5	25.6±2.8	11.90±0.04	-	-	<1.0	<10.22	-6.9 -0.3
HD 105056	7	1.9±1.0	3.3±1.5	4.1±1.1	12.67±0.10	2.7±0.4	1.0±3.1	1.3±0.7	12.48±0.18	-	-	<0.7	>10.26	-3.3±0.1	7.3±0.2	117.3±6.6	12.21±0.02	-0.3 4.9
HD 105056	8	8.1±0.3	1.7±1.0	3.4±0.7	12.62±0.08	8.5±0.4	3.3±3.0	2.3±1.0	12.75±0.15	5.6±1.1	3.4±3.2	2.7±1.2	10.87±0.16	8.1±0.3	1.6±1.5	3.2±0.9	10.60±0.10	4.9 17.1
HD 105056	9	-	-	<1.9	<12.33	-	-	<1.9	<12.63	-	-	<2.4	<10.81	26.7±0.2	4.6±0.4	23.8±1.8	11.46±0.03	17.1 35.9

Table 3. ctd.

Star name	Cmp. Num	Na I (3302.37)				Na I (3302.98)				Ti II (3383.76)				Ca II (3393.66)				Vel. Range
		<i>v</i>	<i>b</i>	EW	log(<i>N</i>)	<i>v</i>	<i>b</i>	EW	log(<i>N</i>)	<i>v</i>	<i>b</i>	EW	log(<i>N</i>)	<i>v</i>	<i>b</i>	EW	log(<i>N</i>)	
HD 145482	1	-	-	<1.0	<12.07	-	-	<1.0	<12.37	-19.5±0.2	4.3±1.7	4.0±1.1	11.06±0.10	-19.4±0.1	3.4±0.5	6.3±0.6	10.89±0.04	-27.1 -15.6
HD 145482	2	-	-	<0.8	<11.93	-	-	<0.8	<12.23	-	-	<0.7	<10.31	-11.8±0.2	1.2±1.1	1.5±0.4	10.25±0.10	-15.6 -7.2
HD 145482	3	-	-	<0.8	<11.95	-	-	<0.8	<12.25	-2.6±0.2	1.4±1.4	0.5±0.4	10.10±0.29	-	-	<0.6	<9.83	-7.2 1.6
HD 145482	4	-	-	<0.9	<12.01	-	-	<0.9	<12.32	5.5±0.5	2.9±2.7	1.2±0.8	10.52±0.22	6.1±0.2	3.1±2.1	1.7±0.6	10.29±0.13	1.6 11.8
HD 157038 ^{4,6}	1	-	-	<1.3	<12.18	-	-	<1.3	<12.48	-	-	-	-	-	-	-	-	-92.0 -78.4
HD 157038 ^{4,6}	2	-	-	<1.4	<12.19	-	-	<1.4	<12.49	-	-	-	-	-	-	-	-	-78.4 -64.3
HD 157038 ^{4,6}	3	-	-	<1.0	<12.07	-	-	<1.0	<12.37	-	-	-	-	-	-	-	-	-64.3 -53.7
HD 157038 ^{4,6}	4	-	-	<1.4	<12.21	-	-	<1.4	<12.51	-47.8	-	-	-	-	-	-	-	-53.7 -39.2
HD 157038 ^{4,6}	5	-	-	<1.2	<12.12	-	-	<1.2	<12.42	-29.4	-	-	-	-	-	-	-	-39.2 -27.2
HD 157038 ^{4,6}	6	-25.2±0.6	3.1±2.9	1.9±0.8	12.34±0.15	-	-	<0.5	<12.06	-23.6	-	-	-	-	-	-	-	-27.2 -22.0
HD 157038 ^{4,6}	7	-	-	<0.3	<11.59	-20.7±0.7	2.2±0.0	1.0±0.7	12.37±0.22	-	-	-	-	-	-	-	-	-22.0 -18.5
HD 157038 ^{4,6}	8	-17.8±0.4	2.4±0.8	5.2±0.8	12.77±0.06	-17.0±0.2	1.0±2.3	1.0±0.5	12.34±0.19	-17.4	-	-	-	-	-	-	-	-18.5 -14.0
HD 157038 ^{4,6}	9	-10.7±0.2	1.0±1.0	1.1±0.6	12.12±0.19	-	-	<0.4	<12.00	-	-	-	-	-	-	-	-	-14.0 -9.6
HD 157038 ^{4,6}	10	-8.0±0.1	4.1±0.2	21.7±1.7	13.43±0.03	-8.8±0.6	3.4±0.5	11.2±1.0	13.38±0.04	-	-	-	-	-	-	-	-	-9.6 -7.2
HD 157038 ^{4,6}	11	-	-	<0.2	<11.23	-	-	<0.2	<11.54	-6.1	-	-	-	-	-	-	-	-7.2 -5.7
HD 157038 ^{4,6}	12	-	-	<0.5	<11.76	-5.1±0.2	1.0±0.0	1.0±0.6	12.37±0.19	-5.8	-	-	-	-	-	-	-	-5.7 -0.4
HD 157038 ^{4,6}	13	5.6±0.4	2.1±0.2	13.1±1.1	13.24±0.03	5.6±0.3	1.7±0.5	6.7±0.7	13.21±0.04	3.5	-	-	-	-	-	-	-	-0.4 2.2
HD 157038 ^{4,6}	14	0.0±0.4	2.3±0.3	13.7±1.2	13.26±0.03	0.0±0.4	2.5±0.5	7.7±0.8	13.28±0.04	-	-	-	-	-	-	-	-	2.2 6.2
HD 157038 ^{4,6}	15	-	-	<0.9	<12.00	13.9±0.8	5.0±3.0	1.0±1.0	12.36±0.29	-	-	-	-	-	-	-	-	6.2 15.3
HD 157038 ^{4,6}	16	-	-	<0.7	<11.92	-	-	<0.7	<12.22	18.2	-	-	-	-	-	-	-	15.3 22.9
HD 143275	1	-	-	<0.6	<11.82	-	-	<0.6	<12.12	-25.9±0.2	1.0±1.0	0.4±0.4	10.10±0.29	-	-	-	-	-27.9 -21.8
HD 143275	2	-	-	<0.6	<11.83	-	-	<0.6	<12.13	-17.7±0.7	4.2±1.7	3.8±1.0	11.03±0.10	-	-	-	-	-21.8 -15.6
HD 143275	3	-13.6±0.7	3.7±3.5	0.8±0.5	11.96±0.20	-	-	<0.5	<12.07	-	-	<0.5	<10.10	-	-	-	-	-15.6 -10.2
HD 143275	4	-	-	<0.6	<11.82	-	-	<0.6	<12.12	-6.9±0.5	3.0±2.8	1.2±0.8	10.54±0.21	-	-	-	-	-10.2 -4.2
HD 143275	5	-1.6±0.4	2.0±0.4	10.4±1.1	13.10±0.04	-1.6±0.1	1.7±0.7	4.8±0.8	13.06±0.06	-1.5±0.1	0.6±0.6	1.3±0.5	10.55±0.15	-	-	-	-	-4.2 0.9
HD 143275	6	-	-	<0.4	<11.69	-	-	<0.4	<11.99	3.3±0.2	1.0±1.0	0.2±0.2	9.80±0.29	-	-	-	-	0.9 5.3
HD 163745	1	-	-	<2.2	<12.40	-	-	<2.2	<12.70	-9.5±0.8	4.8±4.6	3.2±2.0	10.95±0.21	-	-	-	-	-19.1 -5.7
HD 163745	2	-	-	<1.0	<12.07	-	-	<1.0	<12.37	-2.0±0.5	1.7±1.6	2.1±1.1	10.77±0.18	-	-	-	-	-5.7 0.5
HD 163745	3	-	-	<1.4	<12.20	-	-	<1.4	<12.50	3.0±0.2	3.0±0.6	15.8±1.8	11.70±0.04	-	-	-	-	0.5 8.9
HD 155806	1	-	-	<1.9	<12.33	-	-	<1.9	<12.63	-	-	<1.7	<10.67	-37.0±0.1	4.9±0.5	23.5±2.4	11.47±0.04	-46.7 -32.5
HD 155806	2	-	-	<1.3	<12.17	-	-	<1.3	<12.47	-	-	<1.2	<10.51	-28.0±0.4	2.6±0.6	10.8±1.4	11.12±0.05	-32.5 -22.8
HD 155806	3	-	-	<1.7	<12.29	-	-	<1.7	<12.59	-16.3±1.3	10.4	3.1±2.9	10.94±0.28	-18.8±1.0	6.0±0.5	26.1±2.9	11.55±0.04	-22.8 -9.9
HD 155806	4	-	-	<1.3	<12.17	-	-	<1.3	<12.47	-	-	<1.2	<10.51	-2.2±0.4	2.2±0.8	11.6±4.2	11.52±0.06	-9.9 0.0
HD 155806	5	1.4±0.3	1.5±1.5	1.6±0.9	12.27±0.18	2.4±0.3	1.5±1.5	1.1±0.9	12.39±0.26	1.5±0.3	5.9±0.5	23.5±2.5	11.86±0.04	3.2±0.1	8.2±0.2	173.3±12.5	12.49±0.02	0.0 5.4
HD 155806	6	8.0±0.5	2.5±0.4	16.8±1.4	13.35±0.03	8.1±0.1	2.4±0.6	10.0±1.4	13.41±0.05	9.7±1.0	4.8±2.2	6.2±1.6	11.23±0.10	-	-	<0.9	<10.94	5.4 11.7
HD 155806	7	14.1±0.3	1.5±1.5	1.1±0.9	12.10±0.26	-	-	<0.8	<12.23	15.7±4.9	10.0±9.5	4.4±2.9	11.09±0.22	-	-	<0.9	<9.99	11.7 17.4
HD 155806	8	-	-	<1.0	<12.07	-	-	<1.0	<12.37	-	-	<0.9	<10.41	19.9±0.4	2.6±1.2	3.8±1.2	10.85±0.08	17.4 25.1
HD 163758	1	-	-	<2.2	<12.39	-	-	<2.2	<12.69	-	-	<2.1	<10.77	-46.9±1.1	6.4±3.2	2.9±1.0	10.53±0.13	-59.7 -41.0
HD 163758	2	-	-	<1.2	<12.13	-	-	<1.2	<12.43	-	-	<1.1	<10.50	-35.1±0.1	3.0±0.1	17.7±1.0	11.40±0.02	-41.0 -30.8
HD 163758	3	-	-	<1.3	<12.17	-	-	<1.3	<12.47	-26.7±0.8	5.5±1.9	6.7±1.9	11.30±0.10	-26.2±0.1	4.0±0.1	59.9±2.0	11.99±0.01	-30.8 -19.6
HD 163758	4	-	-	<1.3	<12.18	-	-	<1.3	<12.48	-12.0±0.3	7.8±1.1	18.0±2.5	11.75±0.05	-13.7±0.2	6.5±0.1	94.0±3.4	12.23±0.01	-19.6 -8.2
HD 163758	5	-3.8±0.3	1.7±0.4	20.3±1.9	13.48±0.03	-3.6±0.3	1.6±0.4	13.3±1.2	13.56±0.03	-	-	<0.9	<10.41	-3.3±0.1	4.3±0.2	101.2±12.2	12.48±0.02	-8.2 0.0
HD 163758	6	-	-	<0.5	<11.77	-	-	<0.5	<12.07	3.6±0.3	13.8±1.7	51.4±6.3	12.15±0.05	-	-	<0.4	<9.65	0.0 4.5
HD 163758	7	6.4±0.1	4.4±1.0	9.5±1.4	13.03±0.06	6.5±0.2	4.1±1.8	5.1±1.3	13.06±0.10	3.5±0.2	7.2±0.5	33.4±3.5	12.13±0.03	5.3±0.1	4.8±0.2	105.4±15.7	12.59±0.02	4.5 9.8
HD 163758	8	-	-	<1.2	<12.11	-	-	<1.2	<12.42	-	-	<1.1	<10.49	14.2±0.2	5.9±0.1	93.7±2.8	12.15±0.01	9.8 19.7
HD 163758	9	25.8±0.2	3.1±1.5	4.1±1.1	12.66±0.10	26.1±0.3	4.1±3.7	3.0±1.3	12.83±0.16	23.3±1.1	6.4±4.5	4.6±1.9	11.10±0.15	25.4±0.1	4.5±0.1	51.0±1.6	11.91±0.01	19.7 32.0
HD 163758	10	-	-	<3.8	<12.63	-	-	<3.8	<12.93	-	-	<3.7	<11.01	38.9±0.4	6.5±0.8	8.9±1.1	11.02±0.05	32.0 64.6
HD 163758	11	-	-	<3.8	<12.63	-	-	<3.8	<12.93	-	-	<3.6	<11.00	90.4±0.6	3.2±1.9	1.8±0.6	10.32±0.12	64.6 96.7
HD 148184	1	-	-	<1.4	<12.20	-	-	<1.4	<12.50	-13.7±0.1	6.5±1.2	11.6±1.8	11.53±0.06	-14.6±0.4	4.1±0.2	22.9±1.3	11.49±0.02	-24.8 -11.1
HD 148184	2	-	-	<0.8	<11.95	-	-	<0.8	<12.25	-	-	<0.9	<10.41	-8.0±1.1	4.5±0.5	19.2±1.0	11.10±0.04	-11.1 -3.3
HD 148184	3	0.2±0.7	1.0±1.0	0.1±0.1	11.12±0.20	-	-	<0.5	<12.03	2.5±0.3	5.1±4.1	2.8±1.2	10.91±0.15	1.4±0.4	2.3±0.1	39.0±1.2	11.79±0.01	-3.3 1.3
HD 148184	4	1.2±0.4	2.1±0.2	31.4±2.1	13.70±0.02	1.2±0.3	1.9±0.3	24.3±1.5	13.86±0.02	-	-	<0.5	<10.11	-	-	<0.4	<9.69	1.3 5.2

Comments: (1) Poor base-line fitting at 3302Å. No sodium components fitted. (2) Stellar contamination removed in Ti and Ca. (3) Stellar Ca line has been fitted and removed. (4) Ca heavily contaminated by stellar profile, only component velocities given. (5) Components 3,4,5 and 10 may be stellar. (6) Ti heavily contaminated by stellar profile, not fitted. (7) Stellar lines of unknown width. (8) Sodium lines are in poor agreement. (9) LSR velocity of star unknown.

Table 4. Total column density derived by the summation of the individual interstellar components listed in Table 3. We also present the total derived by the AOD method, discussed in Section 3.4.

Star	Na I (3302.37)			Na I (3302.98)			Ti II (3383.76)			Ca II (3393.66)			H I logN
	S/N	logN (Prof)	logN (AOD)	S/N	logN (Prof)	logN (AOD)	S/N	logN (Prof)	logN (AOD)	S/N	logN (Prof)	logN (AOD)	
HD 164794	200	13.54±0.03	13.49±0.05	200	13.63±0.03	13.55±0.11	230	12.08±0.06	12.10±0.03	290	12.49±0.03	12.59±0.01	21.29±0.07
HD 163800	260	13.84±0.02	13.75±0.01	260	13.98±0.03	13.92±0.03	320	12.04±0.05	12.05±0.02	580	12.61±0.02	12.53±0.01	-
HD 170235	210	13.57±0.05	13.60±0.03	210	13.58±0.08	13.60±0.07	220	12.06±0.07	12.07±0.03	300	12.67±0.02	12.65±0.01	-
HD 167264	260	13.52±0.04	13.50±0.05	260	13.53±0.04	13.47±0.09	290	11.98±0.07	11.98±0.03	-	-	-	21.14±0.13
HD 171432	430	13.82±0.03	13.83±0.04	430	13.82±0.04	13.82±0.07	370	12.23±0.04	12.23±0.04	590	12.91±0.02	12.89±0.01	-
HD 169454	240	14.24±0.04	14.17±0.01	240	14.29±0.04	14.23±0.03	340	12.54±0.03	12.53±0.01	-	-	-	-
HD 188294	380	<12.69	<12.69	380	<12.99	<12.99	450	11.34±0.11	11.28±0.06	420	11.33±0.05	11.32±0.03	-
HD 30677	330	13.27±0.04	13.26±0.07	330	13.26±0.04	13.29±0.13	320	12.19±0.07	12.19±0.02	430	12.70±0.02	12.68±0.01	21.10±0.09
HD 36861	330	13.22±0.03	13.10±0.08	330	13.18±0.05	12.99±0.11	340	11.74±0.05	11.74±0.03	370	12.50±0.02	12.48±0.01	20.81±0.12
HD 37490	470	12.84±0.09	12.86±0.14	470	12.76±0.17	12.72±0.19	500	11.66±0.06	11.67±0.04	710	12.30±0.01	12.30±0.01	20.90±0.06
HD 43285	220	<12.63	<12.63	220	<12.94	<12.94	280	11.41±0.12	11.40±0.06	430	12.02±0.02	11.92±0.01	-
HD 36646	330	<12.44	<12.44	330	<12.75	<12.75	400	11.58±0.09	11.56±0.04	470	12.22±0.02	12.27±0.01	-
HD 48099	330	13.40±0.05	13.40±0.03	330	13.36±0.09	13.38±0.06	410	12.11±0.03	12.12±0.01	-	-	-	21.20±0.08
HD 37055	300	<12.73	<12.73	300	<13.03	<13.03	400	11.28±0.09	11.34±0.07	520	11.97±0.03	11.97±0.01	-
HD 33328	550	12.53±0.12	12.36±0.09	550	12.69±0.20	12.63±0.26	470	11.55±0.08	11.54±0.03	660	12.11±0.01	12.11±0.01	-
HD 45725	250	<12.56	<12.56	250	<12.86	<12.86	300	11.12±0.18	11.11±0.09	520	11.56±0.03	11.54±0.01	-
HD 52918	370	<12.66	<12.66	370	<12.96	<12.96	450	11.15±0.16	11.16±0.10	520	11.82±0.03	11.96±0.01	20.38±0.09
HD 46185	310	<12.52	<12.52	310	<12.82	<12.82	350	11.61±0.09	11.62±0.03	550	12.24±0.01	12.24±0.01	-
HD 58343	250	13.29±0.03	13.32±0.03	250	13.31±0.04	13.32±0.05	320	11.38±0.12	11.40±0.04	410	12.07±0.02	12.19±0.01	-
HD 50896	250	12.50±0.13	12.66±0.42	250	12.38±0.26	12.56±0.55	260	12.05±0.07	12.07±0.05	300	12.47±0.02	12.53±0.01	20.54±0.13
HD 58978	500	<12.30	<12.30	500	<12.60	<12.60	520	11.35±0.05	11.28±0.04	620	11.90±0.03	11.91±0.01	20.24±0.10
HD 49131	350	<12.59	<12.59	350	<12.89	<12.89	620	11.31±0.05	11.31±0.05	770	11.98±0.01	11.99±0.01	-
HD 61429	260	<12.26	<12.26	260	<12.56	<12.56	270	11.11±0.08	11.17±0.05	520	10.89±0.07	10.82±0.03	-
HD 58377	300	<12.34	<12.34	300	<12.64	<12.64	370	11.39±0.12	11.35±0.05	-	-	-	-
HD 64972	280	<12.38	<12.38	280	<12.68	<12.68	340	11.41±0.10	11.34±0.04	-	-	-	-
HD 60498	250	<12.97	<12.97	250	<13.27	<13.27	450	11.50±0.19	11.49±0.09	770	-	-	-
HD 90882	120	<12.66	<12.66	120	<12.97	<12.97	120	<11.08	<11.08	190	10.79±0.19	10.79±0.09	-
HD 68761	290	13.58±0.04	13.62±0.07	290	13.55±0.06	13.54±0.11	320	11.91±0.08	11.92±0.06	410	12.58±0.03	12.59±0.01	-
HD 74966	280	<12.78	<12.78	280	<13.08	<13.08	350	11.07±0.16	11.10±0.21	550	11.89±0.03	11.81±0.02	-
HD 72067	280	<13.19	<13.19	280	<13.50	<13.50	430	11.34±0.13	11.38±0.16	450	12.07±0.05	12.13±0.02	-
HD 76341	220	13.88±0.02	13.78±0.02	220	13.96±0.02	13.87±0.06	220	11.76±0.09	11.76±0.07	330	12.24±0.04	12.29±0.01	21.20±0.08
HD 76131	410	12.63±0.12	12.51±0.08	410	12.79±0.16	12.87±0.27	450	11.75±0.06	11.75±0.02	550	12.38±0.01	12.37±0.01	-
HD 67536	340	12.80±0.11	12.67±0.07	340	12.84±0.17	12.79±0.16	340	11.68±0.07	11.67±0.02	550	11.79±0.02	11.72±0.01	20.99±0.09
HD 89587	290	12.71±0.08	12.73±0.15	290	12.70±0.12	12.78±0.29	270	-	-	470	-	-	-
HD 88661	170	<12.83	<12.83	170	<13.13	<13.13	200	11.58±0.10	11.58±0.07	290	12.02±0.06	12.03±0.01	-
HD 92740	320	13.54±0.05	13.55±0.03	320	13.53±0.09	13.52±0.05	380	12.37±0.03	12.38±0.01	430	12.89±0.02	12.89±0.01	21.34±0.10
HD 93131	290	13.49±0.06	13.47±0.06	290	13.50±0.10	13.50±0.11	370	12.42±0.03	12.43±0.01	450	12.92±0.01	12.92±0.01	21.20±0.10
HD 94910	170	13.97±0.08	14.09±0.06	170	13.80±0.08	13.83±0.07	180	12.50±0.05	12.50±0.03	330	-	-	-
HD 96917	240	14.10±0.04	14.07±0.03	240	14.15±0.05	14.13±0.06	290	12.52±0.03	12.52±0.02	390	13.27±0.02	13.26±0.01	21.23±0.11
HD 94963	250	13.12±0.04	13.09±0.19	250	13.12±0.06	13.09±0.33	320	12.32±0.04	12.33±0.03	430	12.65±0.02	12.69±0.01	-

Table 4. *ctd.*

Star	Na I (3302.37)		Na I (3302.98)		Ti II (3383.76)		Ca II (3393.66)		H I				
	S/N	log <i>N</i> (Prof)	log <i>N</i> (AOD)	S/N	log <i>N</i> (Prof)	log <i>N</i> (AOD)	S/N	log <i>N</i> (Prof)		log <i>N</i> (AOD)			
HD 97253	180	14.00±0.05	13.97±0.02	180	14.05±0.06	14.07±0.04	180	12.45±0.06	12.51±0.02	280	12.99±0.03	12.97±0.01	-
HD 100841	170	<12.82	<12.82	170	<13.12	<13.12	240	11.20±0.19	11.19±0.11	260	11.20±0.12	11.19±0.06	-
HD 29138	260	12.79±0.21	12.71±0.50	260	12.47±0.25	12.33±0.45	300	12.28±0.06	12.29±0.02	450	12.44±0.02	12.43±0.01	20.91±0.10
HD 105071	240	13.41±0.06	13.43±0.04	240	13.50±0.10	13.56±0.11	260	-	-	400	-	-	-
HD 106068	120	13.42±0.07	13.41±0.13	120	13.42±0.11	13.49±0.26	150	-	-	330	-	-	-
HD 105056	250	13.08±0.11	13.11±0.14	250	13.10±0.18	13.08±0.24	230	12.28±0.06	12.28±0.03	260	12.63±0.02	12.63±0.01	21.15±0.10
HD 109867	200	13.43±0.07	13.41±0.09	200	13.46±0.10	13.44±0.18	230	12.23±0.07	12.22±0.04	410	12.68±0.02	12.68±0.01	21.11±0.10
HD 112272	130	14.20±0.03	14.16±0.01	130	14.29±0.06	14.27±0.04	140	12.32±0.08	12.32±0.03	370	12.92±0.02	12.86±0.01	-
HD 112842	250	13.63±0.06	13.64±0.04	250	13.70±0.09	13.72±0.08	280	12.39±0.05	12.39±0.02	-	-	-	-
HD 113904	200	13.01±0.13	13.07±0.14	200	13.10±0.22	13.15±0.28	220	12.31±0.10	12.30±0.03	450	12.79±0.02	12.79±0.01	21.15±0.10
HD 115363	100	14.20±0.04	14.16±0.02	100	14.23±0.05	14.23±0.05	160	12.57±0.05	12.57±0.01	290	13.15±0.03	13.14±0.01	-
HD 115842	190	14.10±0.04	14.05±0.01	190	14.16±0.05	14.14±0.03	200	12.21±0.07	12.22±0.03	300	12.80±0.02	12.81±0.01	21.15±0.12
HD 136239	100	14.18±0.07	14.20±0.03	100	14.21±0.08	14.19±0.06	120	12.68±0.06	12.69±0.02	200	13.22±0.03	13.19±0.01	-
HD 143448	250	12.92±0.13	12.96±0.14	250	12.92±0.15	12.96±0.24	270	11.70±0.10	11.64±0.07	380	12.26±0.03	12.26±0.01	-
HD 142758	270	13.55±0.05	13.52±0.05	270	13.51±0.06	13.56±0.10	270	12.71±0.06	12.70±0.01	350	12.99±0.02	12.98±0.01	-
HD 137753	200	12.43±0.15	12.38±0.07	200	12.53±0.25	12.51±0.18	-	-	-	-	-	-	-
HD 148937	210	13.93±0.04	13.93±0.04	210	13.94±0.07	13.96±0.07	280	12.13±0.07	12.13±0.05	370	12.69±0.02	12.67±0.01	21.60±0.10
HD 148379	150	13.98±0.05	13.98±0.02	150	13.99±0.07	14.00±0.05	180	12.33±0.05	12.10±0.04	250	12.84±0.02	12.83±0.01	-
HD 148688	330	13.85±0.02	13.81±0.02	330	13.88±0.03	13.90±0.05	370	12.18±0.04	12.20±0.02	500	12.86±0.02	12.83±0.01	-
HD 154811	290	13.95±0.03	13.97±0.01	290	13.95±0.06	13.96±0.02	270	12.14±0.08	12.15±0.02	380	12.81±0.02	12.80±0.01	-
HD 154873	310	13.95±0.03	13.94±0.02	310	14.00±0.04	14.00±0.04	310	12.01±0.06	12.00±0.04	410	12.69±0.02	12.65±0.01	-
HD 156575	270	13.76±0.04	13.74±0.02	270	13.76±0.07	13.76±0.04	270	12.12±0.05	12.12±0.02	380	12.63±0.03	12.62±0.01	21.26±0.16
HD 156385	280	13.57±0.06	13.55±0.03	280	13.65±0.08	13.65±0.08	350	12.10±0.04	12.12±0.02	450	12.64±0.02	12.64±0.01	-
HD 151932	210	14.12±0.03	14.06±0.02	210	14.21±0.03	14.17±0.05	310	12.29±0.06	12.29±0.03	550	12.93±0.01	12.92±0.01	21.39±0.11
HD 152235	220	14.14±0.03	14.10±0.02	220	14.18±0.02	14.18±0.05	310	12.26±0.05	12.27±0.03	520	12.92±0.01	12.89±0.01	-
HD 152003	210	14.17±0.04	14.10±0.02	210	14.27±0.05	14.20±0.04	240	12.30±0.06	12.27±0.03	340	12.94±0.02	12.92±0.01	-
HD 152270	240	13.86±0.04	13.83±0.02	240	13.93±0.05	13.91±0.05	250	12.25±0.07	12.25±0.03	450	12.89±0.01	12.89±0.01	-
HD 145482	300	<12.60	<12.60	300	<12.90	<12.90	320	11.21±0.14	11.16±0.10	500	11.06±0.07	11.08±0.04	-
HD 157038	300	13.86±0.04	13.85±0.03	300	13.84±0.07	13.84±0.05	280	-	-	410	-	-	-
HD 143275	280	13.13±0.05	13.17±0.06	280	13.06±0.06	13.02±0.08	330	11.29±0.15	11.28±0.07	-	-	-	21.04±0.08
HD 163745	160	<12.72	<12.72	160	<13.02	<13.02	180	11.81±0.08	11.77±0.03	-	-	-	-
HD 155806	200	13.41±0.06	13.43±0.06	200	13.45±0.07	13.48±0.12	230	12.04±0.10	12.04±0.04	240	12.63±0.03	12.62±0.01	21.09±0.07
HD 163758	230	13.66±0.04	13.76±0.06	230	13.74±0.06	13.72±0.11	250	12.56±0.05	12.56±0.02	550	13.09±0.02	13.08±0.01	21.23±0.18
HD 148184	270	13.70±0.02	13.66±0.01	270	13.86±0.02	13.81±0.03	300	11.62±0.08	11.67±0.03	450	12.02±0.02	12.01±0.01	21.15±0.09

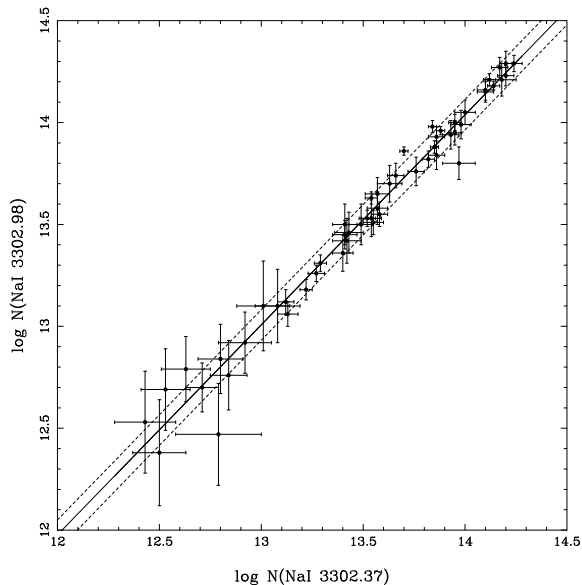


Figure 5. Comparison of the logarithm of the total column density from each line of the Na I UV doublet. The solid and dashed lines represent the best-fitting line and the 1σ standard deviation in the points respectively. The RMS scatter and Pearson correlation coefficient are 0.078 and 0.988 respectively.

case, HD 94910, high velocity features from the weaker line contaminate the stronger line. The 1σ standard deviation of the difference in the column density from each line of the Na UV doublet is 0.08 dex, excluding a few discrepant points at low column density the rms is 0.05 dex. This value compares with the 3σ mode and median error, both of which are 0.06 dex, estimated from the component fits as described in Sect. 3.5.

The uncertainty for the Ti and Ca lines should be less than this, as we can be much more certain about the baseline fit since the S/N ratio is much higher. To test this we have calculated the Ca column density from several Ca II H lines at a range of equivalent width, ($\lambda_{\text{air}}=3968.468 \text{ \AA}$), and compared these to the column density derived from Ca II K. The average difference in the total is less than 0.01 dex, with the maximum being 0.02 dex and the lines were close to saturation in this case. Again this compares well with the total error in the Ca II K column density estimated in Sect. 3.5, which for Ca II is 0.02 dex for both the median and the mode for the total estimated error. We are thus confident that the derived errors in the column densities give a fair approximation of the true errors in the analysis. Since the Ti lines have similar structure to the Ca lines, an average S/N = 300 and do not appear to be saturated, we would not expect the uncertainty in the total column density to exceed 0.05 dex which is the mode of the errors estimated from the component fits as described in Sect. 3.5.

In the rest of this paper we take the total Na I column density as the average of the values derived from each line. We do not take into account saturation effects, as in general they are of a similar order to the standard deviation of the difference in the column density from each line. Because the Ca II H line is severely blended with stellar H I and He I fea-

Table 5. Comparisons with previous work

Star	Species	Total Column Density		Ref.
		This Paper	Other Work	
HD 164794	Na I	13.59	13.58	1
HD 164794	Ti II	12.08	11.84	1
HD 164794	Ca II	12.62	12.63	1
HD 36862	Na I	13.20	>12.89	4
HD 36862	Ti II	11.74	11.73	2
HD 36862	Ca II	12.50	12.52	4
HD 50896	Ti II	12.05	12.18	3
HD 50896	Ca II	12.47	12.45	3
HD 143275	Na I	13.10	>12.79	4
HD 143275	Ti II	11.29	11.02	2

(1) Welsh et al. (1997) (2) Stokes (1978) (3) Hobbs (1984)
(4) Hobbs (1974)

tures, we do not use this species other than for the above comparison, and our Ca column densities are derived from Ca II K only.

3.7 Comparisons with previous work

From an examination of existing data we have found that four of our stars have been previously studied, and column densities determined for some of the species of interest. In Table 5 we compare our results for the total column density with those derived in other studies. The agreement between our Ca II total column density and those of other authors is remarkably good. In the three cases where comparisons could be made, all our values are within ± 0.02 dex of the results reported by the other authors. This is to be expected as the strength of the Ca II spectral line is sufficiently high that it will not be significantly affected by noise in the lower S/N studies of the other authors. Conversely, the Na I UV doublet and the Ti II are much weaker and hence we do not expect to obtain as good an agreement, as many of the weaker features will be obscured by the noise. Indeed, we find differences of up to 0.33 dex for these lines. Although we have been able to compare relatively few sightlines, the agreement we have found is encouraging and we believe that our high S/N spectra allow us to place the best estimates to date on the column densities of Na I UV, Ti II and Ca II towards each of our stellar targets.

4 RESULTS

4.1 Interstellar clouds along each line of sight

The values of v , b , EW and $\log N$ are tabulated in Table 3 for each component of each interstellar line observed towards each sightline. We have associated components in each species based primarily on their velocity. As a general rule, components which lie within 3.0 km s^{-1} have been associated. We note that there remains the possibility that even at a resolution of 3.75 km s^{-1} , the features detected may be blends of several physically different parcels of gas (Welty, Morton & Hobbs 1996), especially when Na is compared with either Ti or Ca, where components are often found not

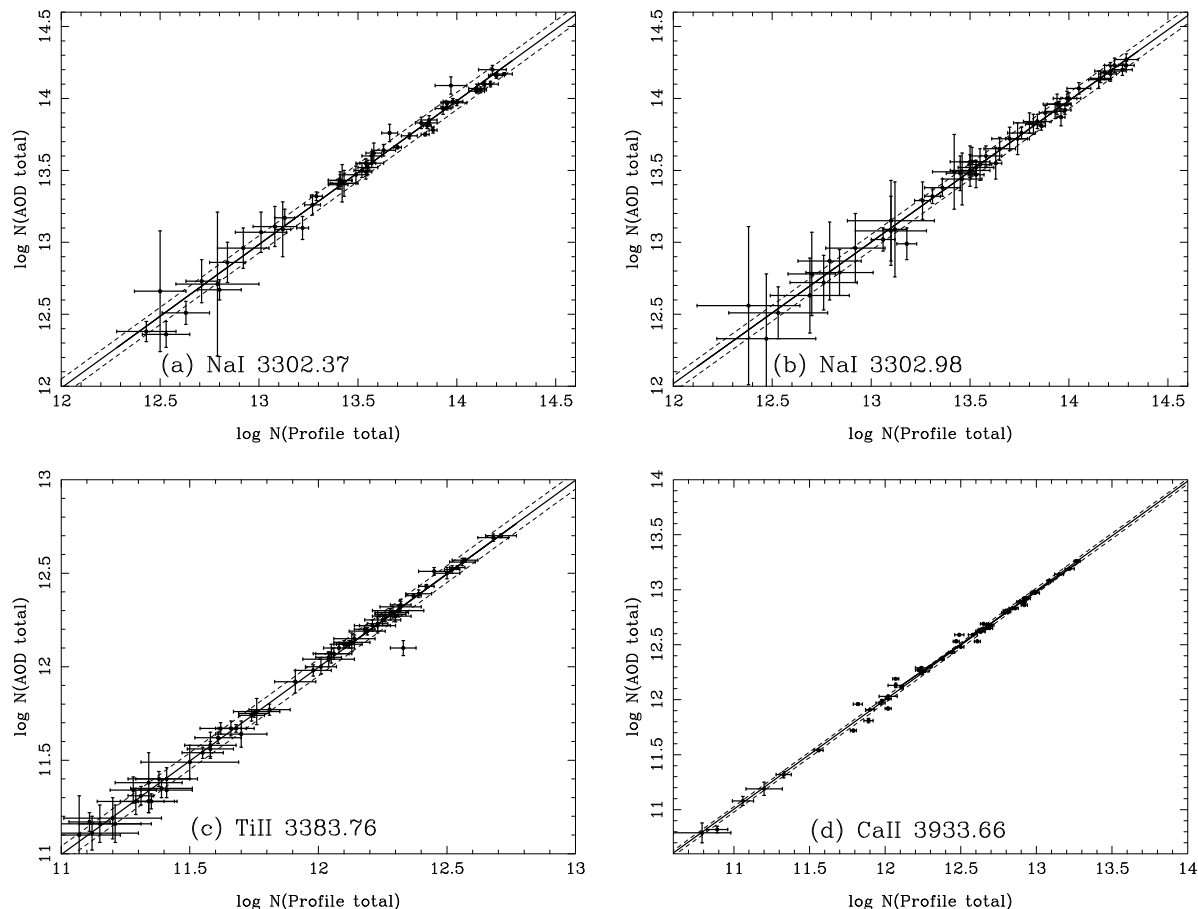


Figure 4. The logarithm of the total column density derived from the component fitting (listed in Table 3) compared to the logarithm of the total column density calculated using the AOD method. The solid and dashed lines represent the best-fitting line and the 1σ standard deviation in the points respectively. The RMS scatter and Pearson correlation coefficients are 0.059, 0.993; 0.055, 0.994; 0.044, 0.997 and 0.027, 0.997 for (a), (b), (c) and (d) respectively.

to match in velocity space. In general, we can usually associate components that appear in Ti with components in Ca.

4.2 Total Column Densities along each line of sight

In Table 4 we present the total column density for the Na I UV doublet (at 3302Å), Ti II at 3384Å and Ca II K at 3934Å. These totals have been calculated as the sum of the individual components, tabulated in Table 3, along each sightline. We also present the S/N ratio measured in the vicinity of each of the lines, along with the total H I column density towards each line-of-sight. The H I data have been taken from the IUE observations of Diplas & Savage (1994) for all sightlines, except for HD 50896, HD 52918 and HD 148184, where the results are from Fruscione et al. (1994), and HD 58978 from Savage, Edgar & Diplas (1990).

4.3 Correlations in total column densities

In this section we discuss correlations in the derived column densities against parameters such as distance, reddening and

H I column density. Where best-fits are performed, all slopes assume all free parameters.

4.3.1 Correlations with distance

In Fig. 6 we plot the logarithm of the total column density derived from profile fitting for each species against the logarithm of the stellar distance (in pc), along with an unweighted linear best fit to the data points. Fig. 6(a) shows a weak correlation between the Na column density and distance, although with the wide scatter of points and small correlation coefficient this correlation may not be significant. However in Fig. 6(b) we see a strong correlation between the Ti column density and the distance, and a similar strong correlation for Ca in Fig. 6(c), both being in agreement with that reported by W97. This supports other studies which find that Ti and Ca have a fairly even spatial distribution, although we should note that there are a number of points in which the column density of Ti can vary by as much as one order of magnitude for stars at similar distances. W97 find this same spread in the column density and conclude that this is expected due to the nonuniform distribution of interstellar gas in the spiral arms. In the W97 survey the majority of the stellar targets lie within 1 kpc. However most

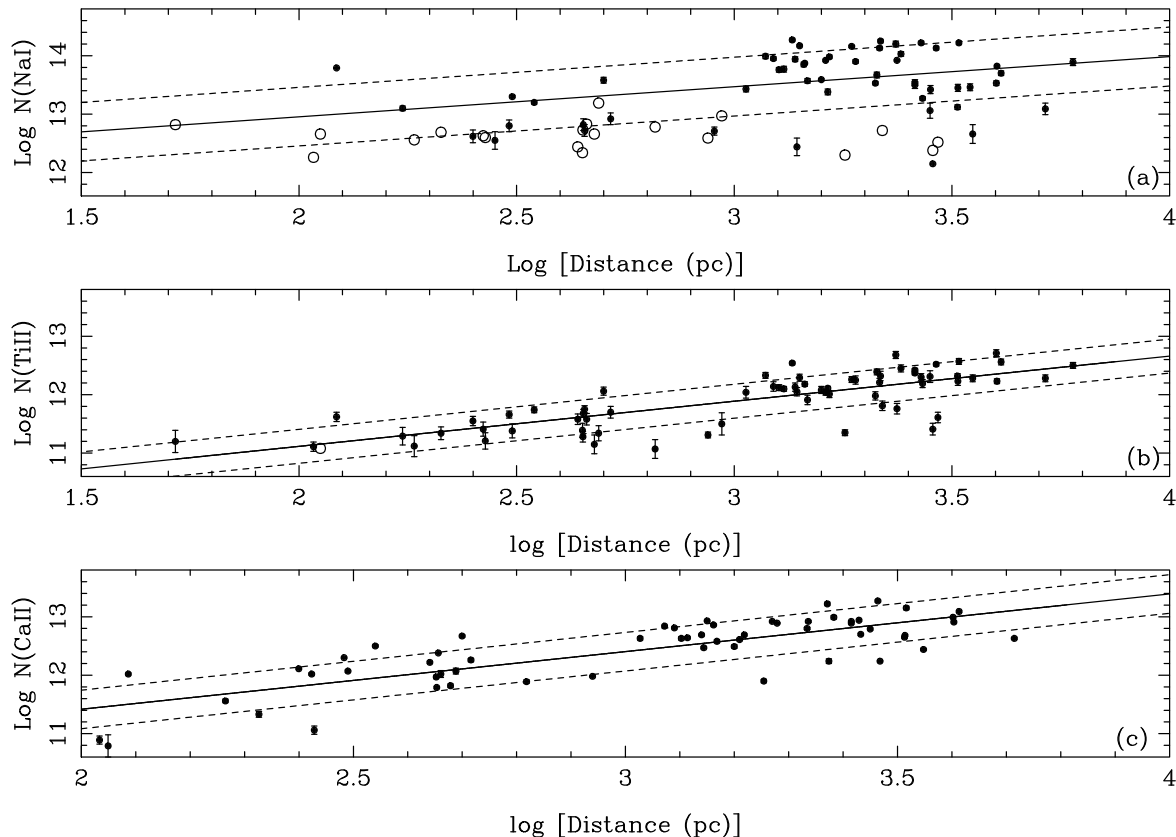


Figure 6. Plots of the logarithm of the total column density of (a) Na I, (b) Ti II and (c) Ca II against the logarithm of the distance to the star (in pc). Open circles represent upper limits to the column density. The solid and dashed lines represent the best-fitting line and the 1σ standard deviation in the points respectively. The error in the distance is 25 per cent (approximately 0.12 dex in the logarithm). The RMS scatter and Pearson correlation coefficients are 0.501, 0.399; 0.287, 0.776 and 0.330, 0.817 for (a), (b) and (c) respectively.

of the targets in our sample lie out to 3.5 kpc. Smoker et al. (2003) observed a greater depletion of Ca II K along sightlines with distances of less than ~ 500 pc and they associate this with the Local Bubble, an elliptical, hot, low-density region of the ISM which has significant X-ray emissivity out to ~ 100 pc and is likely to have been formed via a supernova event, see for example, Frisch (1998), Frisch & York (1983). We do not see this effect in Fig. 6(c) but given the limited number of our sightlines which lie within the Local Bubble, this is unlikely to be significant. Finally, we find that the correlations of Ti and Ca with distance are very similar and this is further evidence that Ti and Ca are mostly associated with the same interstellar regions.

4.3.2 Correlations with distance above the Galactic plane

We also examine the correlation between the total column density of each species and the perpendicular height, z , of the stellar target from the Galactic plane. Following similar methods to W97, we plot the projected column density, $N_{\text{tot}} \times \sin b$ against $|z|$, along with the unweighted linear best-fittings to the data points, for Na, Ti and Ca in Figs. 7(a), (b) and (c), respectively. Again we find a weaker

correlation in the Na plot, but good correlations for both Ti and Ca, with the best-fitting lines having very similar correlation coefficients of 0.880 and 0.864, respectively. We note that distance uncertainties contribute an error of ~ 0.12 dex, compared with the RMS scatter of 0.29 and 0.33 dex for Ti and Ca, hence the Ti and Ca relationships are remarkably tight. Also, although we sample similar Galactic heights to W97, we find a much tighter distribution of the points about the best-fitting line for Ti and Ca. Hence we similarly conclude that the column density of each species increases with height above the Galactic plane, and this trend is in agreement with other sources such as Edgar & Savage (1989). Although our sample does not include lines-of-sight with sufficiently high z to calculate the Galactic scale height of Ti II or Ca II, our results are in agreement with the limits reported. Edgar & Savage (1989) also report the smooth distribution of Ti II and Ca II, in agreement with our results and they find that these species are generally associated with the smooth distribution of the intercloud medium.

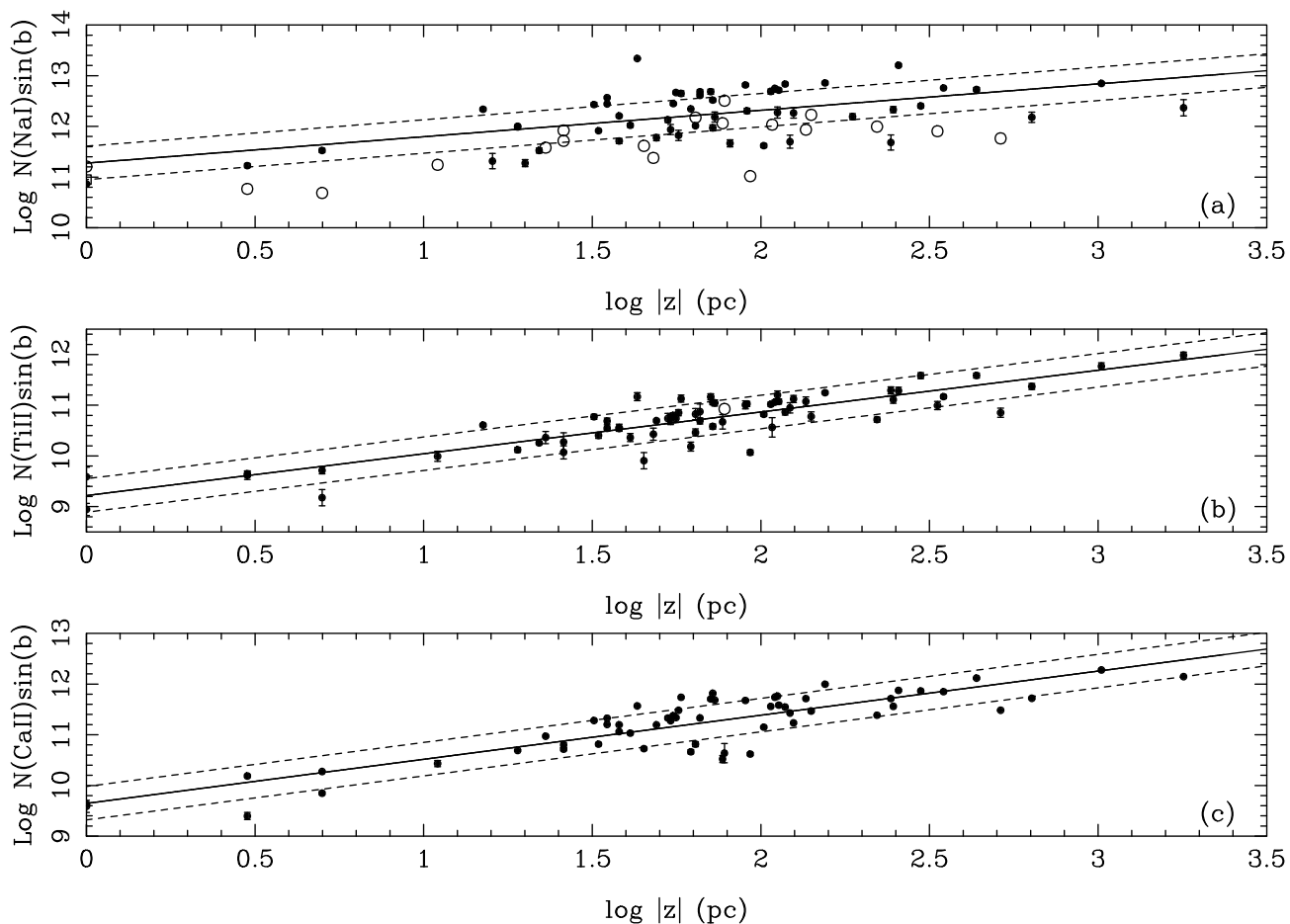


Figure 7. Plots of the logarithm of the total column density of (a) Na I, (b) Ti II and (c) Ca II against the perpendicular distance to the star, z , (in pc). Open circles represent upper limits to the column density. The solid and dashed lines represent the best-fitting line and the 1σ standard deviation in the points respectively. The error in the distance is 25 per cent (approximately 0.12 dex in the logarithm). The RMS scatter and Pearson correlation coefficients are 0.424, 0.564; 0.272, 0.880 and 0.321, 0.864 for (a), (b) and (c) respectively.

4.3.3 Correlations with reddening

In Fig. 8 we plot the correlation between the logarithm of the total column density per parsec and the reddening per kiloparsec along the line-of-sight for each of the three species under investigation. Note that HD 148184 has been excluded from the plot as it appears to have an anomalously high value of reddening per kiloparsec (4.26 kpc^{-1}).

As expected, we find evidence of increasing column density along sightlines with higher reddenings, as reported by Stokes (1978) and W97. At very low values of reddening, we generally do not observe the Na I UV doublet along as many sightlines as we observe Ti or Ca. Hence we see more upper limits at low reddenings per kiloparsec in Fig. 8(a) compared to Figs. 8(b) and (c). The correlation of the total Na column density with reddening appears to be stronger than that of Ti and Ca. The correlation coefficient in Fig. 8(a) is 0.597, compared to Figs. 8(b) and (c) where the correlation coefficients are 0.534 and 0.486 respectively. Although the scatter of points in Fig. 8(a) is greater than in Figs. 8(b) and (c) this stronger correlation appears to be significant. This effect is also seen in W97.

4.3.4 Correlations with total neutral hydrogen column density along the sightlines

In Figs. 9(a), (b) and (c) we plot the correlation between the logarithm of the total column density per parsec and the total neutral hydrogen column density per parsec derived from Ly α absorption for each species, taken from Diplas & Savage (1994), Fruscione et al. (1994) and Savage, Edgar & Diplas (1990). Given the limited number of sightlines for which we have hydrogen column densities and that we sample a range of only 1.5 magnitudes in hydrogen column density per parsec it is difficult to derive accurate correlations. From Fig. 9 it appears that there are similar correlations comparing the column density of both Ti and Ca with the hydrogen column density. The best-fitting line in Fig. 9(a) gives a stronger correlation between the total Na column density per parsec and the total neutral hydrogen column density along the sightline, although given the larger scatter in Fig. 9(a) this may not be significant. The similarity of Fig. 9(b) to Fig. 9(c) may indicate that Ti II and Ca II occur in the same regions of the interstellar medium. Indeed, we see very similar depletion patterns between Ti II and Ca II and this is fully discussed in Section 4.3.6. We note that Wakker & Mathis (2000) also find similar scatters in the

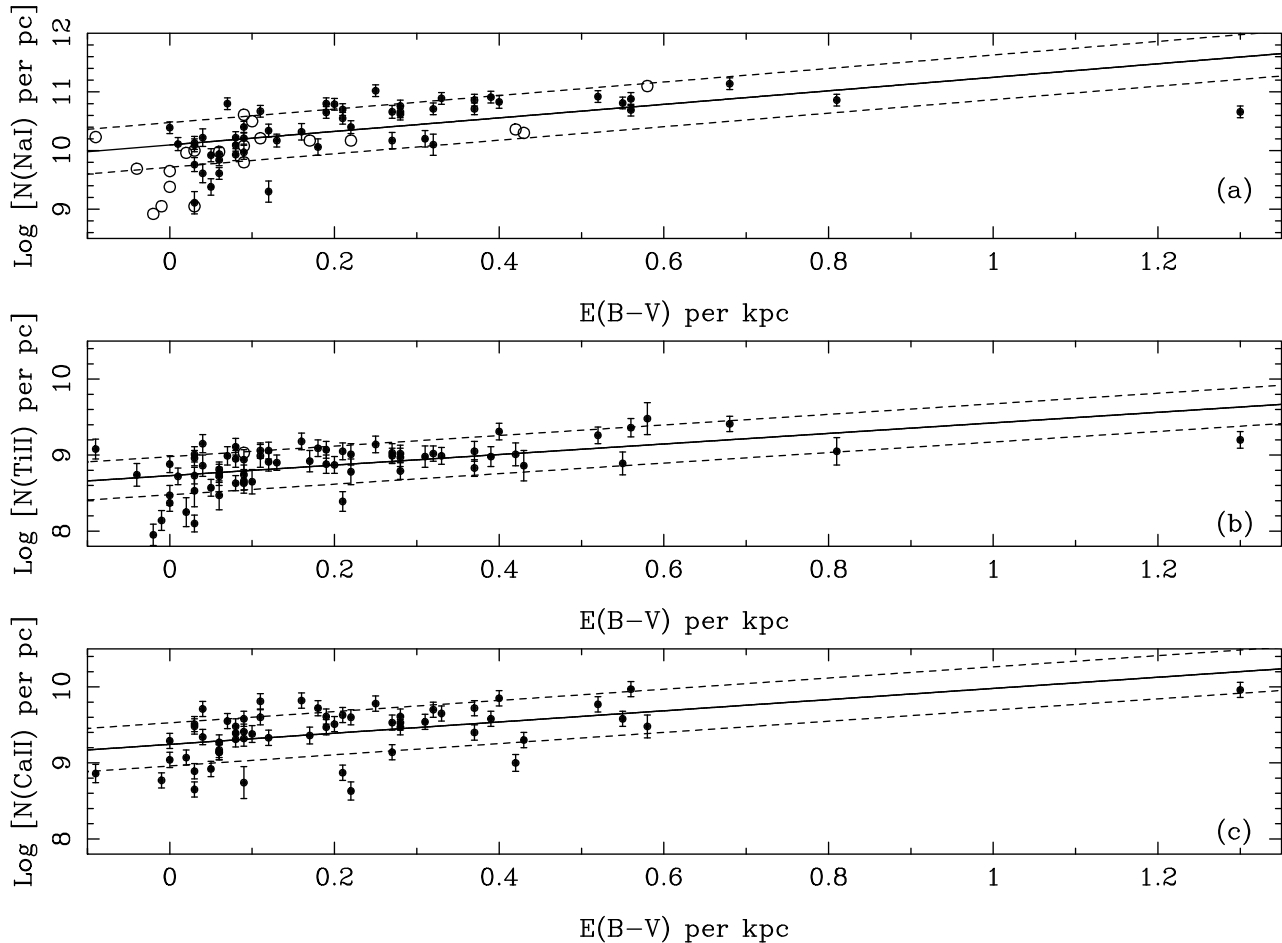


Figure 8. Plots of the logarithm of the total column density of (a) Na I, (b) Ti II and (c) Ca II per parsec against reddening per kiloparsec. Open circles represent upper limits to the column density. The uncertainty in the reddening per kiloparsec is approximately 25 per cent. The solid and dashed lines represent the best-fitting line and the 1σ standard deviation in the points respectively. The RMS scatter and Pearson correlation coefficients are 0.381, 0.597; 0.251, 0.534 and 0.284, 0.486 for (a), (b) and (c) respectively.

plots of Ca and Ti column density with H I column density (a 1σ standard deviation of 0.4 in the log for each species). This disagrees with the findings of W97, who report a much higher degree of scatter in the Ca plot compared to Ti, and reasonably conclude that Ca II absorption is more affected by ionization and depletion than is Ti II. We note that W97 samples a much larger range in $N(\text{H I})$ than do our observations. Our data have values in the rms scatter of 0.29 for Ca II and 0.23 for Ti II. A-priori, the scatter would be expected to be larger in Ca II than in Ti II, as the former is not the primary ionisation stage in the warm ISM, although the observed difference is small and may be a statistical variation.

Ferlet, Vidal-Madjar & Gry (1985) discuss the use of Na I as a tracer of H I in the diffuse interstellar medium via the relationship:

$$\log N(\text{Na I}) = 1.04 \times \log N(\text{H I} + \text{H}_2) - 9.09$$

as derived from Na I D lines. These authors also report that at low reddening ($E(B - V) < 0.3$) this relation is independent of reddening. In Fig. 10 we plot the total Na column density against the value for H I at low reddening, $E(B - V) < 0.3$, and also show an unweighted best-fitting line to the data points. We note that at these reddenings we do not believe the contribution of H₂ to be significant

compared to that of H I. We have also calculated Na column densities from the weaker line of the Na I D doublet at 5893 Å for these sightlines where possible, the results being plotted as triangles. We find excellent agreement between these results and those predicted by the Ferlet et al. (1985) relation. From the best-fitting line to the points plotted as triangles in Fig. 10 (note, this best-fitting line is not shown in the figure) we calculate the relationship between Na I and H I to be:

$$\log N(\text{Na I}) = 1.07 \times \log N(\text{H I}) - 9.66$$

This contrasts with the relationship:

$$\log N(\text{Na I}) = 1.76 \times \log N(\text{H I}) - 23.91$$

derived from the best fitting line to the Na I UV points shown as the solid line in Fig. 10 although given the scatter and low number of data-points the significance of this relation is uncertain. A lack of H I column densities derived in a consistent manner precludes us from deriving a more robust relation.

In W97, it is reported that the ultraviolet Na I UV doublet can underestimate the true Na I column density by up to 20%. We believe this to be due to the fact that higher velocity clouds which appear in the Na I D lines and are significantly offset from the strongest feature do not appear in the UV Na I transitions due to the inherent weakness of

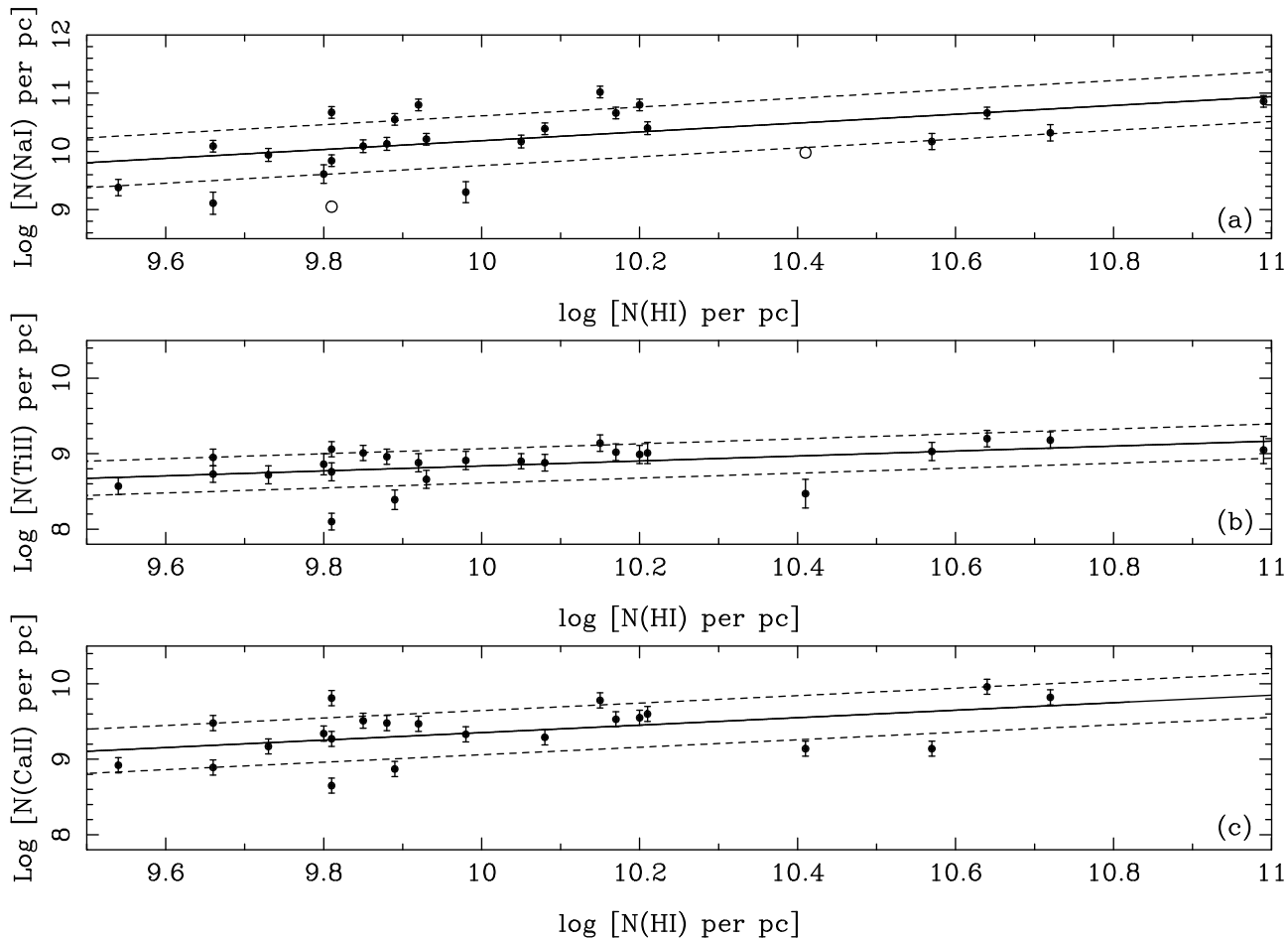


Figure 9. Plots of the logarithm of the total column density of (a) Na I, (b) Ti II and (c) Ca II per parsec against the logarithm of the total H I column density per parsec along the line of sight. Open circles represent upper limits to the column density. The solid and dashed lines represent the best-fitting line and the 1σ standard deviation in the points respectively. The uncertainty in the H I column density per parsec is typically 0.10 dex. The RMS scatter and Pearson correlation coefficients are 0.427, 0.539; 0.227, 0.459 and 0.293, 0.477 for (a), (b) and (c) respectively.

these lines. On the other hand, the high strength of the Na I D lines means that saturation effects cause an underestimate of the column density for the strongest feature of these lines. This effect can be much more important than the under-estimation from the UV lines, which goes some way to explaining the offset between our ultraviolet sodium column density and the column density from the Na I D lines. Savage & Sembach (1991) estimate the correction that one needs to apply to account for saturation, based on the difference between the column density derived from each line of the doublet. We have applied these corrections to the Na I D column density and these are plotted as open circles in Fig. 10. A best-fitting line to these points gives a relationship of:

$$\log N(\text{Na I}) = 1.23 \times \log N(\text{H I}) - 13.01$$

Although this correction reduces the discrepancy between the column densities from the Na I UV and D lines, there is still a significant offset between them. This offset approximately corresponds to an underestimate of 30 per cent in the column density derived from the Na I D lines compared to using the Na I UV transitions.

4.3.5 Correlations between the column density of each species

In Figs. 11(a), (b) and (c) we present plots of the correlations between the column densities derived from each species, and we see good correlation in all three plots. We calculate abundance ratios between the three species to be 0.04 ± 0.01 , 0.30 ± 0.04 and 0.13 ± 0.02 for $N(\text{Ti II})/N(\text{Na I})$, $N(\text{Ti II})/N(\text{Ca II})$ and $N(\text{Ca II})/N(\text{Na I})$, respectively, where the quoted uncertainty is the 1σ standard deviation divided by the square root of the number of points used to determine the ratio. In Fig. 11(b) we see a particularly strong correlation between the Ti II and the Ca II abundance and our $N(\text{Ti II})/N(\text{Ca II})$ ratio agrees well with the value of 0.29 ± 0.03 determined by W97.

In Fig. 12 we plot the column density of individual Ti II components against that of the associated Ca II component listed in Table 3. We have not plotted cases where we see two resolved features in one species and only one feature at a similar velocity in the other species. Similarly, if there are overlapping components of either Ti II or Ca II that lie within the FWHM of either the main or the overlapping component, these components are excluded from the plot. The same rejection criteria were applied with respect to the

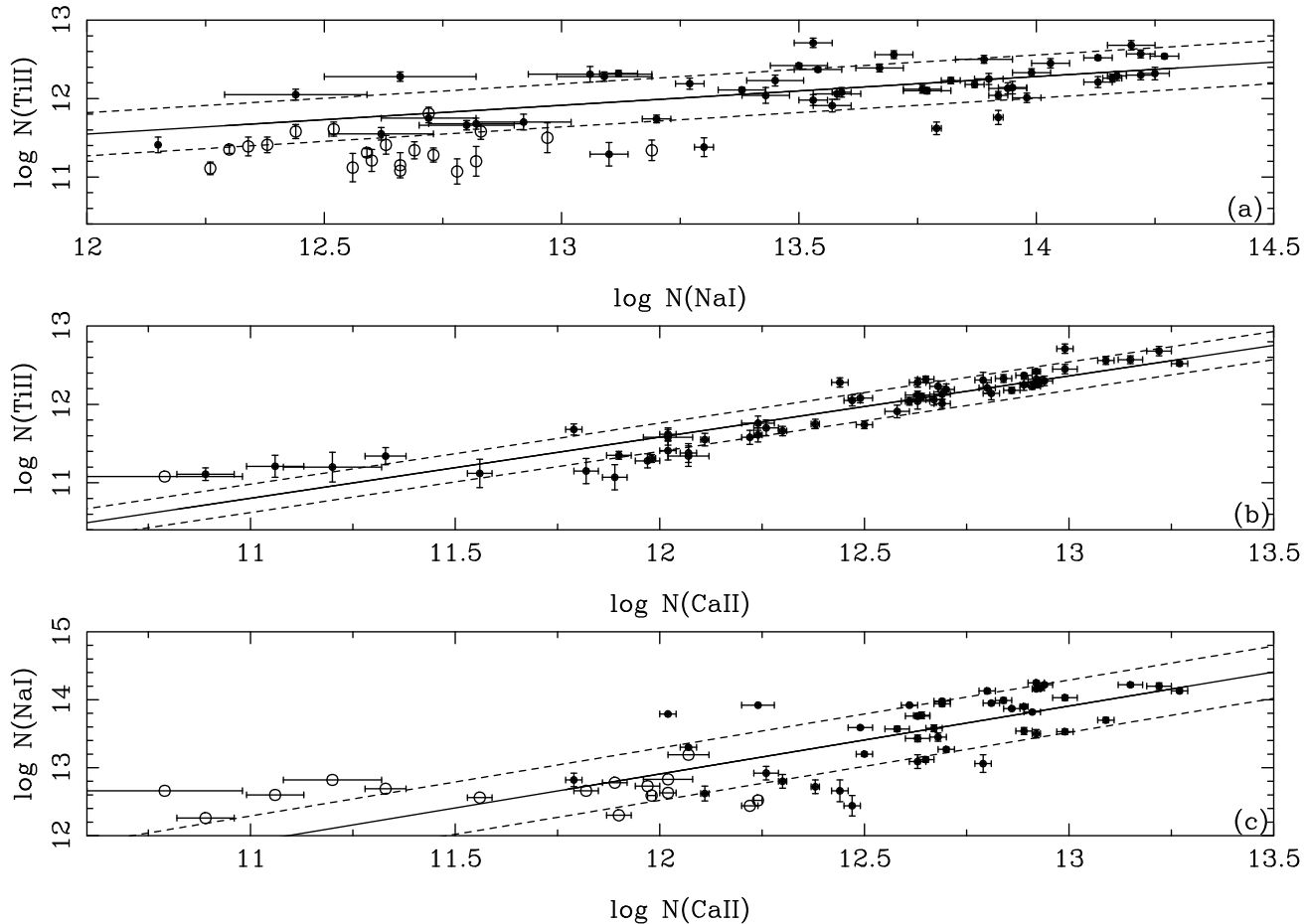


Figure 11. Correlations between the logarithm of the total column densities derived from each species. The open circles represent upper limits to column densities. The solid and dashed lines represent the best-fitting line and the 1σ standard deviation in the points respectively. The RMS scatter and Pearson correlation coefficients are 0.275, 0.573; 0.178, 0.920, and 0.385, 0.643 for (a), (b) and (c) respectively.

upper limits. The $N(\text{Ti II})/N(\text{Ca II})$ ratio based on the components is 0.26 which is in excellent agreement with that derived from the totals. It should be noted that in the derivation of this ratio we have not included those points plotted as open circles. We note that the rms scatter and correlation coefficient are larger and smaller respectively than when comparing the total column density along a line of sight (0.32 dex compared to 0.18 dex for the rms scatter and 0.78 compared to 0.92 for the Pearson correlation coefficient). This may be due to the fact that the components are associated if they lie within 3 km s^{-1} in velocity space, and could in fact be separate parcels of gas.

Finally, we note that for low upper-limit values of Ca II, the points appear to be mainly associated with higher upper limits for Ti II. This may simply be an effect of the higher upper limits for Ti compared to Ca upper limits being due to the weakness of the Ti line compared to the Ca line. For the very low total column densities of Ca, we see a similar effect in Fig. 11(b) although given that this is in only four points on the plots its significance is in doubt. This is in contrast to W97 (Fig. 8(a)) where the opposite effect is seen, low column densities of Ca II seem to correspond to lower than expected upper limits to the Ti column density. Given that this is only seen in the upper limits and not for any real detections

this may be an effect of the methodology which was used to estimate the upper limits. In W97 Fig. 8(c) where they plot Ti against Ca for individual components, this effect is not seen.

4.3.6 Depletions in the column density along each line-of-sight

In Fig. 13 we plot the depletion of the species with respect to the perpendicular height and the reddening along the line-of-sight, in a similar method to that used by W97. The depletion is calculated as the ratio of the abundance of the element to the solar system value. Solar system abundances of 6.37, 5.00, and 6.41 for Na, Ti and Ca, respectively, are obtained from Lodders (2003), where the abundance of the element is taken as its total column density relative to the HI column density along the line-of-sight. Previous work (e.g. Gondhalekar 1985, Crinklaw, Federman & Joseph 1994) indicates that the depletion of both Ti and Ca increase in line with increasing column density. Both elements show the same slope with increasing column density, indicating that these elements only trace the warm intercloud medium. In the current paper we hence restrict ourselves to correlations

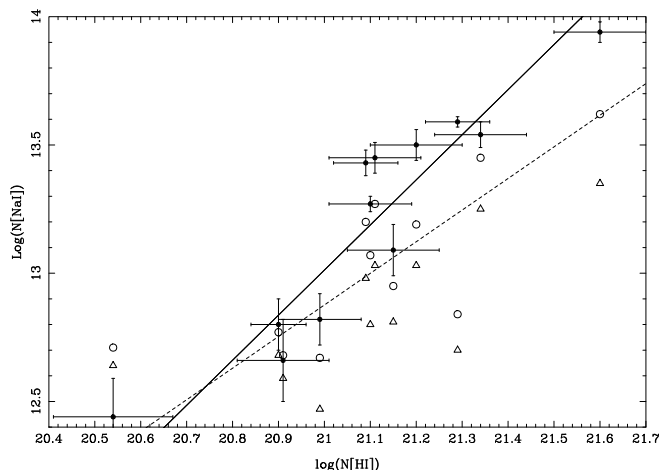


Figure 10. Correlation between the logarithm of the total Na I column density derived from a profile fit of the Na I UV doublet at 3302 Å and the logarithm of the total H I column density at low reddening, $E(B - V) < 0.3$. The solid line represents the best-fit to our data points, given as points with error bars. The triangles represent the Na I column density derived from the weaker line of the Na I D doublet at 5893 Å. The open circles represent the Na I D column density corrected for saturation, using the corrections from Savage & Sembach (1991). The dashed line represents the best-fitting line to these corrected points. The discrepant point at a H I column density of 20.53 dex has not been included in the best-fitting lines.

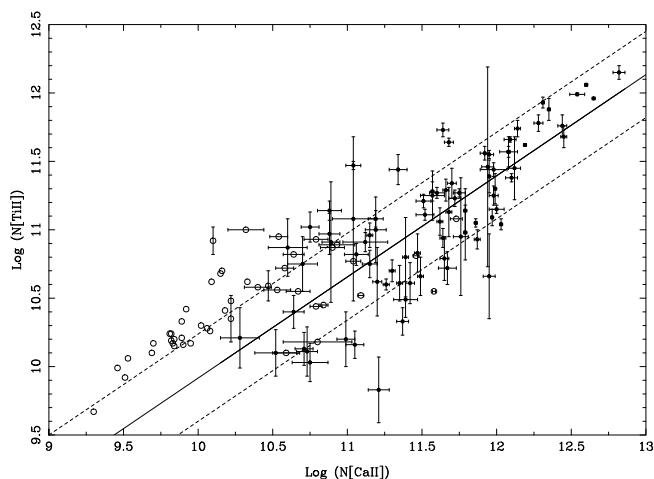


Figure 12. Correlations between the logarithm of the column density of associated components of Ti II and Ca II. The solid and dashed lines represent the best-fitting line and the 1σ standard deviation in the points about this line. The RMS scatter and Pearson correlation coefficient are 0.319 and 0.786 respectively. Open circles represent upper limits to the column density of an individual component.

in depletion of the three species studied with distance above the Galactic plane and reddening in line with W97.

Fig. 13(a) shows a weak correlation between the height, $|z|$, and the depletion for Na I, in the sense of a higher depletion at high z , but given the scatter in the plot (Pearson correlation coefficient of -0.25) this does not appear significant. In Figs. 13(b) and (c) we see evidence for lower depletions of Ti and Ca at higher values of $|z|$, consistent with less dust with increasing distance from the Galactic plane.

In Fig. 13(d) we see a correlation between the depletion of Na and the reddening along the line-of-sight, with again less depletion at higher reddenings. Given the small scatter and large correlation coefficient, the correlation appears to be significant. In contrast, we find evidence of constant depletions of Ti and Ca at all reddenings, shown in Figs. 13(e) and (f). This disagrees with the work of de Boer et al. (1986) who find that the depletion of all metals increases with increasing $E(B-V)$, although for Ti II there were only 8 datapoints. However, our finding of a lack of correlation agrees with W97 who find little evidence in Ti II for such an effect with $E(B-V) > 0.2$. We note that the scatter and range in values of depletion found in the current paper for Ti II of -1.4 to -2.8 dex are somewhat smaller than found by W97 whose depletion values range from -0.5 to -2.7 dex.

Considering the decreasing Na depletion with increasing $E(B-V)$, we associate the sightlines with higher reddenings as having a significant amount of H_2 . We have been able to obtain the H_2 column density for one line-of-sight, HD 148184, at high reddening ($E(B-V)=0.53$) from Fruscione et al. (1994), and we find that this is 30% of the H I column density. For an element that is primarily in clouds, the exclusion of H_2 will cause the total observed H column density to be decreased, causing an observed increase in the abundance of the element and a corresponding decrease in depletion which is what we observe in Fig. 13(d) at high values of reddening. On the other hand, regions with higher $E(B-V)$ values are associated with dust onto which elements are removed from the gas-phase, which causes an increased depletion. Hence the two affects act in different directions. We note that e.g. Phillips, Pettini & Gondhalekar (1984) find that over a range of column densities, the depletion of sodium is essentially constant.

4.3.7 $N(\text{Ti II})/N(\text{Ca II})$ ratio

In order to reliably conclude that Ti II and Ca II do indeed occur in similar environments we plot the $N(\text{Ti II})/N(\text{Ca II})$ ratio against distance to the stellar target, total H I column density along sightline and reddening in Fig. 14(a), (b) and (c), respectively. We also plot the average $N(\text{Ti II})/N(\text{Ca II})$ ratio as a dotted line in these figures. Fig. 14(a) shows a number of “discrepant” points, i.e. with higher than average $N(\text{Ti II})/N(\text{Ca II})$ ratios, towards and HD 100841 and HD 145482. These sightlines have in common that, given errors in their distance estimates, they can be associated within the Local Bubble. The only peculiarities in these sightlines are that for Ca II K in HD 100841 the lines are broad and weak and for HD 145482 the lines are also relatively weak. From each of these plots we conclude that, in general, $N(\text{Ti II})/N(\text{Ca II})$ ratio is constant over distance, cloud density and reddening, and hence we can infer that Ti II and Ca II normally occur in the same regions. The RMS of the scatter when we plot the total column density of Ti II against Ca II is some 0.18 dex. The mode in the errors in the total column densities for each species are 0.02 dex for Ca II and 0.05 dex for Ti II, so the intrinsic scatter on the data is only some 30–40 per cent. We recall that the observed depletion is dependent in each sightline on the fraction of warm and cold gas present in each component (Spitzer 1985), the dust content (ions being removed from the gas-phase by sticking onto grains) and the ionizing radiation field. The

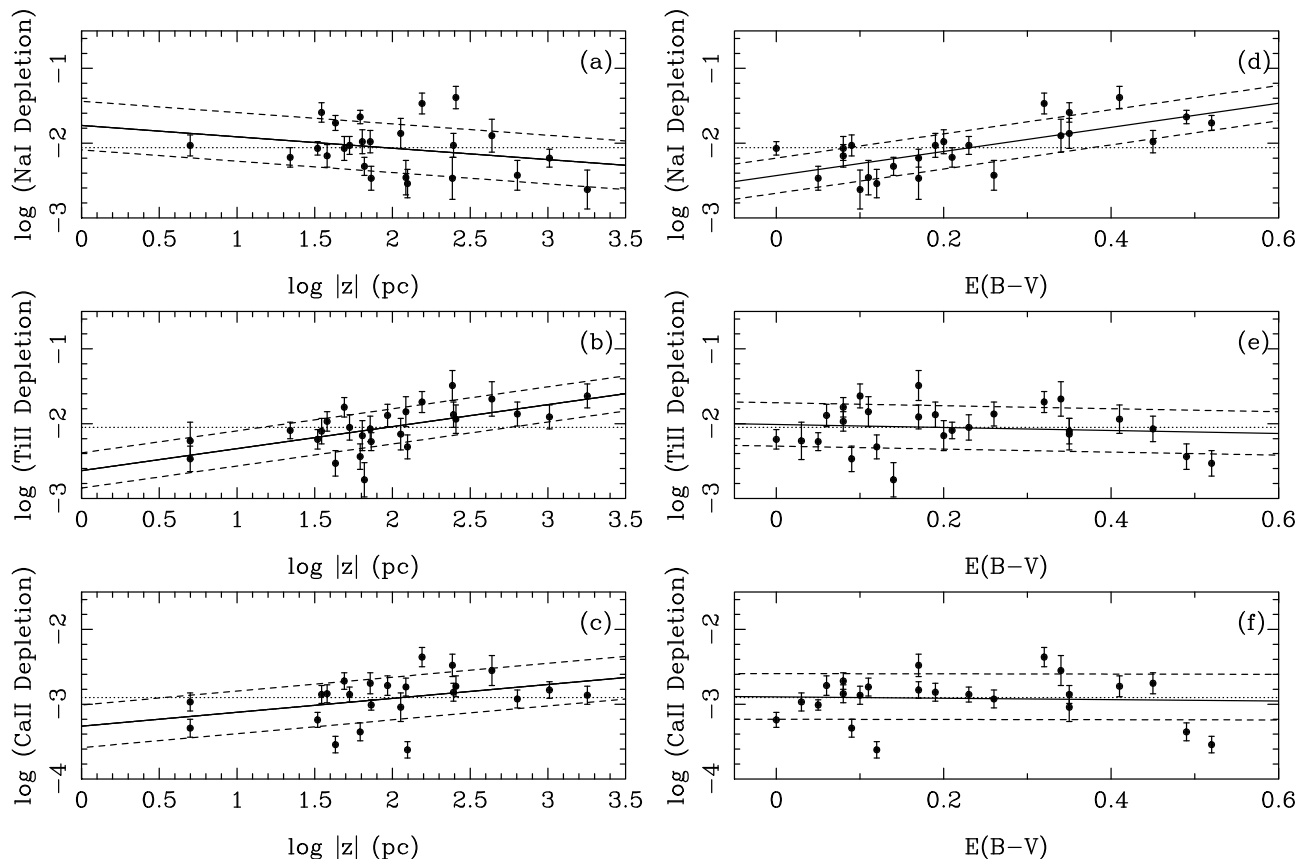


Figure 13. Panels (a), (b) and (c) show the depletion as a function of the perpendicular distance to the star to the Galactic plane for Na I, Ti II and Ca II respectively. Panels (d), (e) and (f) show the depletion as a function of the reddening along the sightline to the star for Na I, Ti II and Ca II respectively. The dotted line represents the average depletion derived from our sample. Open circles represent lower limits to the depletion. The solid and dashed lines represent the best-fitting line and the 1σ standard deviation in the points respectively. The RMS scatter and Pearson correlation coefficients are 0.322, -0.253; 0.236, 0.592; 0.285, 0.370; 0.239, 0.695; 0.291, -0.101 and 0.306, -0.046 for (a), (b), (c), (d), (e) and (f) respectively

fact that Ca II does not vary much with respect to Ti II was initially surprising, as it suggests that the amount of Ca II (not the dominant ionisation stage) does not change much with the radiation field. However, at least when comparing the warm interstellar medium to low-density H II regions, the work of Sembach et al. (2000) predicts that the relative fraction in these transitions remains constant. For example, in their composite model of the warm interstellar medium (WIM) by Sembach et al. (2000), the ionisation fraction is 0.21 for Ca II, 0.79 for Ca III, 0.59 for Ti II, and 0.41 for Ti III. For WIM regions with the fraction of neutral hydrogen x_{edge} , is greater than 0.1, the corresponding values of the ionisation fraction for their model is 0.19 for Ca II, 0.79 for Ca III, 0.45 for Ti II and 0.52 for Ti III. Finally, for the $x_{\text{edge}}=0.1$ model for a low-density H II region, the ionisation fractions are 0.06 for Ca II, 0.94 for Ca III, 0.18 for Ti II and 0.63 for Ti III. In these models at least, the relative Ti II/Ca II ionisation fractions are thus a factor 3 different in both cases. Hence if the models are accurate and the sightline is comprised only of WIM and H II regions, the strong correlation between Ti II and Ca II is not unexpected. Of course, the above discussion

does not take into account the presence of dark clouds in which both elements are heavily depleted.

4.4 Components

4.4.1 Intermediate and High velocity components

In order to classify the interstellar components we have observed as low-, medium- or high velocity (LVCs, IVCs and HVCs, respectively), we have calculated the expected velocity range in which one would expect to see interstellar clouds based on the direction of the sightline and the distance to the stellar target. To calculate the velocity range we use the methodology of Wakker (1991), in that we assume a flat rotation curve with $v_{\text{rot}} = 220 \text{ km s}^{-1}$ at $r > 0.5 \text{ kpc}$, decreasing linearly towards the Galactic centre, together with equations from Mihalas & Binney (1981). A deviation velocity for interstellar cloud components which lie outside the expected velocity range is calculated, where the deviation velocity is defined as the difference between the velocity of the component and the nearest limit of the expected velocity

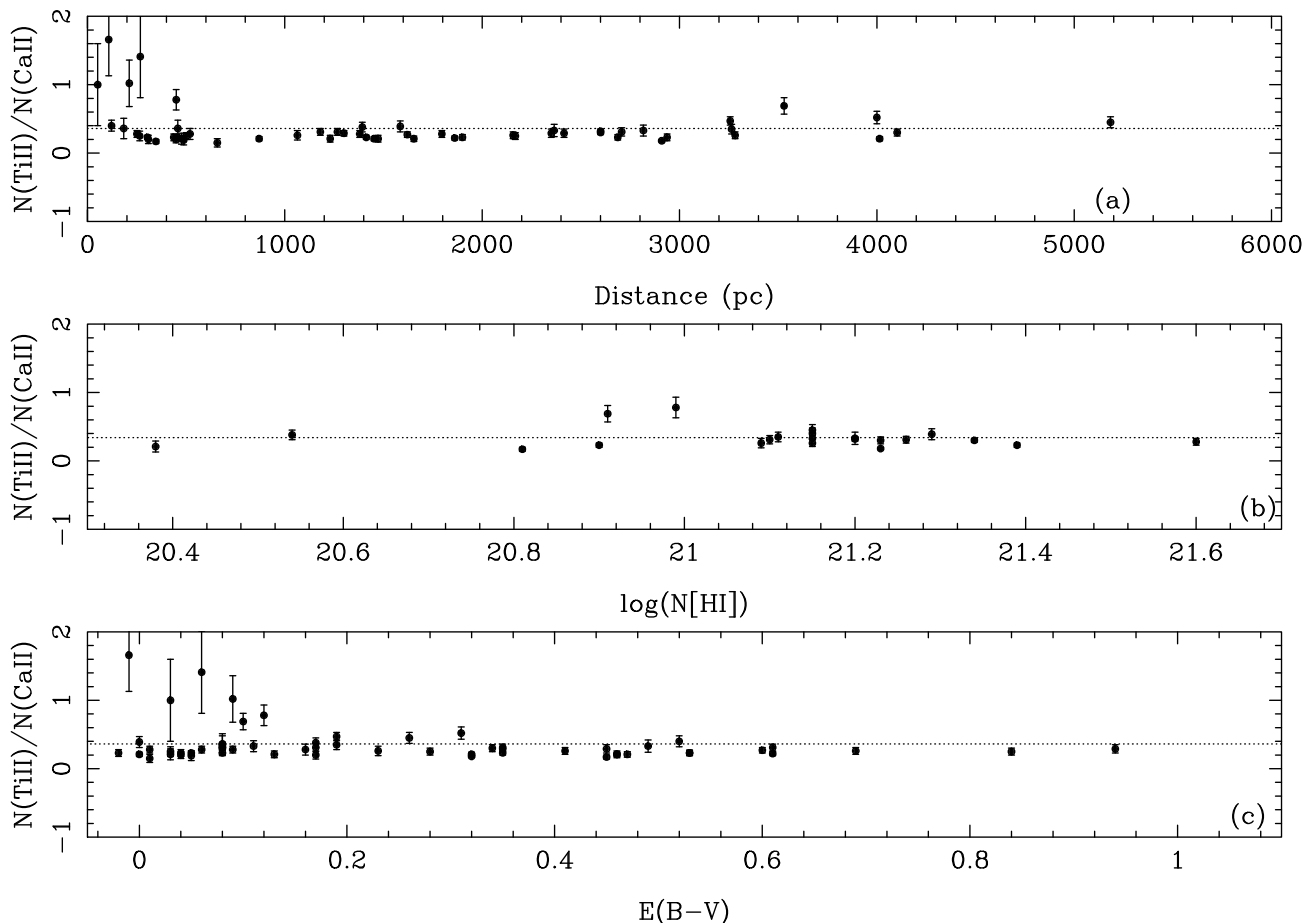


Figure 14. (a), (b) and (c) plot the $N(\text{Ti II})/N(\text{Ca II})$ ratio as a function of distance to the target, total H I column density and reddening respectively. The dotted lines represent the average $N(\text{Ti II})/N(\text{Ca II})$ ratio.

range (Wakker 1991). We classify LVCs as having absolute values of their deviation velocities below 30 km s^{-1} , IVCs between 30 km s^{-1} and 90 km s^{-1} , and HVCs greater than 90 km s^{-1} . In Table 6 we tabulate all the IVCs and HVCs detected along our sightlines. As the present paper is not primarily concerned with IVCs and HVCs, and we also do not have access to H I emission spectra at present, we are hence unable to confirm that our detected IVCs and HVCs are real interstellar clouds. We must emphasise that given the nearby nature of many of the stars, it is unlikely that they are true HVCs/IVCs but this possibility should not be discounted. Although high velocity clouds are thought to reside either in the Galactic halo or possibly at extragalactic distances (e.g. Wakker & van Woerden 1997, Braun & Burton 1999), they can also arise from shocks created in the ISM by supernova blast waves. In the present paper we will restrict ourselves to a brief discussion of several of the more interesting sightlines, although a full study of both IVCs and HVCs will be carried out in a future paper.

4.4.2 HD 171432

We see 5 IVCs in the Ca II K line and these have also been identified in the Ca II H feature and hence these lines are unlikely to be stellar transitions of another species. We have correlated our sightline with data from the H I survey of

high velocity interstellar clouds in the Southern Hemisphere (Morras et al. 2000), and we do not find any nearby H I clouds at similar velocities to our HVCs, although we have not inspected the actual H I data.

HD 171432 lies along the line of sight to the Scutum Supershell and Callaway et al. (2000) report a kinematically-derived distance to the Supershell of 3.3 kpc with a diameter of ~ 290 -pc. Our spectroscopic distance estimate puts the star at a distance of 4.0 kpc and so the IVC's appear to be associated with this feature. We also see some evidence for IVCs in the Ti II spectra although these have not been fitted. On closer inspection of the spectra, we see evidence of many small strength features which do not appear to be noise. Based on the FWHM of the stellar lines of the star, these features are clearly not stellar in nature (unless there is a binary companion present), but they may be evidence of small scale structure in the Scutum Supershell.

4.4.3 HD 72067

We see a single strong HVC along this sightline which also appears in Ca II H. This sightline lies along the same sightline as the Vela supernova remnant which Cha, Sembach & Danks (1999) report to lie at a distance of 250 pc. Our distance estimate of 488 pc would place HD 72067 within and possibly beyond the Vela supernova remnant and as many

previously observed HVC's have been seen along sightlines which pass through this remnant, for example, as reported by Slavin, Nichols & Blair (2004), our observation of an HVC is not unexpected.

4.4.4 HD 94910

This is the only sightline in which we detect an HVC in the Na I UV data, and also appears in the Ca II K line. Note that we have not fitted the interstellar components of the Ca II K line due to the difficulty of accurately fitting a base-line to the continuum. The SIMBAD database classifies HD 94910 as a Wolf-Rayet star and the high velocity feature we see may be associated with the star rather than the interstellar medium, as Wolf-Rayet stars are known to have many peculiar features (Leitherer & Chavarria 1987), such as stellar-wind bubbles this could explain our high velocity features. Indeed, we find that over two thirds of our stellar targets which are classified as Wolf-Rayet's show IVCs or HVCs.

4.4.5 HD 163758

Again we have confirmed the existence of the high velocity feature in the Ca II H line, although similarly to HD 94910 this star is classified as a Wolf-Rayet star and as such the HVC may be a circumstellar feature. A search of the Morras et al. (2000) H I database does not find any nearby HVCs at a similar velocity to our detected feature.

5 CONCLUSIONS

We have obtained spectra towards 74 early-type stellar targets from the UVES POP survey, at a velocity resolution of 3.75 km s^{-1} . We have studied the interstellar Na I UV doublet at 3302 \AA , Ti II at 3383 \AA and Ca II at 3933 \AA . The average S/N ratio per pixel for the spectra are 260, 300 and 430, respectively, which far exceeds that in previous work in a sample of this size. Column densities were measured for each component along each line-of-sight, with the individual components being summed to obtain the total. This quantity was also calculated by the AOD method, which is in excellent agreement with the total generated by the fitting of each individual component. There is also good agreement between the total column densities derived from each line of the Na I UV doublet. The median of the errors in individual components are 0.06 dex, 0.06 dex and 0.02 dex for Na, Ti and Ca components respectively. In general, we have not studied cases where the stellar line is of a similar width and velocity to the interstellar profile, and so we have avoided stellar contamination of our derived column densities.

5.1 General correlations

We have investigated the dependence of the total column density of each species along the line-of-sight to a star with distance, reddening and total H I column density. Our stars span distances from 52 pc to 6000 pc, with the maximum height from the Galactic plane, $|z|$, being 1793 pc. We find a strong positive correlation between Ti and Ca column densities and distance, and a similar correlation for Na

although with much more scatter. We also find a good correlation between the column densities and $|z|$, although again the correlation is weaker in Na. Our sightlines have values of reddening $E(B - V)$ of up to 1.0, and some correlation between the column density per parsec of each species and the reddening per kiloparsec has been found. We find similar correlations between the H I column density per parsec and the column density per parsec of Ca and Ti. There is evidence of a stronger correlation between Na and H I but given the scatter of the points this may not be significant. Wakker & Mathis (2000) have previously found this large dispersion, and have thus cautioned against for example using non-detections of Na to set limits on the distances of High Velocity Clouds. The observed scatter in Na and H I is attributed by these authors to the fact that it is not the dominant ionisation stage in the ISM, so ionisation effects may play a more important role. This certainly calls into question the accuracy of using the Na column density as an indicator of the value for H I. We also find that the column density derived from the Na I D lines, generally used to predict the H I values, appears to underestimate the column density relative to the UV lines that we have studied. Even when the saturation corrections of Savage & Sembach (1991) are applied to the column density derived from the Na I D lines it still appears to underestimate the Na column density. For Na column densities greater than 13 dex the corrected values underestimate the column density by as much as 0.3 dex relative to column density derived from the UV lines.

5.2 Depletions

The depletion of each species relative to the solar system value has been correlated with $|z|$ and $E(B - V)$. We find some evidence for decreasing depletion with increasing z for both Ti and Ca, with no correlation with depletion and reddening for these species. For Na, we find decreasing depletion with increasing $E(B - V)$, some of which may be caused by the conversion of H I to H₂.

5.3 $N(\text{Ti II})/N(\text{Ca II})$ ratio

We find a good correlation between the Ti II and Ca II column densities, both in the total values and those from individual components that are observed in both species. The ratio from the total is 0.30 compared to that from the individual components of 0.26. Our ratios compare very well with the value of 0.29 ± 0.03 calculated by W97. The similarity between our plots of the correlation of Ti and Ca with each of the different parameters reinforces the possibility that the species show good correspondence if the Ca ionisation balance is controlled by the average interstellar radiation field, and the relative Ca and Ti depletions are relatively constant in the clouds (Welty et al. 1996, Wakker & Matthis 2000).

5.4 Future work

As discussed in Section 4.4.1, many of our sightlines show strong IVC and HVC features. A future paper will involve a

Table 6. List of sightlines showing intermediate and high velocity features in absorption.

Star	l (deg.)	b (deg.)	$d(\text{pc})$	Cmp. No.	Na I(3302)		Ti II(3384)		Ca II(3934)		Type
					v_{LSR}	v_{Dev}	v_{LSR}	v_{Dev}	v_{LSR}	v_{Dev}	
HD 164794	6.01	-1.21	1585	2	-	-	-31.2	-31.2	-	-	IVC
HD 167264	10.46	-1.74	2109	5	-	-	43.7	30.9	-	-	IVC
HD 171432	14.62	-4.98	4014	1	-	-	-	-	-65.2	-65.2	IVC
HD 171432	14.62	-4.98	4014	2	-	-	-	-	-62.5	-62.5	IVC
HD 171432	14.62	-4.98	4014	3	-	-	-	-	-47.2	-47.2	IVC
HD 171432	14.62	-4.98	4014	12	-	-	-	-	92.6	48.7	IVC
HD 171432	14.62	-4.98	4014	13	-	-	-	-	117.4	73.5	IVC
HD 169454	17.54	-0.67	1359	1	-	-	-40.2	-40.2	-	-	IVC
HD 37490	200.73	-14.03	304	1	-	-	-	-	-45.7	-45.7	IVC
HD 50896	234.76	-10.08	1393	1	-	-	-	-	-65.0	-65.0	IVC
HD 60498	247.20	-6.64	936	1	-	-	-	-	-41.2	-41.2	IVC
HD 60498	247.20	-6.64	936	2	-	-	-	-	-31.2	-31.2	IVC
HD 60498	247.20	-6.64	936	12	-	-	-	-	53.4	44.3	IVC
HD 68761	254.37	-1.62	1473	1	-	-	-	-	-55.3	-55.3	IVC
HD 68761	254.37	-1.62	1473	2	-	-	-	-	-39.2	-39.2	IVC
HD 68761	254.37	-1.62	1473	10	-	-	-	-	50.8	38.8	IVC
HD 74966	258.08	3.93	658	7	-	-	-	-	35.7	31.8	IVC
HD 74966	258.08	3.93	658	8	-	-	-	-	50.5	46.6	IVC
HD 72067	262.08	-3.08	488	1	-	-	-	-	-105.8	-105.8	HVC
HD 89587	279.83	5.19	900	1	-	-	-	-	-40.1	-37.4	IVC
HD 93131	287.67	-1.08	2600	1	-	-	-	-	-67.4	-57.1	IVC
HD 93131	287.67	-1.08	2600	2	-	-	-	-	-51.4	-41.0	IVC
HD 94910	289.18	-0.69	6000	1	-117.3	-105.1	-	-	-	-	HVC
HD 94910	289.18	-0.69	6000	2	-79.4	-67.2	-	-	-	-	IVC
HD 94910	289.18	-0.69	6000	3	-64.5	-52.3	-66.2	-54.0	-	-	IVC
HD 96917	289.28	3.06	2910	1	-	-	-	-	-70.8	-58.5	IVC
HD 96917	289.28	3.06	2910	11	-	-	-	-	60.1	60.1	IVC
HD 94963	289.76	-1.81	3257	1	-	-	-	-	-89.0	-76.1	IVC
HD 94963	289.76	-1.81	3257	2	-	-	-	-	-54.0	-41.0	IVC
HD 94963	289.76	-1.81	3257	3	-	-	-	-	-44.8	-31.9	IVC
HD 97253	290.79	0.09	2415	1	-	-	-	-	-47.4	-33.7	IVC
HD 29138	297.99	-30.54	3530	1	-	-	-	-	-77.6	-56.9	IVC
HD 106068	298.51	-0.41	2824	1	-	-	-	-	-85.0	-61.3	IVC
HD 106068	298.51	-0.41	2824	2	-	-	-	-	-75.6	-51.9	IVC
HD 109867	301.71	-4.35	3264	1	-	-	-63.0	-33.3	-63.1	-33.4	IVC
HD 136239	321.23	-1.75	2350	1	-	-	-65.2	-31.6	-64.2	-30.6	IVC
HD 148937	336.37	-0.22	1380	1	-	-	-	-	-102.4	-87.3	IVC
HD 148688	340.72	4.35	1452	1	-	-	-41.7	-28.0	-46.1	-32.4	IVC
HD 148688	340.72	4.35	1452	8	-	-	-	-	34.1	34.1	IVC
HD 151932	343.22	1.43	1413	1	-	-	-	-	-56.2	-44.4	IVC
HD 151932	343.22	1.43	1413	2	-	-	-	-	-44.0	-32.2	IVC
HD 151932	343.22	1.43	1413	11	-	-	-	-	51.5	51.5	IVC
HD 152235	343.31	1.10	1861	1	-	-	-	-	-75.3	-58.8	IVC
HD 152235	343.31	1.10	1861	13	-	-	-	-	39.8	39.8	IVC
HD 152003	343.33	1.41	2687	1	-	-	-	-	-62.9	-36.3	IVC
HD 152270	343.49	1.16	1900	10	-	-	-	-	31.7	31.7	IVC
HD 157038	349.95	-0.79	1444	1	-	-	-	-	-87.3	-79.6	IVC
HD 157038	349.95	-0.79	1444	2	-	-	-	-	-69.6	-61.9	IVC
HD 157038	349.95	-0.79	1444	3	-	-	-	-	-59.1	-51.4	IVC
HD 157038	349.95	-0.79	1444	4	-	-	-47.8	-40.1	-48.9	-41.2	IVC
HD 155806	352.59	2.87	1064	1	-	-	-	-	-37.0	-33.0	IVC
HD 163758	355.36	-6.10	4103	1	-	-	-	-	-46.9	-30.8	IVC
HD 163758	355.36	-6.10	4103	10	-	-	-	-	38.9	38.9	IVC
HD 163758	355.36	-6.10	4103	11	-	-	-	-	90.4	90.4	HVC

more detailed analysis of these components, using the Villa-Elissa HI survey and the current observations to provide improved distance limits to IVCs and HVCs.

ACKNOWLEDGEMENTS

We would like to thank the staff of the Very Large Telescope, Paranal for the work involved in producing the POP survey. ESO DDT programme ID 266.D-5655, <http://www.eso.org/uvespop>. IH and JVS gratefully acknowledge the ESO Director Generals Discretionary fund which provided financial support for IH for this work. FPK is grateful to AWE Aldermaston for the award of a William Penney Fellowship. This research has made use of the SIMBAD database, operated at CDS, Strasbourg, France. We would also like to thank the referee who provided many useful comments and suggestions to the initial draft of the paper.

REFERENCES

- Albert C. E., Blades J. C., Morton D. C., Lockman F. J., Proulx M., Ferrarese L., 1993, *ApJS*, 88, 81
- Ballereau D., Chauville J., Zorec J., 1995, *A&AS*, 111, 423
- Bagnulo S., Jehin E., Ledoux C., Cabanac R., Melo C., Gilmozzi R., 2003, *ESO Messenger* no. 114 Page 10
- Braun R., Burton W. B., 1999, *A&A*, 341, 437
- Callaway M. B., Savage B. D., Benjamin R. A., Haffner L. M., Tuft S. L., 2000, *ApJ*, 532, 943
- Cha A. N., Sembach K. R., Danks A. C., 1999, *ApJ*, 515, 25
- Conti P. S., Garmany C. D., de Lore C., Vanbeveren D., 1983, *ApJ*, 274, 302
- Conti P. S., Vacca W. D., 1990, *AJ*, 100, 431
- Crinklaw G., Federman S. R., Joseph C. L., 1994, *ApJ*, 424, 748
- Diplas A., Savage B. D., 1994, *ApJS*, 93, 211
- Edgar R. J. Savage B. D., 1989, *ApJ*, 340, 762
- Ferlet R., Vidal-Madjar A., Gry C., 1985, *ApJ*, 298, 838
- Frisch P. C., 1998, *LNP*, 506, 269
- Frisch P. C., York D. G., 1983, *ApJ*, 271, 59
- Fruscione A., Hawkins I., Jelinsky P., Wiercigroch A., 1994, *ApJS*, 94, 127
- Gondhalekar P.M., 1985, *ApJ*, 293, 230
- Goraya P. S., Tur N. S., 1988, *AJ*, 96, 346
- Grady C. A., Bjorkman K. S., Snow T. P., 1987, *ApJ*, 320, 376
- Hartmann J., 1904, *ApJ*, 19, 268
- Hobbs L. M., 1974, *ApJS*, 191, 381
- Hobbs L. M., 1978, *ApJS*, 38, 129
- Hobbs L. M., 1984, *ApJS*, 56, 315
- Hoekzema N. M., Lamers H. J. G. L. M., van Genderen A. M., 1993, *A&AS*, 98, 505
- Howarth I. D., Murray J., Mills D., Berry D. S., 2003, *Starlink User Note SUN 50*, Rutherford Appleton Laboratory/CCLRC
- Hurwitz M., Bowyer S., 1996, *ApJ*, 465, 296
- Krelowski J., Schmidt M., Snow T. P., 1997, *PASP*, 109, 1135
- Leitherer C., Chavarria-K C., 1987, *A&A*, 175, 208
- Lallement R., Welsh B. Y., Vergely L., Crifo F., Sfeir D., 2003, *A&A*, 411, 447
- Lodders K., 2003, *ApJ*, 591, 1220
- Mennickent R. E., Vogt N., Barrera L. H., Covarrubias R., Ramirez A., 1994, *A&AS*, 106, 427
- Mihalas D., Binney J., 1981, *Galactic Astronomy; Structure and Kinematics*, 2nd edition, San Francisco, W. H. Freeman and Company
- Morras R., Bajaja E., Arnal E. M., Poppel W. G. L., 2000, *A&AS*, 142, 25
- Morton D. C., 2003, *ApJS*, 149, 205
- Morton D. C., 2004, *ApJS*, 151, 403
- Penny L. R., 1996, *ApJ*, 463, 737
- Phillips A.P., Pettini M., Gondhalekar P.M., 1984, *MNRAS*, 206, 337
- Savage B. D., Edgar R. J., Diplas A., 1990, *ApJ*, 361, 107
- Savage B. D., Sembach K. R., 1991, *ApJ*, 379, 245
- Schmidt-Kaler Th., 1982, in Schaifers K., Voigt H. H., eds, *Landolt-Boernstein*, group VI, subvol. b, *Stars and Star Clusters*, Vol. 2 Springer, Berlin, p. 17
- Sembach K. R., Danks A. C., Savage B. D., 1993, *A&AS*, 100, 107 (SDS93)
- Sembach K. R., Danks A. C., 1994, *A&A*, 289, 539 (SD94)
- Sembach K. R., Howk J. C., Ryans R. S. I., Keenan F. P., 2000, *ApJ*, 528, 310
- Slavin J. D., Nichols J. S., Blair W. P., 2004, *ApJ*, 606, 900
- Slettebak A., 1982, *ApJS*, 50, 55
- Smoker J. V., et al., 2003, *MNRAS*, 346, 119
- Spitzer L. J., 1985, *ApJ*, 290, 21
- Stokes G. M., 1978, *ApJS*, 36, 115
- Vacca W. D., Garmany C. D., Shull J. M., 1996, *ApJ*, 460, 914
- Vallerga J. V., Vedder P. W., Craig N., Welsh B. Y., 1993, *ApJ*, 411, 729
- Vergely J. -L., Freire Ferro R., Siebert A., Valette B., 2000, *A&A* 366, 1016
- Wakker B. P., 1991, *A&A*, 250, 499
- Wakker B. P., van Woerden H., 1997, *ARA&A*, 35, 217
- Wakker B. P., Mathis J. S., 2000, *ApJ*, 544, 107
- Wallace P., Clayton C., 1996, *rv*, *Starlink User Note SUN 78*, Rutherford Appleton Laboratory/CCLRC
- Wegner, W., 1994, *MNRAS*, 270, 229
- Wegner, W., 2000, *MNRAS*, 319, 771
- Welsh B. Y., Sassen T., Craig N., Jelinsky S., Albert C. E., 1997, *ApJS*, 112, 507 (W97)
- Welty D. E., Hobbs L. M., Kulkarni V. P., 1994, *ApJ*, 436, 152
- Welty D. E., Morton D. C., Hobbs L. M., 1996, *ApJS*, 106, 533 (W96)
- Winkler H., 1997, *MNRAS*, 287, 481